2014

Effects Of Drill-pipe Whirling Motion On Cuttings Transport Performance For Horizontal Drilling

Yasin Demiralp
Louisiana State University and Agricultural and Mechanical College, ydemir1@lsu.edu

EFFECTS OF DRILL-PIPE WHIRLING MOTION ON CUTTINGS TRANSPORT PERFORMANCE FOR HORIZONTAL DRILLING

A Thesis

Submitted to the Graduate Faculty of the
Louisiana State University and
Agricultural and Mechanical College
in partial fulfillment of the
requirements for the degree of
Master of Science

in

The Department of Petroleum Engineering

by
Yasin Demiralp
B.Sc., Istanbul Technical University, 2007
December 2014

ACKNOWLEDGEMENTS

First of all, I would like to thank my academic and thesis advisor, Prof. Mayank Tyagi, for his helpful insights that lead me to this thesis topic, for his patience and guidance that made this thesis scientific, and for his great personality that made my stay at LSU very fruitful and enjoyable.

I wish to thank my thesis committee: Prof. Andrew K. Wojtanowicz, and Prof. Krishnaswamy Nandakumar, for their suggestions and efforts that help in guiding and writing this thesis. Also, I would like to thank all faculty members of Craft & Hawkins Petroleum Engineering Department for their critical contributions to my personal and professional skills during my graduate education.

My deepest thanks are also for my family, especially my parents, Naside and Adnan Demiralp, my sister Nese and my brother Sahin, and my girlfriend Aylin Amedova for their continuing encouragement and support over the years. Also, I express my appreciation to Gursat Altun and Yusuf Catal to give me the opportunity for studying here by going surety for the sponsorship agreement.

Special thanks to Turkish Petroleum Corporation for their financial sponsorship and material support during the time I spent in the U.S.A.

I sincerely would thank my roommate, Efecan Demirci for his endless supports and making the life in the US more enjoyable and livable. In addition, I appreciate everything Sultan Anbar did to help me with my research project.

I would like to thank my colleagues for their helpfulness and encouragement over the years, particularly, my dear office mates: Sadé Garcia, Negar Dahitaleghani, Muhammed Zulqarnain, Ildar Akhmadullin, Aaron Harrington, Oscar Molina, and Masoud Mohandessi. I also would like to thank my friends in Nandakumar research group, Oladapo Ayeni, Abhijit Rao, Rupesh Reddy, and Yuehao Li for their supports with CFD strategies and HPC utilization.

Finally, my huge thanks are for my dear Turkish Community in Baton Rouge, Kenan Gedik, Isil&Mert Akyuz, Elif&Bahadir Dursun, Koray Ozhan, Kahila Mokhtari, Volkan Kanat, Gorkem Aydin, Pelin&Abdullah Tekin, Fatih Oz, Selim Oz, Doguhan Yilmaz and Dogus Saracoglu for their limitless support that made me pleased and successful at LSU.

TABLE OF CONTENTS

LIST OF TABLES

LIST OF FIGURES

NOMENCLATURE

F_g	Gravity force	K	Flow consistency index
F_b	Buoyancy force	V_t	Inner pipe tip velocity
F_d	Drag force	U_b	Bulk velocity
F_l	Lift force	N_{RE}	Reynolds Number
F_{wal}	Van der Walls force	D_o	Outer pipe diameter
α	Hole inclination from vertical	D_i	Inner pipe diameter
u	Fluid velocity	D_H	Hydraulic diameter
u_p	Particle velocity	L	Computational length
t	Time	$F_{pressure}$	Pressure gradient force
$\bar{u}$	Mean velocity	$F_{virtual\_mass}$	Virtual mass force
u'	Fluctuating velocity	$F_{Saffman's\_lift}$	Saffman's lift force
ν	Kinematic viscosity	$F_{gravitation}$	Gravitational force
p	Pressure	F_{other}	Other forces
ϕ	Scalar quantity	m	Particle mass
ρ	Fluid density	ρ_p	Particle density
k	Turbulent kinetic energy	$\boldsymbol{\omega}$	Rotating speed of the drill-pipe
ϵ	Turbulent dissipation rate	$\boldsymbol{\Omega}$	Whirling speed of drill-pipe
ω	Specific dissipation rate	P	Point P on Drill-pipe
σ_{ij}	Stress tensor	ε	Whirling radius
τ_{ij}	Sub-grid scale stress	r_w	Wellbore radius
τ	Shear stress	r_p	Drill-pipe radius
γ	Shear rate	V_s	Slip velocity
ΔP	Pressure gradient	C_c	Cuttings concentration
n	Flow behavior index	$\bar{V}_T$	Ave. Transport Velocity

ABBREVIATIONS

ERW	Extended Reach Well
WOB	Weight on Bit
ROP	Rate of Penetration
ECD	Equivalent Circulating Density
VKI	von Karman Institute
METU	Middle East Technical University
MTV	Minimum Transport Velocity
RANS	Reynolds-Averaged Navier-Stokes
CFD	Computational Fluid Dynamics
DEM	Discrete Element Method
DPM	Discrete Particle Method
DNS	Direct Numerical Simulations
LES	Large-Eddy Simulations
DES	Detached Eddy Simulation
SGS	Subgrid-Scale Model
SRS	Scale-Resolving Simulation
CPU	Central Processing Unit
UDF	User Defined Function
SST	Shear Stress Transport
RNG	Re-Normalization Group
RSM	Reynold's Stress Model
DRW	Discrete Random Walk Model
BHP	Bottom Hole Pressure

ABSTRACT

Dispersion, deposition, and suspension of particulate materials in the carrier fluid play a significant role in the oil industry. Increasing the cuttings transport performance in deviated wells is difficult due to the rolling/sliding transport, and cuttings settling on the low side of the annulus. Insufficient cuttings transport may lead to some crucial problems such as pipe sticking, increasing in torque and drag, material damage and bed cementing quality. Increasing flow rates and improving mud properties may not be applicable for a proper hole cleaning because of the hydraulic and mechanical limitations. In such cases, additional pressure may be generated, and this causes formation fractures and drilling fluid losses. Under these circumstances, the other major contribution to cuttings transport is provided by drill-pipe rotation.

In this study, the effect of drill-pipe rotation on cuttings transport behavior is investigated for eccentric horizontal wells. Whirling motion of drill-pipe is also analyzed. During drilling, drill-pipe is subjected to axial, lateral and torsional loads due to the dynamic vibrations. These loads cause that drill-pipe to lose its stability and generate snaking and/or whirling type of motion. Dynamic behavior of drill-pipe plays a significant role on cuttings transport and stationary bed removal.

Turbulence modeling becomes very complicated when cuttings transport includes deposition and sliding effects. Advanced turbulence models are required to get accurate flow predictions while optimizing computational resources requirements. Unsteady SST k-ω turbulence model is applied due to its practicability and reliability in predicting cuttings transport behavior. Discrete phase is modeled with discrete element method (DEM) by including particle-particle and particle-fluid interactions with a commercial ANSYS FLUENT™ 15.0 CFD package using LSU high performance computing (HPC) resources.

It is concluded that cuttings concentration significantly decreases with increasing flow rate. Drill-pipe rotation around its own axis causes cuttings swaying and distribute asymmetrically along the circumferential direction. Orbital motion of the drill-pipe contributes more to cuttings transport performance. Low whirling rotary leads to increase in annular pressure losses in low flow rates. In the turbulent flow regime, however, annular pressure losses increase with increasing whirling speed.

CHAPTER 1: INTRODUCTION

1.1 Overview of Cuttings Transport Phenomena

In the oil industry, transportation of drilled cuttings plays a significant role from the point of wellbore stability and cement job reliability in any kind of well inclinations. Effective hole cleaning is essential in order to achieve successful drilling. Otherwise, costly consequences may happen. Majority of the cuttings transportation phenomena can change with the wellbore configuration, formation type, designing of the bottom-hole assembly, and drilling fluid contamination in time. Drilling fluid, which usually has a non-Newtonian fluid rheology, is capable of carrying cuttings from the bottom hole to the surface. Drilling mud properties such as plastic viscosity and yield point demonstrate the ability to carry cuttings out of the annulus during circulation. Also, the gel strength indicates the capacity of suspension of the drilled cuttings in the static condition. To clarify, drilled cuttings tend to fall down under settling condition when drilling fluid is not circulated. In a non-Newtonian drilling fluid, cutting settling velocity is a function of the shear stress generated by the density differences between the fluid and cuttings, and the gel strength of the drilling fluid. Drilled cuttings are all suspended if the stress is less than the gel strength since the particle settling velocity equals to zero [1]. Observing mud properties during drilling provides awareness of understanding how effective cuttings are transported. In summary, drilling fluid properties can be controlled to avoid mud contamination and subsequently improve hole cleaning performance.

In vertical and near vertical wells, drilled cuttings transport has been well understood. Particles are mainly lifted by drilling fluid when the axial velocity of the carrier fluid is bigger than the cuttings settling velocity. This behavior also brings about the hole cleaning efficiency in terms of the transport ratio, which is the ratio of the net rising velocity of drilled cuttings to the annular fluid velocity. Also, net rising velocity of cuttings is defined as the difference between the annular fluid velocity and the particle slip velocity. However, effective hole cleaning is a challenging problem in complex structural wells like highly deviated wells, horizontal wells, extended reach wells (ERW), etc. as illustrated in Figure 1-1 [2]. For hole angles between 30° and 55°, it is very difficult to maintain the wellbore stability and remove cuttings because the stationary bed slides downward against the flow [3]. Nevertheless, greater attention is required in

highly inclined sections of ERW due to the fact that generated drilled cuttings tend to accumulate as part of the suspension by forming a bed in the lower section of the annulus [4].

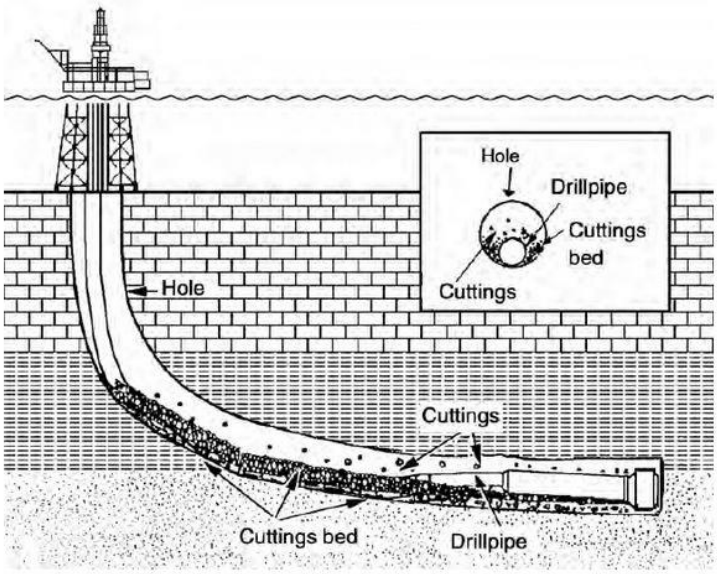

Figure 1-1: Schematic of cuttings bed build-up during directional drilling [2]

Inadequate cuttings removal can lead to several problems. Excessive frictional drag and torque, tool wear, significant decrease in rate of penetration (ROP), difficulty in casing cementing and well logging, formation fracturing, and mechanical pipe sticking are the most serious concerns that can be caused by poor hole cleaning [5-7]. It was stated that many stuck pipe problems occurred because of insufficient hole cleaning, and may lead to significant financial losses, or well abandonment [8].

Cuttings transport phenomena can be positively or negatively affected by several parameters. Cuttings characteristics, drilling fluid properties and operational factors are the main functions influencing the cuttings transportation. To clarify the key elements, cuttings shape and size, cuttings density, and cuttings distribution (volume fraction) can be categorized under the cutting characteristics. Formation type, bit selection, weight on bit (WOB) and rotary speed determines the characteristics of the cuttings. Moreover, fluid viscosity, annular velocity, flow regime, and fluid rheology can be evaluated under the drilling fluid characteristics. In addition, annular eccentricity, ROP, inclination angle, hydraulic diameter, and drill-pipe rotation are also significant operational factors that have substantial impacts on hole cleaning. Some of these variables regarding fluid properties and operational parameters can be controlled and

manipulated by engineers before, after and during a drilling operation. However, it is considerably very problematic to manage drilled cuttings properties due to the uncertainty and instability of variable cuttings parameters. When corrosion of drill bit, cuttings growth by coalescence and agglomeration are taken into consideration during drilling, it becomes difficult to predict or estimate the cuttings parameters such as particle shape, size, density, etc.

1.2 Basic Physics of Cuttings Transport Phenomena

Before describing the possible cuttings transport mechanisms in complex structural wells, macroscopic behavior of cuttings in a fluid domain must be fully understood. This behavior is affected by the interaction between individual cuttings, surrounding fluid and the wall (inner pipe and/or wellbore). Therefore, cuttings on a sedimentary bed are subjected to different types of forces such as, static forces, hydrodynamic forces and inter-particle forces [9]. Figure 1-2 illustrates these forces acting on a particle. Within this context, gravity and buoyancy are determined as static forces because of the properties with regard to the cuttings and its surrounding fluid, and shown as F_g and F_b, respectively. Drag and lift are the hydrodynamic forces resulting from the fluid characteristics.

In fluid dynamics, drag force, F_d, is described as fluid resistance or frictional force between a particle and its surrounding fluid. On the other hand, lift force, F_l, opposes the weight of the particle and holds the cuttings in the drilling fluid. It is also perpendicular to the flow direction as shown in Figure 1-2. Due to the non-Newtonian behavior of the drilling fluid, shear stress provides a lift force on the particles. The hydrodynamic forces depend on the local velocity of the drilling fluid around the particle. Therefore, cuttings are transported when the axial component of the terminal velocity is positive [10].

Inter-particle forces exist between the contacting particle and the non-contacting particle. Van der Waals forces, F_{val}, are inter-particle forces that significantly affect the particle accumulation and fluid flow behavior of particles [11]. The macroscopic behavior of particulate matter is described in detail in the following chapters.

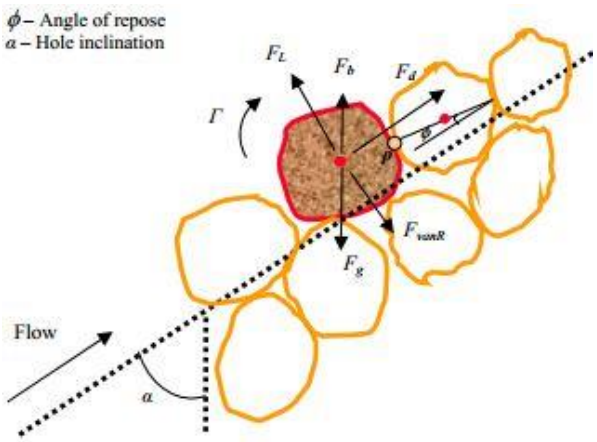

Figure 1-2: Forces applied on a particle in a deviated well [9]

Another analogy can be made here. Williams and Bruce conducted an experiment in order to show the behavior of flat particles in a vertical annulus [12]. Their aim was to investigate the reasons of particle motion in the drilling fluid by considering the inner pipe rotation and turbulence as shown in Figure 1-3. Due to the parabolic shape of the laminar flow velocity, velocity values near the wall are smaller; therefore, drag and lift forces on the flat cuttings are not distributed equally. This behavior causes a recycling motion as seen in the Figure 1-3 (a). However, inner pipe rotation plays a crucial role for hole cleaning performance. Transport efficiency increases because of the helical motion of the flat cuttings near the inner pipe as depicted in Figure 1-3 (b).

The centrifugal forces produced by the inner pipe rotation make the flat cuttings drag along the high velocity region. Hence, a proper hole cleaning can be achieved. Furthermore, turbulent flow also improves the transport ratio of the flat cuttings in a vertical section. The recycling of the flat cuttings near wall does not exist in the turbulent annular flow as illustrated in the Figure 1-3 (c). Also, velocity values near the wall are relatively higher in turbulent flows than they are in the laminar flow. Thereby, turbulent flows cannot be defined by a parabolic velocity profile. Consequently, particle motion in a carrier fluid is affected by the inner pipe rotation and flow regime as experimentally investigated by [12]. However, cuttings transport phenomena becomes more complex in inclined and horizontal wells. The transport mechanisms in such geometries will be explained in detail in the following section.

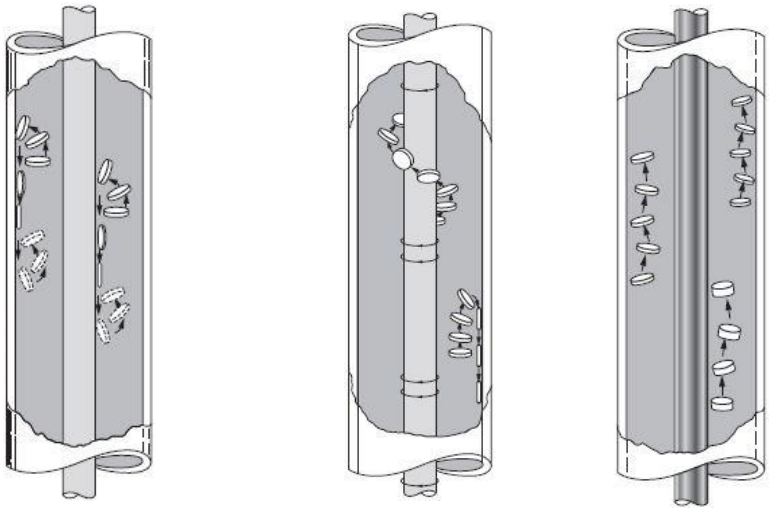

(a) (b) (c)

Figure 1-3: (a) Flat particles in the annular section without inner pipe rotation, (b) Helical motion of the flat particles with inner pipe rotation, and (c) Flat particles transported in turbulent flow without inner pipe rotation [12]

1.3 Cuttings Transport Mechanism in Inclined and Horizontal Wells

In the deviated wells, cuttings are affected not only by the axial, but also the radial component of the gravitational force. Cuttings deposition occurs at the bottom in the axial direction when the fluid velocity is not sufficient to overcome the axial component of the gravitational force. In addition, drilled cuttings are likely to accumulate on lower section of the annulus due to the radial component of the gravitational force in the same manner. However, if drilling fluid force acting on a cutting is bigger than the gravitational force; drilled cuttings would be in the suspension and carried effectively as shown in the Figure 1-4, provided by Zhang *et al.* [13].

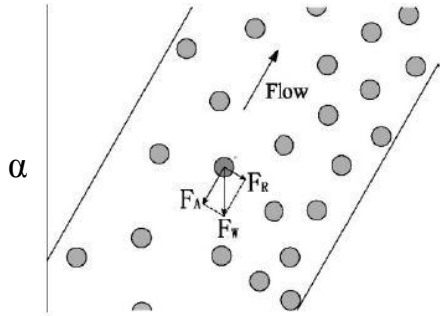

Figure 1-4: Suspension transport in inclined well
(α represents deviation from vertical) [13]

Drilled cuttings can accumulate at the lower side of the annulus if the radial component of the gravitational force becomes more dominant than the drilling fluid force acting on a particle; therefore, drag force on the particle decreases with diminishing flow rate due to increasing inclination angle. Thereby, stationary bed occurs at the lower section while rolling/sliding action arises at the top of the non-moving bed as seen in the Figure 1-5 [13].

Further, cuttings deposition continues with decreasing flow rate; therefore, cuttings bed height increases gradually. Accumulated cuttings start moving downward after the axial component of the gravitational force reaches a critical value. Hence, stationary bed avalanches downward while rolling/sliding action keeps taking place at the top of the sedimentary bed due to the moving particle-fluid interaction as shown in Figure 1-6 [13].

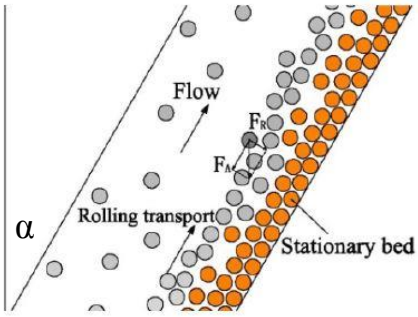

Figure 1-5: Rolling/sliding transport in inclined well [13]

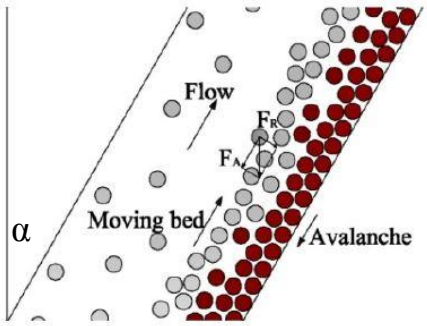

Figure 1-6: Moving bed transport and avalanche in inclined well [13]

In a horizontal well, when parabolic velocity profile is considered, maximum fluid velocity is reached at the center of the annulus while it is zero at the wall due to the shear forces. However, the gravity leads to an eccentric drill-pipe; therefore, fluid velocity profile is not distributed uniformly in the annulus. At lower side of the annulus, fluid velocity is less than the velocity in the larger section. Particles also tend to deposit on the narrow part of the annulus under the effect of gravitational force.

Flow rate plays an important role in order to achieve successful cuttings transport in horizontal wells. With increasing velocity, particles on the sedimentary bed surface begin moving through a rolling and jumping action. On the other hand, moving all particles along the cuttings bed height is challenging if adequate condition is not provided like larger flow rate, drill-pipe rotation, etc. because drag force of the drilling fluid does not reach a certain value in which particles are conduced to move. Therefore, particles below the sedimentary bed surface remain motionless as a result of compaction as illustrated in the Figure 1-7 [13]. However, particles below the sedimentary bed surface begin to move after the fluid velocity reaches a threshold value where a stationary state turns into a moving state.

Accelerating flow rate brings about an increase in the drag force of the drilling fluid, and momentum and mass exchange generated from particle-fluid and particle-particle interaction. Consequently, a moving bed occurs on the surviving stationary bed. This transport phenomenon is called moving bed transport in the horizontal well and demonstrated in Figure 1-8 [13].

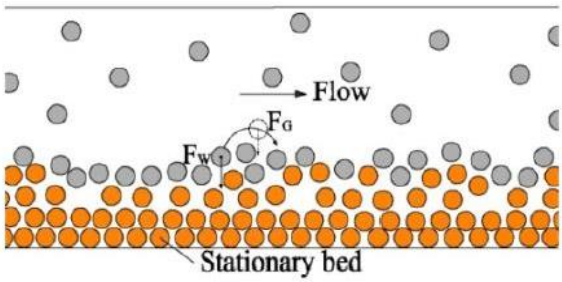

Figure 1-7: Rolling/Sliding transport in horizontal well [13]

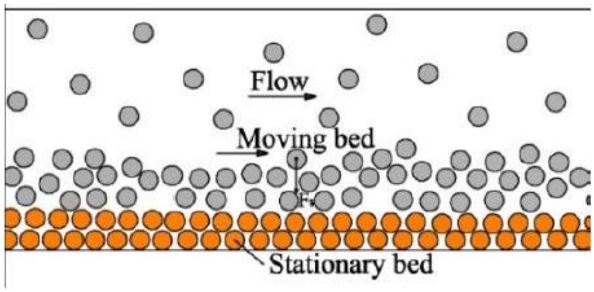

Figure 1-8: Moving bed transport in horizontal well [13]

In addition to moving bed transport state, if fluid velocity increases continuously, cuttings in the sedimentary bed tend to begin moving because of the lift force and fluctuation of the fluid due to the propagation of the turbulence. Thus, all particles are suspended in the drilling fluid and transported as shown in the Figure 1-9 [13].

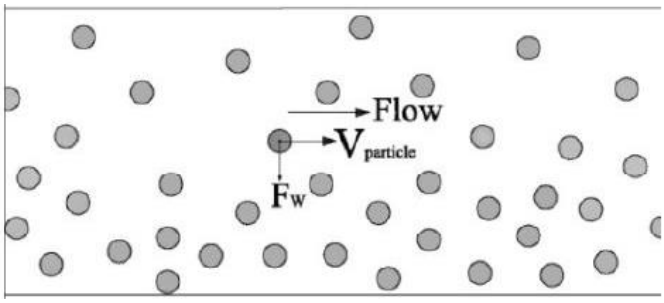

Figure 1-9: Suspension transport in a horizontal well [13]

Particle transport in deviated and horizontal wells is more complicated than it is in vertical wells due to the complexity of the problem as explained so far. An effective hole cleaning is needed for optimizing drilling and hydraulic parameters in such geometries for environmental aspects and economic reasons. After describing the physics of cuttings transport phenomena in complex wells, the objective of this study and proposed methodology are discussed in the following chapters.

1.4 Scope of the Study

The objective of this research was to develop a numerically robust model to investigate the effects of drill-pipe rotation on cuttings transport in eccentric horizontal wells. To reach this aim, a multi-step approach was required.

- The first goal was to implement unsteady turbulence modeling rather than using steady RANS (Reynolds-Averaged Navier-Stokes) calculations to accurately describe the flow and turbulence structures in the flow stream. Continuous phase is solved accurately because particle tracks are affected by turbulence modulation due to its interaction with the dispersed phase.

- The second goal was to consider particle-particle and particle-wall interactions to increase the accuracy of the numerical model for improved cuttings transport performance. Particle collisions cannot be neglected in such a system that drill-pipe rotates with a certain rpm and volume-fraction occupied by the particles is more than 10% of the annular volume (Severe numerical restriction as stated in the ANSYS FLUENT^{TM} documentation [14]). Therefore, Discrete Element Method (DEM) was applied for the collision model.
- The third and main goal was to successfully take account of the whirling motion of the drill-pipe arising from the vibrations created by the dynamic loads. The numerical setup was designed to predict the cuttings concentration and annular pressure losses including particle-fluid and particle-particle interactions, and whirling motion of the rotating drill-pipe in eccentric horizontal wells.

CHAPTER 2: LITERATURE REVIEW

2.1 Cuttings Transport in Complex Structural Wells

In this part of the study, most interesting experimental and numerical cuttings transport studies regarding with the drill-pipe rotation in complex structural wells are discussed. Some background on CFD based unsteady turbulent flows is also presented. Finally, recent works about coupled CFD-DEM simulations are argued with respect to cuttings transport studies.

2.1.1 Experimental Studies

Tomren *et al.* conducted an experiment to investigate the cuttings transport in deviated wells [3]. They aimed to use long enough test section, which was 40.0 ft (12.2 m), in order to obtain the steady state flow conditions to get more realistic results on cuttings transport for various drilling parameters such as drill-pipe rotation, pipe eccentricity, hole inclination from 0 to 90°, and drilling fluid and rheology. They highlighted that the higher annular velocities was required in deviated wells to clean the hole effectively and hole inclinations between 40 to 50° had a significant impact on cuttings transport as the generated cuttings bed began to slide downward against the flow. They also deduced that fluid rheology played an important role on effective hole cleaning; such as using a high-viscosity drilling fluid. Furthermore, the effect of inner pipe rotation was also investigated in inclined annulus. However, it was observed that pipe rotation slightly contributed the cuttings transport in deviated annulus.

Peden *et al.* investigated the influences of rotation and eccentricity of drill-pipe on cuttings transport in inclined wells by considering the minimum transport velocity (MTV) [15]. Transport capacity of a drilling fluid could be determined by estimating the MVT for various conditions in order to achieve an effective hole cleaning. Accordingly, an extensive parametric study was conducted for observing the effects of fluid rheology, cuttings diameter, hydraulic diameter and flow rate on hole cleaning performance. According to the results, fluid rheology and flow regime contributed the most to the cutting transport depending on the pipe eccentricity and hydraulic diameter. Additionally, it was observed that pipe rotation had a crucial impact on MVT when a high viscosity fluid was used, and a small annuli or gravity dependent eccentricity was present. In concentric annulus, drill-pipe rotation did not play a critical role on adequate hole cleaning.

They also induced that smaller cuttings seemed to be carried easier than the larger cuttings. On the contrary, at near vertical or vertical wells with a high viscosity fluid, an effective hole cleaning was provided with larger particles.

Sanchez *et al.* experimentally studied the impact of rotating drill-pipe on cuttings transport performance in deviated wells [16]. A wellbore simulator by 8 in. x 4.5 in. 100-ft long was used in this research. In addition to drill-pipe rotation, effects of hole inclination, fluid rheology, annular fluid velocity and cuttings diameter were also considered for providing an effective hole cleaning. Results indicated that drill-pipe rotation played a major role on cuttings removal. This study was differed from the previous works because dynamic behavior of the drill-pipe was also implemented in the experiments. Therefore, drill-pipe was not only rotated around its own axis, effect of whirling motion of drill-pipe on cuttings transport was also observed. It was noticed that whirling rotary significantly improved the hole cleaning efficiency. It was suggested that orbital motion of drill-pipe was required for the enhancement of the hole cleaning. On the other hand, smaller cuttings were observed to be removed harder. However, increase in pipe rotation speed with high viscosity drilling fluid enhanced cuttings transport performance for smaller cuttings.

Duan *et al.* conducted a field scale flow loop (8 in. x 4.5 in. 100-ft long) study to mainly investigate the effects of cuttings size ranging from 0.45 to 3.3 mm on hole cleaning efficiency in extended-reach wells [17]. They observed that higher cuttings concentration would be provided with smaller cuttings when the carrier fluid was water. However, lower cuttings concentration could be obtained with smaller cuttings if a Non-Newtonian fluid with 0.25-ppb polyanionic cellulose (PAC) was tested. They concluded that the efficiency of smaller cuttings transport significantly increased by applying PAC solutions as a carrier fluid. They also analyzed the effect of pipe rotation and fluid rheology on smaller cuttings transport in the flow loop. They finally developed a mathematical correlation by employing the experimental results into their model to measure the cuttings concentration and to predict the bed height in order to apply practically in the field applications.

Ozbayoglu *et al.* performed an experimental work to analyze the effects of drill-pipe rotation on cuttings transport performance in highly inclined and horizontal wells [18]. METU cuttings transport flow loop was used for the purpose of this research. They were motivated from the point of that increasing flow rates could not be a solution for the removal of cuttings due to the

hydraulic and physical limitations of the drilling operations. A proper hole cleaning could be provided with increasing drill-pipe rotation speeds. Therefore, a sensitivity analysis was implemented for different water-based drilling fluids to observe the impacts of drill-pipe rotation on cuttings transport performance for hole inclination angles in the range of 50° to 90°, rate of penetrations between 15 and 45 ft/hr, and fluid flow velocities changing from 2.1 ft/s to 7.2 ft/s. Drill-pipe rotation speed was also varied from 0 to 120 rpm. According to the results, an effective hole cleaning was ensured with the drill-pipe rotation as well as the orbital motion of it. Moreover, pipe rotation obviously contributes to removing of cuttings bed sustaining a lower fluid velocity than the minimum fluid velocity needed for non-rotating drill-pipe cases. On the other hand, an effective hole cleaning could be tolerated with mud viscosity if low rotation speeds were present.

Osgouei conducted an experimental study on cuttings transport in gasified drilling fluids [19]. He aimed at analyzing the hole cleaning performance and cuttings behavior in horizontal, deviated and vertical wells when drilling fluid was gasified. He also conducted some experiments on cuttings transport as the carrier fluid was water before he went through the cuttings transport properties with gasified fluids. He applied digital image processing for observing the cuttings behavior and defining the flow pattern type. Experimental set up consisted of a 21 ft long, 2.91 in. x 1.85 in. eccentric annulus. Drilling parameters such as ROP, pipe rotation and hole inclination on cuttings transport performance were investigated in this study. Osgouei deduced that total cuttings concentration was increased with increasing ROP. This also caused higher annular pressure losses. Furthermore, it was observed that increasing fluid velocity provided a better cuttings transport performance. However, drill-pipe rotation did not significantly change the total cuttings concentration in horizontal annulus when the cuttings injection rate, liquid and gas velocities remained constant. On the other hand, he developed a mechanistic model using the experimental results to determine the volumetric distribution of each phase during cuttings transport process using gasified fluid in order to predict the annular pressure losses in horizontal annuli by taking account of the influence of pipe rotation and eccentricity.

Duan *et al.* conducted an experiment to investigate the hole cleaning performance using foam with rotation of drill-pipe [20]. Their purpose was to indicate the impact of drill-pipe rotation on cuttings concentration and annular pressure losses along with a horizontal well. They used a 73 ft

long, 7.76 in. x 3.5 in. eccentric annular section to analyze the pipe rotation, fluid rheology and fluid velocity on an essential hole cleaning. Experimental results showed that pipe rotation played a critical role on cuttings transportation as results of decreasing particle concentration and reducing annular frictional pressure losses. Their suggestion was to rotate drill-pipe between 80 to 160 RPM during drilling with foam in the deviated well. Furthermore, they focused on the pressure and temperature effect on the cuttings concentration by using a constant foam quality. In particular, pressure had a positive influence on annular pressure drop while temperature had a negative impact. However, cuttings concentration was not significantly affected with pressure and temperature.

Han *et al.* studied on cuttings transport problem in inclined wells including drill-pipe rotation [21]. In their experimental set-up, annular fluid velocities changed between 0.4 m/s and 1.2 m/s. Both laminar and turbulent flow regimes were implemented in the laboratory experiments. They aimed at observing the effects of drill-pipe rotation varying from 0 rpm to 400 rpm, and inclination from 0° to 60° on the hydraulic transport of the particles in a slim hole drilling annulus. A non-Newtonian drilling fluid was selected for the carrier fluid. It was stated that drill-pipe rotation generally enhanced the cuttings transport ratio, in particular, at the low flow rates. On the other hand, annular frictional pressure losses increased with increasing fluid velocity, inclination and drill-pipe rotation. It was also observed that the impact of rotating drill-pipe on cuttings transport in water was higher than it was in the non-Newtonian fluid solutions due to the shear-thinning behavior of the drilling fluid. They also developed a numerical model using commercial CFD software, Fluent. They compared the experimental results with the numerical solutions, and both results agreed satisfactorily.

Ytrehus *et al.* conducted another experimental study to investigate the cuttings transport efficiency of water based drilling fluids [22]. A 12 m-long flow loop with 2 in. x 4 in. eccentric horizontal annulus was used for the tests. They observed that hole cleaning performance showed discrepancy when different drilling fluids were used even though they had same rheological properties according to the API standards as well as same density (1370 kg/m^3). In particular, bentonite and KCL were mainly used as drilling fluid. In addition, they also studied the effects of the drill-pipe rotation with free whirling movement on annular pressure losses and hole cleaning performance. Based on the results, pressure drop with particle injection did not change remarkably with a low rotation speed (6 rpm) for bentonite and KCL fluids. On the other hand, at

high rotation speed (150 rpm), pressure losses along the annulus decreased. Critical fluid velocity was determined as 0.3 m/s in order to avoid from plugging the flow loop at 6 rpm; therefore, the lowest flow was selected as 0.54 m/s. However, there was no deposition at even the fluid velocity of 0.54 m/s at 150 rpm. Otherwise, cuttings transport ratio was not significantly affected with the low rotation speed for either fluid. Furthermore, it was observed that bentonite fluid had a better transport efficiency than KCL fluid at 150 rpm, while hole cleaning performance using KCL fluid was provided better at 6 rpm.

2.1.2 Theoretical and Numerical Models

Gavignet and Sobey developed a two-layer model for solid particle transport in an eccentric annulus for a Non-Newtonian drilling fluid [23]. This model was one of the first cuttings transport models and was originated from the previous slurry transportation models. In the study, they concluded that cuttings deposition began to occur if the flow rate was under the critical value when Reynolds number was high enough to create turbulence flow. The study revealed that this criterion was strongly dependent on pipe eccentricity, particle size, pipe and hole diameter. Otherwise, fluid rheology, pipe rotation and hole inclination greater than 60° did not affect much that criterion. Another important result from the mechanistic model was that friction coefficient of drilled cuttings against the wall had a significant impact upon the bed accumulation at high hole inclinations. They also compared their model with experimental results conducted by Tomren *et al* [3], and it was seen that there was a fair agreement between the predictions of the mechanistic model and experimental observations. Drill-pipe rotation was not included in their study.

Hyun *et al.* presented a three-segment hydraulic model to understand the cuttings transport phenomena in inclined wells [24]. In the model, it was assumed that stationary bed was layered at the bottom of the annulus. Above the stationary bed, there was a moving bed in which the cuttings were transported. Third layer was the heterogeneous suspension layer where cuttings were suspended. They aimed at determining a reasonable pumping rate and optimizing fluid rheology for a better hole cleaning. In the model, they divided the annulus into three segments such as deviation of 60-90°, 30-60° and 0-30°. They particularly applied mass balance and transport equations for each segments. The effects of annular flow rate, fluid type, and hole

inclination on wellbore cleaning were found to be important with respect to economical and operational aspects. Moreover, a better cutting transport was provided with a high viscous fluid when the flow regime was turbulence. Pipe rotation was neglected in this model.

Ramadan *et al.* developed a mechanistic model to estimate the critical flow rate in order to move the spherical cuttings bed in deviated wells [25]. They aimed at predicting the critical velocities in different sand beds with various particle sizes. They also carried out some experiment using an 80 mm flow loop to measure the critical velocities in order to initiate the movement of the sedimentary bed. They compared their model predictions with experimental results. They provided a good agreement in critical velocities. Consequently, results indicated that fluid properties, flow parameters, and particle size significantly affected the critical velocity. Furthermore, Ramadan *et al.* also developed a three-layer model for transportation of solid particles in highly deviated wellbores to estimate the annular friction pressure losses and cuttings transport capacity in Newtonian and Non-Newtonian power law fluid [26]. They modified their previous study in order to predict a better hole cleaning performance in deviated wells. Though, similar procedure was employed. They measured average transport ratios and critical flow rates by implementing the three-layer model and conducting experiment. Even though the model had a good agreement with the experiment, it was demonstrated that the model had some limitations. This model could be applied for both Newtonian and Non-Newtonian power law fluids to estimate the transport rate when the particle Reynolds number was no less than 15 and no more than 400. Effect of drill-pipe rotation for determining the critical flow rates on cuttings transport was not considered in this study.

Malekzadeh and Mohammadsalehi developed a new method to optimize hole cleaning performance, and obtain critical flow rate in extended-reach wells by compensating the negative hole inclination effects [27]. This model combined two previous studies: Moore's correlation to estimate the slip velocity of the cuttings, and Larsen's model to predict the minimum flow rate in order to provide the cuttings removal [27]. According to the study, one of the purposes of this model was also to minimize the negative effects of extreme flow rates resulting from drilling fluid loss in the formation to obtain an effective hole cleaning. The procedure of the model was to make comparison the outcome flow rate with the one was needed to move cuttings settling by obtaining a maximum bit hydraulic horsepower. When the resultant flow rate became higher than

the one for cuttings removal, the procedure was completed and final results gave the optimum flow rate for efficient cuttings removal.

Wang *et al.* developed a dynamic three-layer (stationary, moving, suspension) mechanistic model for cuttings transport including momentum and mass exchange between layers, and the effect of pipe rotation speed from 0 rpm to 150 rpm [28]. The purpose of this study was to determine the thickness of sedimentary bed in an extended reach well, and also analyze the most effective parameter to avoid an annulus blockage. Accordingly, ECD was determined to be used as a key element to estimate the dynamic thickness. Based on the results, increasing flow rate and drill-pipe rotation played a significant role to decrease cuttings bed height. On the other hand, ROP had a relatively low impact on cuttings bed height. Increasing ROP lead to produce more cuttings and resulted in a dense cuttings deposition. In consequence, higher drill-pipe rotation speed with low ROP would provide a better hole cleaning based on the observations and analysis for this study.

Haolin *et al.* developed a mechanistic model based on momentum and force balance equations for estimating the critical incipient velocity for particle movement in deviated pipes [29]. For enhancement of the model, various drag coefficients predicted from different equations were applied in the mechanistic cuttings transport model. Model predictions were compared with the experimental data for the best estimation of the critical incipient velocity of cuttings. It was deduced that critical incipient velocity is a function of particle size, inclination angle and fluid properties. Based on the analysis, suspension transport was observed at near vertical pipes. However, when the inclination angle increased from vertical to horizontal, rolling/sliding action was present unless sufficient fluid velocity was provided to carry the cuttings. Maximum incipient velocity of cuttings was reached when the inclination angle was 60°. Otherwise, the minimum incipient velocity of cuttings was obtained at lower inclination angle.

2.1.3 Computational Fluid Dynamics (CFD) Approach

One of the first studies for investigating the characteristics of cuttings transport by applying CFD was conducted by Bilgesu *et al.* [30]. They studied the impacts of particle size, fluid rheology and flow rate on hole cleaning efficiency. They applied a solid-liquid multiphase model with a Non-Newtonian power law fluid and Newtonian fluid (water). According to their

results, annular velocity was a critical parameter for removing cuttings from the annulus. They also compared their results with the laboratory data, and obtained a satisfactory agreement. Bilgesu *et al.* also analyzed cuttings transport phenomena in an annular section by implementing 3D CFD simulations in order to analyze the importance of various parameters on hole cleaning performance [31]. In this model, they used an Eulerian-mixture multiphase model to simulate the behavior of cuttings transport. They embedded effects of drill-pipe rotation and hole inclination into their model to observe the impacts of these parameters on the cuttings transport performance. Results indicated that a better cuttings transport could be provided with the pipe rotation if smaller particles were present. In addition, cuttings transport in enhanced hole inclination angles was observed to be more difficult because of the accumulation and rolling/sliding action of particles.

Mishra mostly concentrated on investigating the effects of different fluid properties, various cuttings diameters and variable operational conditions such as pipe rotation and eccentricity on cuttings transport efficiency by using a steady-state Eularian-mixture model [32]. Results demonstrated that decreasing hole inclination from horizontal to medium angle (90° ➔ 60°) created difficulty for adequate hole cleaning. They also showed that increasing flow rate, particularly for larger cuttings, contributed to a reduction in the cuttings concentration. According to this study, smaller particles were harder to remove from the annuli by using water as a carrier fluid. Furthermore, impact of drill-pipe rotation played a critical role on hole cleaning performance, however transportation of smaller cuttings was more effective when pipe was rotating than the one for larger particles. This model was limited to 20% of cuttings concentration in the annulus.

Wang *et al.* focused on the impact of drill-pipe rotation on hole cleaning in extended reach wells [33]. Eulerian multiphase flow model was implemented in their CFD set-up. Cuttings bed height for different rotation speed was investigated. Based on the results, solid phase was observed to be asymmetrically deposited in the annulus due to the rotation effect. Furthermore, drill-pipe rotation contributed to cuttings transport by reducing the solid phase concentration. On the other hand, a parametric study was conducted to derive an empirical correlation in order to estimate the cuttings bed height in horizontal wells. Thereby, parameters such as eccentricity, fluid viscosity, fluid density, volume fraction occupied by solid phase, and particle diameter were used to obtain an empirical formulation for predicting the cuttings bed height. This formula

was compared with an experimental study conducted by Wang *et al.* [34] with a maximum error of 12% and minimum error of 1.2%.

Sorgun studied drilling fluid hydraulics and characteristics to analyze cuttings transport behavior in highly deviated and horizontal wells [35]. First, an extensive experimental study was performed using METU flow loop to address the effects of various parameters on cuttings behavior in water and several drilling muds: hole inclination, flow rate, ROP and drill-pipe rotation. Second, a CFD model was developed and numerical results were compared with the experimental data. A satisfactory agreement was achieved. Based on the results, fluid velocity was found to be the most effective parameter which influence the cuttings transport performance in deviated and horizontal wells. He also pointed out that drill-pipe rotation improved cuttings removal; in particular, if the orbital motion of drill pipe was present. Additionally, increasing rotation speed prevented cuttings bed accumulation and decreased the critical fluid velocity which was needed to suspend particles in the flow stream. However, increasing pipe rotation did not contribute cuttings transport performance after a critical rotation speed.

Yilmaz developed a CFD model to investigate the cuttings bed height and moving bed velocities in highly deviated and horizontal wellbores [36]. He employed DPM simulations to track particles in the flow domain. He neglected particle collisions due to low cuttings concentration. He also implemented his studies using two-equation SST k-ω turbulence model. Yilmaz validated the CFD simulations with previous experimental data for estimating velocity profiles of Herschel-Bulkley fluid flow, predicting cuttings height in stationary layer, and calculating moving bed velocities [36, 37]. He projected the thickness of a stationary bed by analyzing the change in particle characterization between annular flows and various bed heights. He also estimated the moving bed velocities using unsteady particle tracking approach with DRW model because particle injections were released randomly into the fluid domain. His results for estimating the cuttings bed height and moving bed velocities had a satisfactory agreement with the experiment conducted by [38]. After the validation, he performed a parametric study to investigate the effects of different parameters on cuttings transport. He analyzed the effect of inclination angle, drill-pipe rotation, and fluid rheology on hole cleaning performance. He also took consideration of different particle sizes with variable sphericity and implemented one-way coupling where the particle motion (discrete phase) is affected by the fluid flow (continuous phase), however the continuous phase is not affected by the discrete phase.

Increased cuttings concentration would require using a two-way coupling scheme with/without particle collisions.

Ofei *et al.* developed an Eulerian-Eulerian multiphase flow model to predict annular pressure losses and cuttings concentration in eccentric horizontal annuli taking into account various drilling parameters such as flow rate, fluid rheology, hydraulic diameter, and drill-pipe rotation [39]. CFD results were successfully compared with experimental data [21]. According to the results, increasing flow rate lead to an increase in annular pressure losses and a reduction in cuttings concentration in eccentric horizontal annuli. When the ratio of inner pipe diameter to outer pipe diameter was 0.9, increasing flow rate provided the most effective hole cleaning performance for both drilling mud and water as carrier fluids. Furthermore, impact of drill-pipe rotation on pressure losses and cuttings concentration was also analyzed. Results indicated that increasing pipe rotation speed from 80 rpm to 120 rpm did show insignificant increment in pressure losses for either carrier fluids. In addition, increasing inner-pipe rotary speed had an insignificant effect on hole cleaning because of the slight reduction in the cuttings concentration. The most effective scenario was observed when the ratio of inner pipe diameter to outer pipe diameter was 0.7 and also at low flow rates.

Sun *et al.* performed CFD simulations to investigate the impacts of drill-pipe rotation on hole cleaning performance in complex structural wells applying an Euler multiphase model [40]. They studied critical parameters that affect cuttings transport behavior: inclination from 45° to 90°, rotation speed changing from 80 rpm to 240 rpm, and flow rate in the range between 30 L/s and 50 L/s. Results demonstrated that pipe rotation circumferentially played a significant role on resulting in asymmetrical distribution of the solid particles. Accordingly, increasing drill-pipe rotation speed caused producing more drag force in the tangential direction. This brought about an important decrease in cuttings bed deposition, and an improvement on cuttings transport ratio which is the ratio of the net upward cutting velocity and average annular velocity. They observed that the effect of drill-pipe rotation on cuttings concentration and annular pressure losses did not show an alteration at high flow rates after a critical rotation speed of 180 rpm.

2.2 Modeling of Unsteady Turbulent Flows

Magagnato studied unsteady turbulent flows in turbo-machines [41]. He emphasized that non-linear turbulence models and unsteady calculations were needed to increase the accuracy of CFD methods when complex flow fields were analyzed. CFD calculations were compared with the experimental data for two cases: flow past a cylinder and VKI (von Karman Institute) turbine blade. According to the results, turbulence models coupled with unsteadiness were capable of capturing the turbulence characteristics better than steady state turbulence calculations for turbo-machines.

Chung *et al.* performed direct numerical simulations (DNS) for a turbulent flow in concentric annuli in order to obtain the statistics of turbulent quantities [42]. They mainly focused on the transverse curvature effects of turbulence characteristics on near wall. Average velocity profile normalized by the bulk velocity was compared with experimental data in a good agreement even though there was a slight discrepancy in center region. An excellent agreement was satisfied when rescaling the data with respect to normalization process. On the other hand, it was deduced from their study that turbulent intensities and Reynolds shear stresses of the outer wall were bigger than those of the inner pipe. It was also stated that because surface area of the outer wall was bigger than the one of the inner pipe, the outer pipe supplied more turbulent kinetic energy; therefore, energy transfer was observed to be bigger in the outer wall.

Feiz *et al.* studied larde eddy simulations (LES) in swirling channel flows [43]. Smagorinsky subgrid model and dynamic model were performed to investigate the effect of rotation speed in fully developed turbulent flows. LES results were compared with DNS data in the literature. Although there were some discrepancies with DNS results, a satisfactory agreement was mainly achieved. They deduced that an increase in pipe rotation caused a gradual reduction in intensity of turbulence in rotating pipe flows because of the stabilizing impact of centrifugal forces. Furthermore, it was also remarked that LES with dynamic model provided more accurate results than LES with Smagorinsky model to simulate the turbulent pipe flow with or without pipe rotation. It is because an external constant with respect to the rotation speed was not required in the Smagorinsky model.

Liu and Lu simulated turbulent flows in a rotating annular channel by using LES coupled with a dynamic sub-grid scale model (SGS) [44]. Their purpose was to determine the turbulent

flow characteristics near walls of swirling concentric annular flow. They also aimed at observing the impressiveness of LES method to accurately estimate the flow behavior exposed to the rotation. They examined velocity profiles, intensity of the turbulent, Reynolds stresses, and flow structures near inner and outer walls. LES results were confirmed successfully with the previous experimental and DNS studies. Results showed that radial and azimuthal turbulence intensities changed remarkably with the rotation while turbulence intensities in the axial direction were not affected much by the rotation. As a result of an increase in rotation speed, intensities of turbulence in the radial and azimuthal direction developed in center of the fluid domain, and maximum values of the turbulence intensities increased near pipe walls.

Chung and Sung modeled turbulent flow in a concentric annulus including the pipe rotation by using LES [45]. Their purpose was to investigate the turbulent structures near inner and outer walls due to the swirling effect. Three different rotation rates (N =0.2145, 0.429, 0.858) were applied with a constant Reynolds number (Re = 8900). The rotation ratio was defined as the ratio of the mean velocity component in the θ direction and bulk mean velocity. They validated their results with previous experimental and numerical studies. LES results demonstrated that pipe rotation had a significant effect on the overall turbulent statistics and velocity profiles. It was also observed that higher rotation rates leaded to increments in efficiency of producing eddies.

Ninokata *et al.* studied on analysis of turbulent flows in an eccentric annulus by applying DNS to investigate the turbulence particularities [46]. First, they solved a fluid flow simulation in concentric annuli and compared the DNS results with the previous numerical studies implemented by spectral method in order to show the accuracy of the DNS. After satisfactory agreement was achieved, they applied DNS method for solving the turbulent flow in an eccentric annulus. Axial velocity profiles along the widest and narrowest gap were calculated. It was stated that DNS and experimental data did not match directly because Reynolds number on experiment was twice of that of DNS calculations.

Zhao *et al.* studied various turbulence models to accurately simulate airflow and turbulence in enclosed environments applying CFD [47]. They performed eight different turbulence models, and performance of all models was compared with experimental data from the literature. They included unsteady RANS modeling, DES, and LES simulations in their study. Zero-equation model, two-equation models such as RNG k-ε, low Reynolds Number k-ε, and SST k-ω, $\overline{v^2} - f$

three-equation model, and RSM were implemented in URANS simulations. They aimed at comparing their simulations with the experiment in predicting the air velocity and temperature profiles, Reynolds Stresses, and turbulent heat fluxes. This study demonstrated the importance of turbulence modeling in complex physics and geometries. According to the results, the most detailed flow behavior was provided by using LES simulations. They also concluded that LES simulations required more computing time than URANS simulations. Furthermore, it was observed that LES simulations could not always give the best accurate results depending on the wall effect performance.

2.3 Particulate Flow Modeling using CFD-DEM Coupling

Cleary and Sawley presented a numerical study in order to analyze the effect of particle shape on hopper discharge [48]. They included DEM method into their simulations to increase the accuracy of particulate flow. They deduced that particle shape had a significant impact on flow rate and flow patterns. The importance of particle shape on the flow of hopper discharge systems had been studied greatly in this study. Based on the results, the flow rates for elongated particles could be reproduced up to 30% lower than for circular particles; therefore, circular shapes did not really represent the granular materials. Hence particles with circular shape showed lower resistance to the frictional forces [48]. They also concluded that DEM modeling could be accurately used for the process optimization and equipment design due to its capability of modeling the inter-particle collisions.

Bertrand *et al.* performed various numerical simulations in order to demonstrate the applicability of DEM in mixing of granular materials [49]. Their purpose was to emphasize DEM model by not only considering the suitability but also revealing the limitations in modeling of particulate flows in mixing processes. They showed many studies in the literature by including current state of the art with respect to granular flows. They pointed out that CPU time (or process time) and number of particles could be a challenging problem for modeling even though DEM had capability of capturing the real physics in mixing of granular materials, Therefore, modeling of particulate flows regarding DEM collisions could be time consuming and required parallel programming in high performance computers.

Tsuji *et al.* studied flow characteristics of gas-fluidized bed by implementing CFD-DEM coupling [50]. In the study, spontaneous flow pattern in 3D bubbling gas-fluidized bed was analyzed by applying the parallel programming with 16 processing pores in order to model 4.5 million aluminum particles. Characteristics of bubble shapes were also visually investigated. They presented one of the largest particulate systems in gas-fluidized bed simulations.

Martins *et al.* investigated gravel packing process during horizontal well completions by CFD-DEM coupling [51]. CFD was used for the fluid flow calculations while DEM was applied for prediction of particle trajectory. They aimed at estimating the alpha wave height during the gravel displacement process by taking into account the particle-particle interaction. Due to large number of particles, they implemented 2D simulations to observe the propagation of gravels and predict the bed height in horizontal wells. They compared their numerical results with the experimental data provided by Petrobras [51]. Coupled CFD-DEM simulation results had a satisfactory agreement with the experiment in terms of bed height prediction, velocity profile in the annulus of gravel packing operation, and determined the flow regimes during the displacement process.

Mezhericher studied of modeling of horizontal pneumatic conveying of polyethylene pellets by implementing two different granular flow methods: DPM and DEM [52] to predict the particle trajectories. In DEM method, inter-particle and particle-wall collisions were considered by using a soft-spheres approach. In DPM model, a hard-spheres approach for particle-wall collision was used. In addition, particle-particle collisions were ignored in DPM method. They concluded that larger solid fractions could be achieved by using DEM method while DPM would be applied for the modeling of particulate flow in which solid concentration was less than 10% of the numerical domain.

Chu *et al.* conducted a numerical study of multiphase flows in a dense medium cyclone (DMC) combining DEM and CFD [53]. Their primary objective was to analyze particle density impact on the flow in a DMC in the coal industry by taking into account the particle-particle, particle-wall, and particle-fluid interaction forces. They observed that the flow pattern in a DMC significantly changed with altering particle density and concluded that the density effect influenced particle trajectories and interaction forces between the particle and fluid domain.

CHAPTER 3: STATEMENT OF PROBLEM AND NUMERICAL APPROACH

Flow behavior of particulate materials in the carrier fluid plays an important role in petroleum engineering applications. Cuttings can accumulate in the lower part of a horizontal annulus and block the well caused by insufficiently controlled drilling parameters. Inadequate hole cleaning results in crucial drilling problems such as formation fracturing, drilling fluid losses into the formation, and erosion of drilling materials; therefore, an effective removal of drilled cuttings is extremely essential especially for deviated and horizontal wells [5-7].

Technological development and growing energy demand has led to an increase in associated drilling operations. This situation has also provided oil companies an opportunity to invest heavily in deeper drilling operations to meet the demand; therefore, unconventional and offshore drilling operations have become important state of the art technologies. As it is well known, unconventional reservoirs are produced by the way of directional and horizontal drilling. During drilling in complex structural wells, an effective cuttings transport is more difficult than it is in the vertical well [13]. Hence, due to the complexity of well structure in such geometries, essential hydraulic requirement and proper hole cleaning performance are essential for well design optimization and cost minimization.

In order to predict cuttings behavior and estimate critical properties, several experiments have been conducted. Furthermore, numbers of mechanistic and numerical studies have been performed by researches as reported earlier in the background and literature review. However, it can be noted that there are still practical limitations in experiments due to its difficulty over whole trajectory of cuttings in extended-reach wells. Furthermore, as the purpose of this study, inner pipe is believed to be rotated freely in order to make some orbital motion rather turning on its own axis. In the real drilling operations, drill-pipe not only rotates around its own axis, but also does a whirling or a snake motion particularly in eccentric horizontal wells. Furthermore, energy is transferred to drilling flow due to the dynamic motion of drill-pipe arising from the mechanical vibrations which occurs during drilling. This behavior is called whirling motion of the drill-pipe and causes more turbulence; therefore, orbital motion due to the eccentricity of the inner pipe would contribute to improved cuttings transport. Many experiments about cuttings transport with inner pipe rotation do not include this type of rotation as mentioned earlier. On the other hand, there is still a lack of fundamental understanding of numerical modeling of drilled

cuttings transport phenomenon to produce a reliable method. Although some assumptions that have been made in the mechanistic and numerical models provide convenience to solve cuttings transport problem, realistic approaches cannot be provided by taking into account the steady state considerations in these methods; therefore, the best strategy for hole cleaning efficiency could not be decided yet. To overcome these deficiencies, more physics based computational models are necessary. For this purpose, impacts on major parameters such as turbulence regime, cuttings interaction and collision, and orbital motion of the drill pipe on cuttings transport performance in eccentric horizontal wells is discussed in the following chapters.

In general, cuttings transport simulations in horizontal wellbores were conducted by coupling CFD and DEM. Included in the methodology, the Eulerian-Lagrangian multiphase flow method was used for coupled CFD-DEM simulations as already reported. An upwind discretization method was implemented for solving the unsteady RANS equations in the continuous phase. Computational domain was divided into the quadrilateral, finite volumes where the conservative laws were applied for each finite volume cell. SST k-ω turbulence model was determined to be used for solving the continuous phase after an optimization study was completed in the following chapter. For axial swinging of eccentric drill-pipe, a user defined function (UDF) written in C programming language was implemented in FLUENT. Particles were also injected randomly from the inlet boundary. Non-uniform distribution of particles was believed to be more accurate particularly when the whirling motion was present. Particle path in the carrier fluid was tracked by DPM with DEM collision method. Further details could be found in ANSYS documentations [14, 54]. Simulation procedure is organized as shown in Figure 3-1.

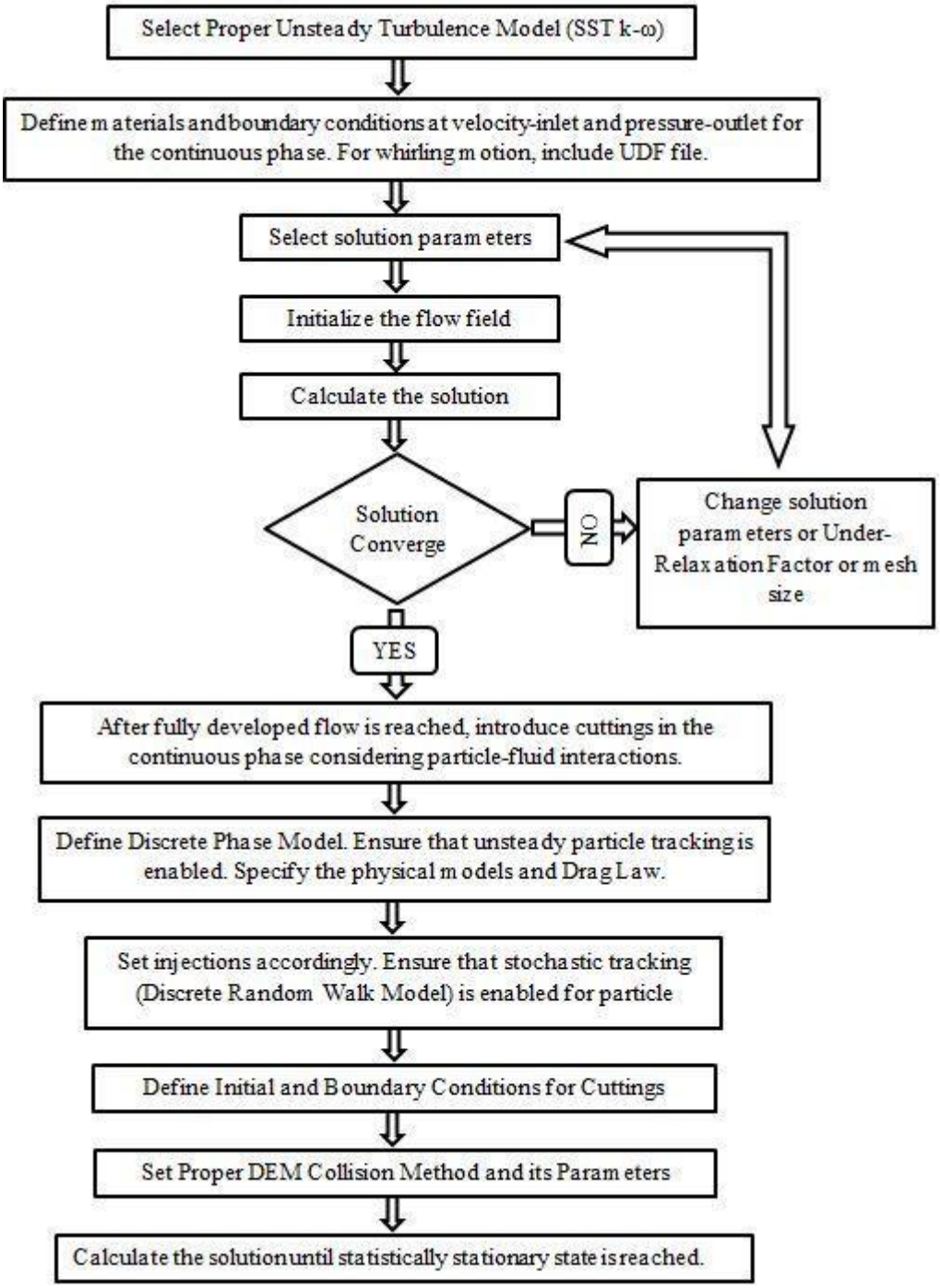

Figure 3-1: Simulation procedure for CFD-DEM coupling simulations

CHAPTER 4: TURBULENT FLOW EFFECT ON CUTTINGS TRANSPORT PERFORMANCE

In fluid dynamics, turbulence modeling is one of the most difficult issues and the most critical factor to obtain a robust and accurate computer simulation of engineering flows. Turbulence has a big impact on the fluid flow characteristics such as drag and lift forces [55]. In simple CFD applications, applying various turbulence models to a problem may not significantly affect the simulation results. A good approach to these problems is usually to select any turbulent models which need less computing time and effort. However, when more complex simulation domains are solved, advanced turbulence models are required to get accuracy and optimize computational resources. In this study, drilled cuttings transport was modeled in an eccentric horizontal annulus. Complexity of geometry makes the problem very difficult because transport mechanism changes continuously through the well depending on hole angle due to the particle-fluid interaction. Settling and dispersion of particles in the annulus play a critical role in drilling engineering applications. Numerical simulation of cuttings transport requires modeling of the continuous phase, discrete phase, and interaction between them for coupling [11]. Continuous phase significantly impacts the discrete phase since particles are dispersed by random motion of the turbulence. Thus, continuous phase must be solved properly so that particle trajectories and particle deposition are represented accurately.

One of the main factors in particle lifting in complex geometries is irregular and aperiodic motion in the fluid flow. In drilling operations, velocity profiles do not distribute uniformly in the annulus due to the eccentricity of drill-pipe. In the lower part of an annulus, velocity may not be sufficient to carry the particles. However, in the larger area, velocity may be high enough to suspend or transport cuttings. As a result, flow rate determines the turbulence of fluid domain, and cuttings in the lower section of the annulus may be transported due to the turbulent flow [56]. An accurate turbulent flow is essential to provide the best physics based model for complex systems. Fluid velocity is determined by a proper turbulent method, and plays a critical role on particle motion; therefore, particle-fluid interaction forces are needed to be considered properly [11].

In consequence, any models particularly those in sophisticated geometries should perform the continuous phase behavior as accurately and properly as possible. In most CFD applications,

there are generally two types of turbulent flows: steady-state turbulence modeling, and unsteady turbulence modeling with scale-resolving simulations [14].

4.1 Turbulence Modeling in CFD Applications

Turbulent flows are defined by fluctuating velocity fields in the fluid domain. The velocity term in Navier-Stokes Equations is solved by a turbulence model which is the major aspect for such a strongly three-dimensional and unsteady flow [57]. This particular flow is characterized by a wide range of length and time scales for the Reynolds Number (the ratio of the inertial forces to the viscous forces) of practical, industrial applications. In other words, turbulent flows include a wide range of eddy sizes. Large eddies carry small eddies in energy cascade as shown in Figure 4-1 [58]. Here, l and η respectively represent the large eddy size and dissipative eddy size.

Energy injected by the mean flow is transported to smaller structures. Deformation of the eddy structure is caused by the fluid dynamics. Energy is dissipated by fluid viscosity when the Reynolds Number is extremely high. This process is called energy cascade in which the kinetic energy is transported from the large scale eddies to small dissipating eddies as presented in Figure 4-1. Although large eddies have various behavior in each flow, small eddies conversely have more universal behavior in nature. In many engineering applications of turbulence modeling, small eddies either can be ignored or modeled [57]. In Direct Numerical Simulations, both large and small eddy scales are resolved instead of modeling as also demonstrated in Figure 4-1. Resolving these large and small sizes by a time accurate and three-dimensional computations with very high temporal and spatial resolution seems to require more computational time and effort, because grid size should be scaled according to the smallest scale of turbulence. It is impractical in the most of engineering models, and computationally expensive for the complex structural geometries.

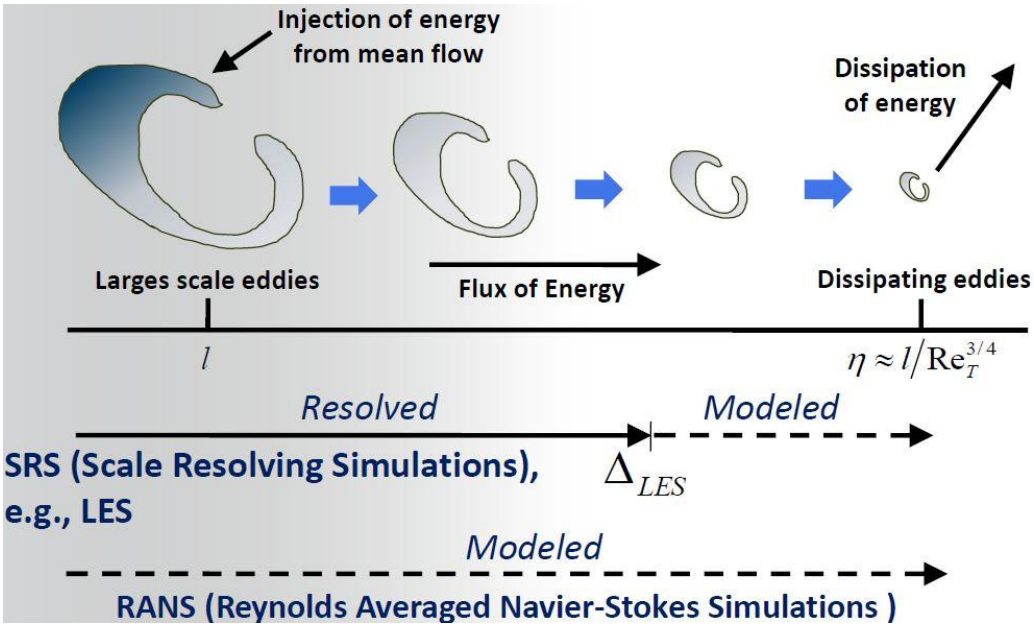

Figure 4-1: Dissipation of eddies in Energy Cascade [58]

4.1.1 Reynolds-Averaged Navier Stokes Turbulence Modeling

It is considered in this study that a viscous and incompressible flow with constant parameters for turbulent flow is applied. In this model, a statistical approach is considered for the instantaneous Navier-Stokes equations by inserting the mean values in terms of time-averaged, space-averaged, and ensemble-averaged. Navier-Stokes equations are decomposed into mean and fluctuating parts which results in Reynolds (Ensemble)-averaged Navier-Stokes (RANS) equations. Fluctuating quantities are also considered by averaging unsteadiness of the turbulence. In addition to the averaged terms, RANS also includes Reynolds Stresses resulting from using the sum of average velocity and fluctuation on the average velocity. Reynolds Stresses are impossible to be represented uniquely with regards to mean quantities. This means the system is no longer closed; as a result, closure of RANS equations is required only through consideration of approximations that provide the Reynolds Stresses in averaged values.

Navier-Stokes and continuity equations are respectively given by Equation 4.1 and 4.2:

$$\frac{\partial u_i}{\partial t} + u_j \frac{\partial u_i}{\partial x_j} = -\frac{\partial p}{\partial x_i} + \nu \nabla^2 u_i \tag{4.1}$$

$$\frac{\partial u_i}{\partial x_i} = 0 \tag{4.2}$$

where u_i is the velocity vector, p is the pressure, and ν is the kinematic viscosity of the fluid [14, 59]. The average bulk velocity is not changing in the axial direction; therefore, $\frac{\partial u_i}{\partial x_i}$ is equal to zero. The velocity and other scalar quantities such as pressure, energy, or species concentration are decomposed into mean and fluctuating components. For velocity components, instantaneous velocity is described by Equation 4.3:

$$u_i = \bar{u}_i + u'_i \tag{4.3}$$

where $\bar{u}_i$ is mean velocity and u'_i is the fluctuating velocity.

On the other hand, instantaneous value for the other scalar quantities is generalized as Equation 4.4:

$$\emptyset = \bar{\emptyset} + \emptyset' \tag{4.4}$$

where ∅ symbolizes a scalar quantity as already noted above.

Further details can be obtained in the bibliography part [14, 59]. These flow variables are substituted into the instantaneous continuity and momentum equations. In order to find the ensemble-averaged momentum equations, time average is taken and the over-bar on the mean velocity, $\bar{u}_i$, is dropped [14]. Continuity and momentum equations can be shown in the Cartesian tensor form as follows, respectively:

$$\frac{\partial \rho}{\partial t} + \frac{\partial}{\partial x_i}(\rho u_i) = 0 \tag{4.5}$$

$$\frac{\partial}{\partial t}(\rho u_i) + \frac{\partial}{\partial x_j}(\rho u_i u_j) = -\frac{\partial p}{\partial x_i}\left[\mu\left(\frac{\partial u_i}{\partial x_j} + \frac{\partial u_j}{\partial x_i} - \frac{2}{3}\delta_{ij}\frac{\partial u_l}{\partial x_l}\right)\right] + \frac{\partial}{\partial x_j\left(-\rho\overline{u'_\iota u'_J}\right)} \quad (4.6)$$

where $-\rho\overline{u'_\iota u'_J}$ is the Reynold stresses.

Equation 4.5 and 4.6 are called Reynolds-averaged Navier-Stokes equation [14] and a closure problem arises due to the non-linear term '$-\rho\overline{u'_\iota u'_J}$'. Closing the RANS equations needs modeling the Reynold's stress term; therefore, mean velocity and other scalar quantities are determined once Reynolds stress tensor is modeled for the closure. A transient case of fluid flowing is considered in this study; thus, unsteady RANS or URANS was included in the simulations by adding an unsteady term in the momentum equation. This term '$\frac{\partial}{\partial t}(\rho u_i)$' is expressed in Equation 4.6.

Several turbulent models are available in order to close the equation above and mainly based on the Boussinesq assumption where the effective viscosity determines the Reynolds stress tensor. The standard k-ω model, shear-stress transport (SST) k-ω model, standard k-ε, RNG k-ε, realizable k-ε, and Reynolds Stress Model (RSM) are some of turbulent models used in the commercial ANSYS FLUENT™ software.

4.1.2 Scale Resolving Simulation

The governing field equations for Large Eddy Simulations (LES) are determined by filtering the time-dependent Navier-Stokes equations. If the eddy scale is smaller than the filter width, eddies are effectively filtered out. This process is called filtering process in scale resolving simulations [14]. LES solves the large eddy size motions and models the small eddy motions as shown in Figure 4-1. LES is a widely accepted and promising numerical approach to the turbulent flow problems. It is a time dependent and three-dimensional numerical model. LES requires fine grid sizes with respect to URANS models, however coarser than those for Direct Numerical Simulations in which all time and space scales are resolved instead of modeling. The fluid flow is separated spatially into two parts with the purpose of spatial and temporal filters

applied in the inertial sub-range of the turbulent energy spectrum in LES modeling: one part is resolved and one part is modeled to obtain the subgrid scale Reynolds stress [14]. The modeled part is also called sub-grid scale model (SGS) and various SGS models are present in CFD applications. In Scale-Resolving Simulation (SRS) models, numerical simulations are necessary for additional information which cannot be obtained from the URANS formulations.

The filtered Navier-Stokes and continuity equations are given by Equation 4.7 and 4.8 [14]:

$$\frac{\partial}{\partial t}(\rho\bar{u}_i) + \frac{\partial}{\partial x_j}\left(\rho\bar{u}_i\bar{u}_j\right) = \frac{\partial}{\partial x_j}\left(\sigma_{ij}\right) - \frac{\partial\bar{p}}{\partial x_i} - \frac{\partial\tau_{ij}}{\partial x_j} \tag{4.7}$$

$$\frac{\partial\rho}{\partial t} + \frac{\partial}{\partial x_i}(\rho\bar{u}_i) = 0 \tag{4.8}$$

where $\sigma_{ij}$is the stress tensor because of the molecular viscosity. The shear stress tensor is defined by Equation 4.9:

$$\sigma_{ij} = \left[\mu\left(\frac{\partial\bar{u}_i}{\partial x_j} + \frac{\partial\bar{u}_j}{\partial x_i}\right)\right] - \frac{2}{3}\mu\frac{\partial\bar{u}_l}{\partial x_l}\delta_{ij} \tag{4.9}$$

In Equation 4.7, the term "τ_{ij}" is the subgrid-scale stress and defined by Equation 4.10:

$$\tau_{ij} = \rho\overline{u_i u_j} - \rho\bar{u}_i\bar{u}_j \tag{4.10}$$

LES and unsteady RANS models were implemented in this study for the accuracy of the numerical approach. Velocity and pressure profiles as well as turbulence structures predicted by unsteady Reynolds Averaged Navier–Stokes equations were satisfied with the experimental data, and the solution provided a less computational effort; therefore, URANS was implemented instead of LES approach for the rest of the simulations, and only the results of the URANS are shown. In the validation part, different types of unsteady RANS turbulent models were investigated for the optimization of the fluid flow field by considering time and accuracy.

4.2 Non-Newtonian Turbulent Flows in Concentric and Eccentric Annulus without and with Inner Pipe Rotation

4.2.1 Initial and Boundary Conditions for Concentric Annular Flow

Different unsteady turbulence models were simulated for a non-Newtonian drilling fluid in a concentric annulus, and results were compared with the experimental data reported by Nouri and Whitelaw [60]. Effect of inner pipe rotation on velocity and turbulence structures was also investigated. Experimental apparatus was suitably designed as 0.04030 m of outer pipe diameter and 0.02015 m of inner pipe diameter. The non-Newtonian fluid was a 0.2% aqueous solution of CMC at 25 °C with density of 1000 kg/m^3. The relationship between shear rate and shear stress in the non-Newtonian Power Law fluid was shown by Equation 4.11 as follows:

$$\tau = 0.044\gamma^{0.75} \tag{4.11}$$

where the power-law consistency index (a measure of the average viscosity of the drilling fluid) was 0.044 Pa.s, and power-law index (a measure of the deviation of the drilling fluid from Newtonian rheology) was 0.75.

Mean velocity for turbulent flow was 2.78 m/s for the case in which the inner pipe did not rotate, and 2.76 m/s for which the inner pipe tip velocity was 0.314 m/s corresponding to 300 rpm. In the experiment, bulk fluid velocity was measured by a calibrated orifice plate; however, the velocity values by the orifice plate were underestimated by 16% of the bulk velocities obtained from the integration of the average velocity profiles. Hence, the velocity values were corrected accordingly [60]. Flow properties and geometric dimensions for the simulations were summarized in Table 4-1. Figure 4-2 also demonstrates the flow configuration in vertical concentric annulus that was used in the numerical simulations for the representation of the test section.

Table 4-1: Geometric details and non-Newtonian drilling fluid properties for the computational set-up

	Without Rotation (0 rpm)	With Rotation (300 rpm)
Geometric Details		
Outer Pipe Diameter, (D_o, m)	0.04030	0.04030
Inner Pipe Diameter, (D_{in}, m)	0.02015	0.02015
Hydraulic Diameter, (D_H, m)	0.02015	0.02015
Computational Length, (L_z, m)	0.5	0.5
Flow Properties for Non-Newtonian CMC Solution		
Bulk Velocity, (U_b, m/s)	2.78	2.76
Inner Pipe Tip Velocity, (V_t, m/s)	0	0.314
Bulk Reynolds Number, (N_{Re})	9000	9000
Power-Law Consistency Index , (Pa.s)	0.044	0.044
Power-Law Index	0.75	0.75
Density of the CMC, (ρ, kg/m^3)	1000	1000
Temperature of the CMC, (°C)	25	25

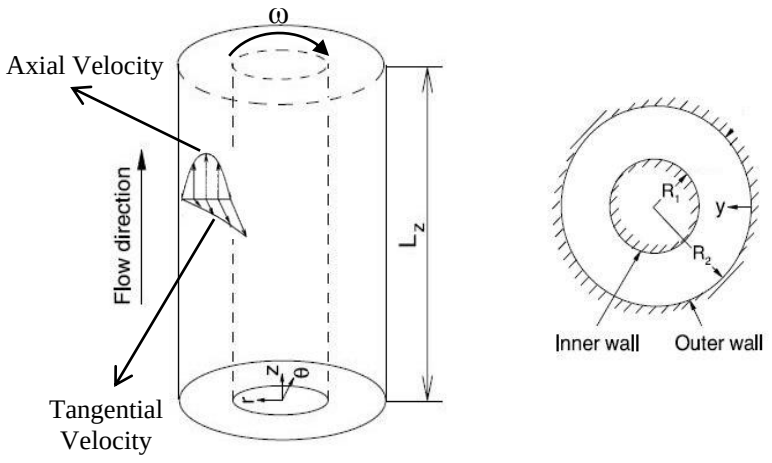

Figure 4-2: Geometric demonstration of computational set-up for concentric annuli (redrawn from Chung *et al.*, 2002)

Numerical simulations for concentric annuli were conducted using ANSYS FLUENT^{TM} 15.0. Convergence criterion was set to 10^{-4}, and computational time was 1.5 seconds with a time step size of 10^{-3} for unsteady RANS simulations. Several types of turbulence models were carried out in order to obtain the most accurate model for the experimental data. For that purpose, k-ω SST, k-ω Standard, k-ε Standard, k-ε Realizable Standard, k-ε RNG with two equation turbulence models and RSM Linear with seven equation turbulence models were simulated.

A grid independence study was also implemented with different element sizes. Hence, 0.00025 m, 0.00050 m, and 0.0010 m of grid sizes were tested for the grid independence study. It was confirmed that there was no significant differences in velocity profiles between fine and coarse mesh; therefore, it was determined to use 0.001 m of grid size for the simulations. However, finer mesh was defined near wall in order to achieve higher order accuracy. This was provided with the wall function procedure creating inflation layers near wall. Furthermore, the y plus (y^+) value was determined to be lower than 10. Figure 4-3 shows the unstructured mesh used in the computational domain for concentric annuli. The number of elements in the computational domain was 116600 for the concentric case.

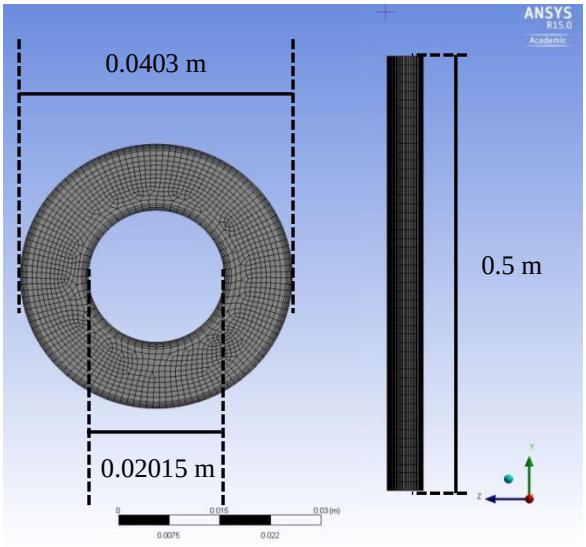

Figure 4-3: Concentric computational grid with inflation near wall

It was also noted in the experiments that maximum uncertainties in mean velocity values was 5% for the non-Newtonian fluid; therefore, this error applied in the experimental data as shown in the following figures.

4.2.2 Results: Velocity Profiles for Non-Rotating and Rotating Flows in Concentric Annulus

Velocity profiles for the simulated and experimental results in concentric annulus are shown in Figure 4-4 and Figure 4-5. The x axis, $\frac{r_1}{S}$, is the ratio of the radial distance from the outer wall and the gap between the inner and outer wall. Also, the y axis, $\frac{U}{U_b}$, is the ratio of the axial velocity and the bulk velocity. In particularly, Figure 4-4 demonstrates the comparison of various turbulence models with the experimental data for non-rotating flows. The effect of inner pipe rotation with rotary speed of 300 rpm can be seen in Figure 4-5.

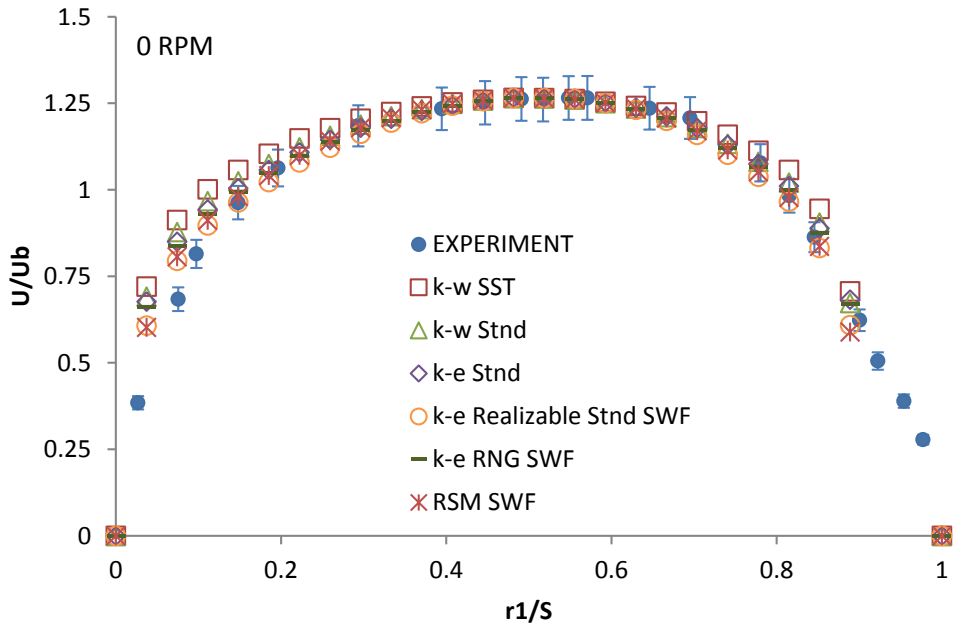

Figure 4-4: Simulated and experimental results for axial velocity profiles normalized with bulk velocity in the concentric annuli without inner pipe rotation

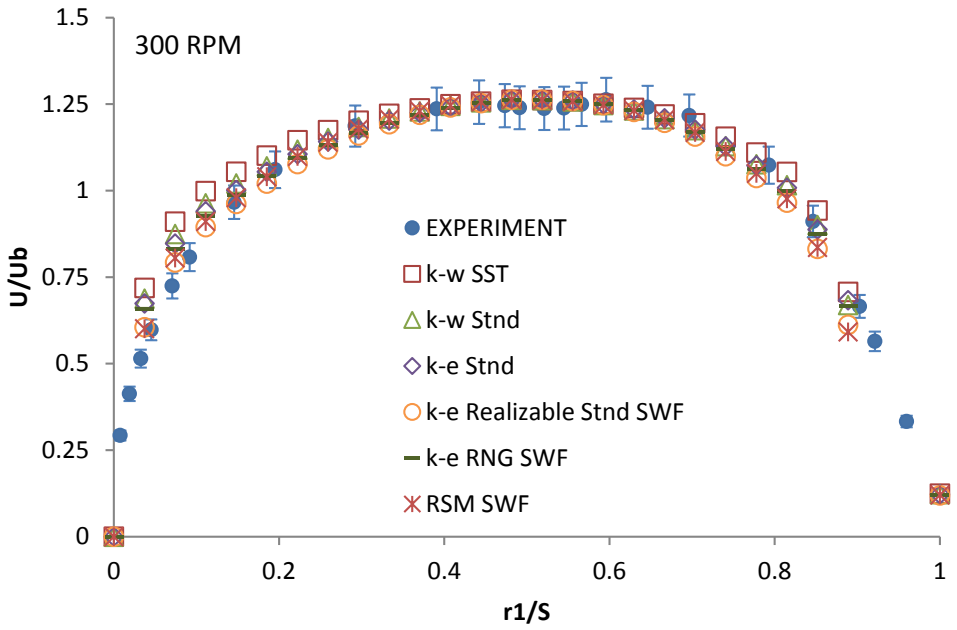

Figure 4-5: Simulated and experimental results for axial velocity profiles normalized with bulk velocity in the concentric annuli with inner pipe rotation (300 rpm)

Simulation results provided by six different approaches give satisfactory agreement with the experimental data for the non-rotating and rotating flows; especially excellent agreement is obtained near the inner wall at which the normalized radius is 1. Otherwise, velocity profile close to outer pipe, where normalized radius is 0, has some discrepancy from the experimental data. The relative error is usually less than 5% for each turbulence model. Contours of velocities in concentric annulus with non-rotating and rotating flows can be seen in the Figure A-1 and Figure A-2, respectively. Although, velocity contours for six turbulence models show similar behavior, turbulence kinetic energy and eddy viscosities differ from each other as illustrated in Figure A-3 to Figure A-6 in Appendix A. This situation can be explained by each turbulence model that uses different methodology and closure equations. According to the results, it was observed that inner pipe rotation did not significantly affect the velocity profile in concentric annulus. Furthermore, similar observation was obtained that turbulent kinetic energy and eddy viscosity were not influenced by rotation of the inner pipe as well.

4.2.3 Initial and Boundary Conditions for Eccentric Annular Flow

In addition to flow in a concentric annulus, different unsteady turbulence models were simulated for a non-Newtonian drilling fluid in an eccentric annulus, and results were compared with the experimental data reported by Nouri and Whitelaw [61]. Similar procedure was implemented in order to investigate the effect of inner pipe rotation on velocity and turbulence structures. Geometric details and flow properties were demonstrated in Table 4-1. However, bulk velocity of the non-Newtonian fluid was 2.76 m/s for non-rotating flow and 2.72 m/s for rotating flow in the eccentric case. Figure 4-6 shows the flow configuration in vertical eccentric annulus that was used in the numerical simulations. Eccentricity is defined as the deviation of the center of the inner pipe from the center of outer pipe. It is the ratio of distance between the centers of inner and outer pipes, l, and hydraulic radius, R_H. Plane 1 and Plane 3 represent the smallest and largest gap in the annulus, respectively.

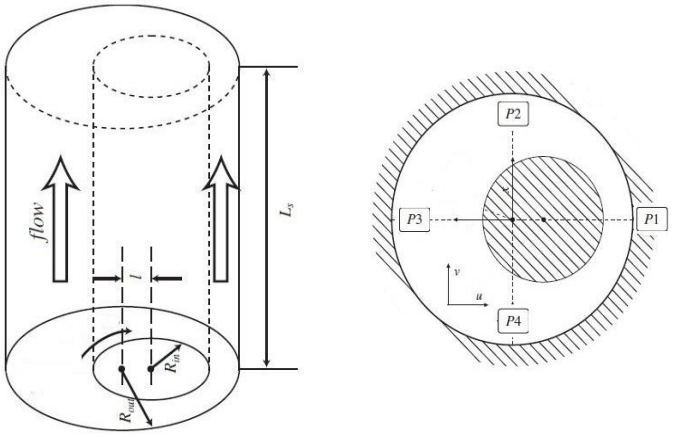

Figure 4-6: Geometric demonstration of computational set-up for eccentric annuli: Locations of the lines Plane 1 to Plane 4 (redrawn from Ninokata *et al.,* 2006)

Figure 4-7 shows the unstructured mesh used in the annulus with an eccentricity of 0.5. Each turbulent model was simulated by applying this computational grid with element size of 0.001 m. The number of elements in the computational domain was 194900.

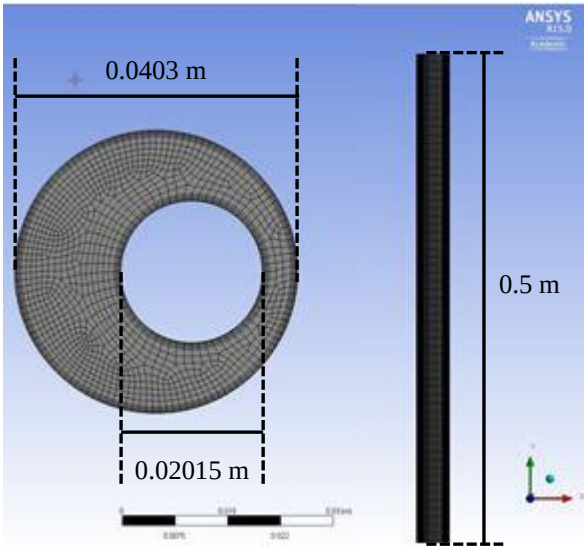

Figure 4-7: Eccentric (e = 0.5) computational grid with inflation near wall

4.2.4 Results: Velocity Profiles for Non-Rotating Flows in Eccentric Annulus

Velocity profiles for non-Newtonian fluid flow in eccentric annulus are depicted in Figure 4-8 to Figure 4-11. Simulated results for the radial distribution of the normalized axial velocities for non-rotating flow were also compared to the experimental data [61]. Velocity distribution was obtained similar to experimental results in Plane 2-4. However, in the smallest gap, Plane 1, the velocity profile does not have a good agreement with the experiment, especially at the near wall region. Simulated results overestimated the experimental results near the inner and outer pipe wall. On the other hand, each turbulence model captures the flow characteristics accurately in the center region for non-rotating, non-Newtonian fluid flow. It can also be observed that axial velocities normalized with the bulk velocities are smaller in the smallest gap (Plane 1) when compared to other planes. Otherwise, normalized velocities are almost 1.4 times bigger than the bulk velocity in the largest area (Plane 3). This is caused by channeling phenomenon due to low shear and resistance to flow in that region that is the most preferred path for the non-Newtonian fluid flow.

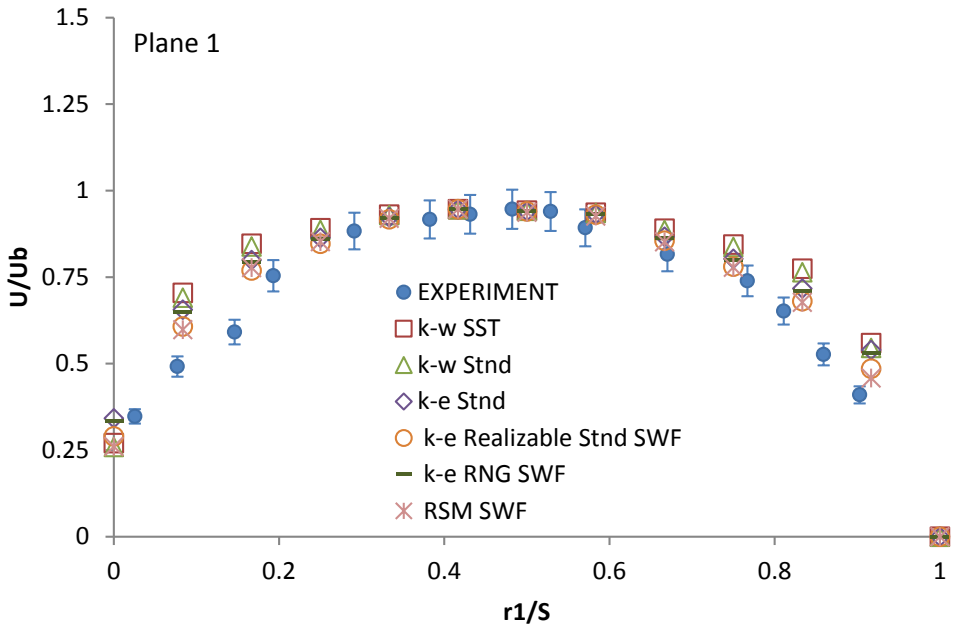

Figure 4-8: Simulated and experimental results for axial velocity profiles normalized with bulk velocity for Reynolds Number of 9300 in the eccentric annuli without inner pipe rotation at Plane 1

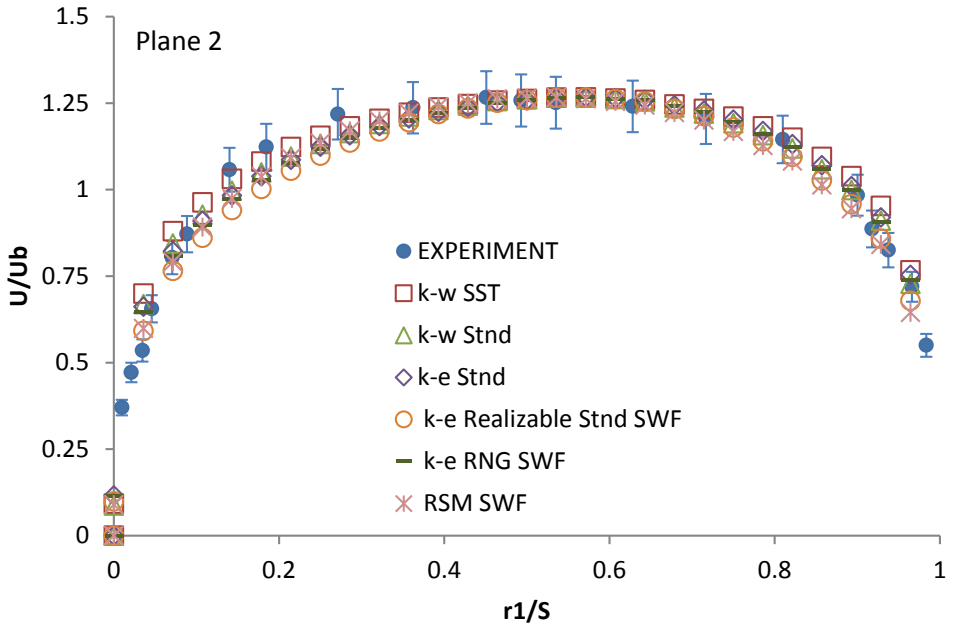

Figure 4-9: Simulated and experimental results for axial velocity profiles normalized with bulk velocity for Reynolds Number of 9300 in the eccentric annuli without inner pipe rotation at Plane 2

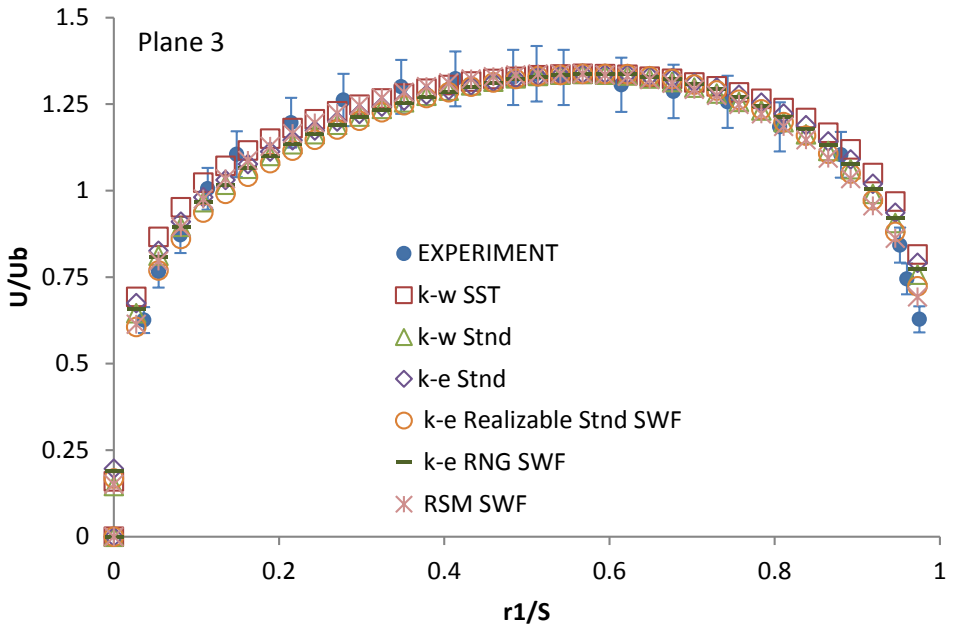

Figure 4-10: Simulated and experimental results for axial velocity profiles normalized with bulk velocity for Reynolds Number of 9300 in the eccentric annuli without inner pipe rotation at Plane 3

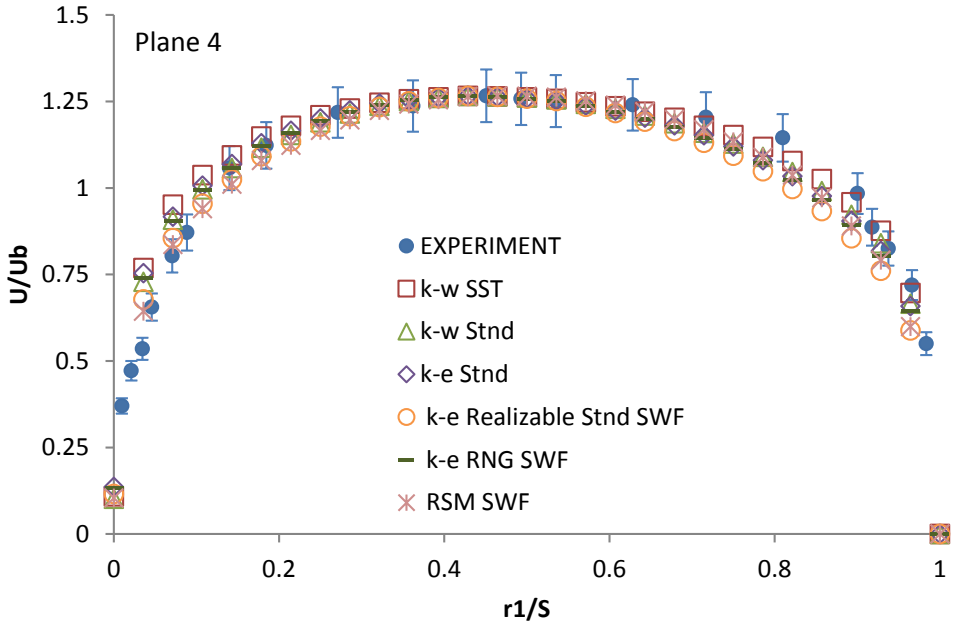

Figure 4-11: Simulated and experimental results for axial velocity profiles normalized with bulk velocity for Reynolds Number of 9300 in the eccentric annuli without inner pipe rotation at Plane 4

4.2.5 Results: Velocity Profiles for Rotating Flows in Eccentric Annulus

The effect of inner pipe rotation on axial velocities normalized with bulk velocity in eccentric annulus with inner pipe rotation (300 rpm) is presented in Figure 4-12 to Figure 4-15. Simulated results show a good agreement with the experimental results; however, velocities are over predicted near outer pipe in Plane 1, 2 and 4. A perfect fit with the experiment is provided in the largest gap (Plane 3) as shown in the Figure 4-14. Furthermore, it is deduced from the results that inner pipe rotation increases the axial velocity values normalized with the bulk velocity in the smallest gap. Likewise, inner pipe rotation has a positive effect on velocity profiles in the smallest region. Otherwise, velocities slightly decrease in Plane 2, 3 and 4 with inner pipe rotation. It can be explained that inner pipe rotation conduced a distribution of the axial velocities normalized by the bulk velocity across the annulus and made higher velocity profile shift into the smallest gap in the direction of the rotation. This behavior can be seen by going over the contours of velocities for each turbulence model in Figure B-2 in Appendix B.

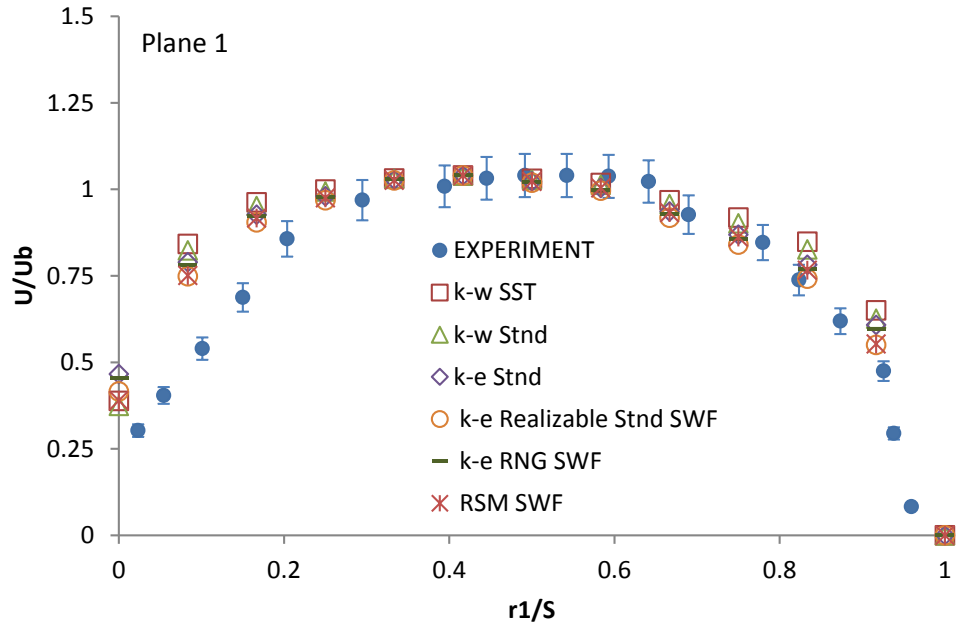

Figure 4-12: Simulated and experimental results for axial velocity profiles normalized with bulk velocity for Reynolds Number of 9200 in the eccentric annuli with inner pipe rotation (300 rpm) at Plane 1

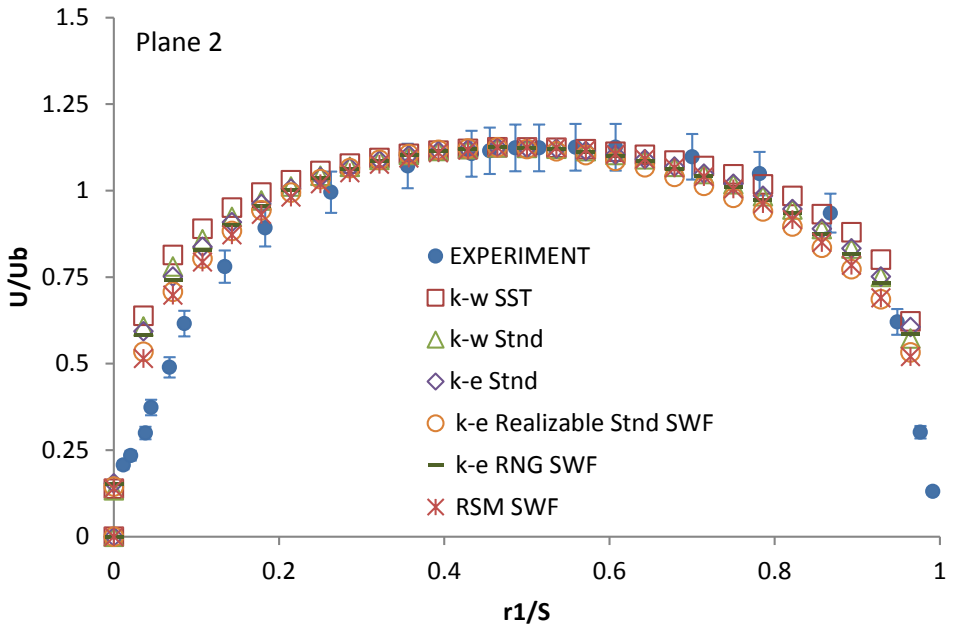

Figure 4-13: Simulated and experimental results for axial velocity profiles normalized with bulk velocity for Reynolds Number of 9200 in the eccentric annuli with inner pipe rotation (300 rpm) at Plane 2

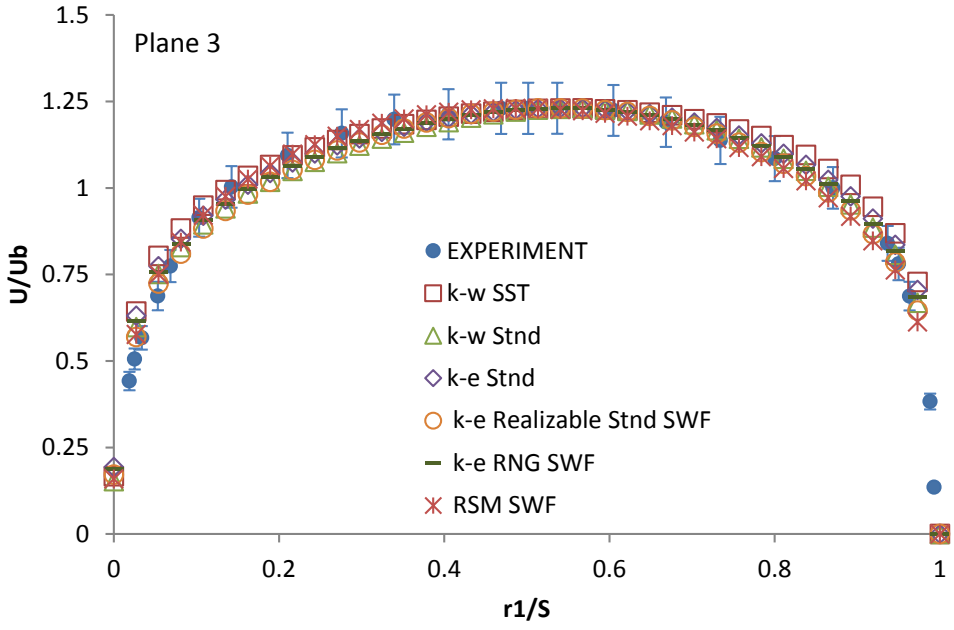

Figure 4-14: Simulated and experimental results for axial velocity profiles normalized with bulk velocity for Reynolds Number of 9200 in the eccentric annuli with inner pipe rotation (300 rpm) at Plane 3

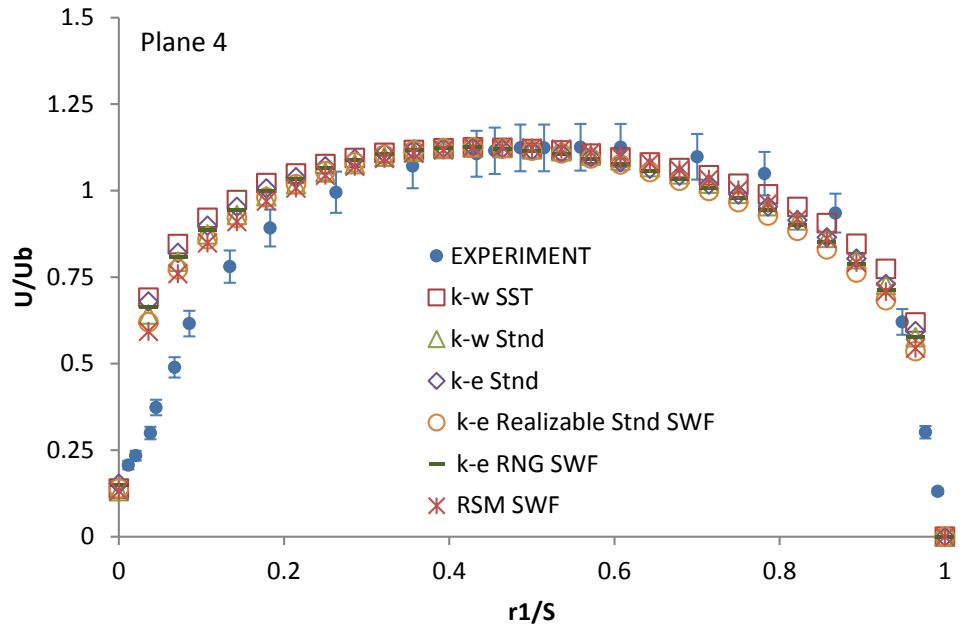

Figure 4-15: Simulated and experimental results for axial velocity profiles normalized with bulk velocity for Reynolds Number of 9200 in the eccentric annuli with inner pipe rotation (300 rpm) at Plane 4

4.3 Conclusion

Particle settling is most likely to occur in the narrow part of the annulus in the horizontal and directional drilling due to the low velocity in the narrow section as depicted in Figure 4-8. This behavior demonstrated a tendency towards laminarization of the turbulent flow in the narrow gap region. Increasing eccentricity decreases the velocity distribution in the smaller gaps because of the resistance of fluids flowing through the annulus; therefore, that situation may cause cuttings deposition and pipe sticking problem.

Furthermore, it was observed form the results that there was a potential of occurrence of a secondary flow at wider section of the annulus with presence of the eccentricity as shown in Figure B-1 and Figure B-2. There was no secondary flow at the concentric annulus (Figure A-1 and Figure A-2). Tangential velocity increases with increasing inner pipe rotation; therefore, cuttings close to inner pipe may be dragged into the secondary flow region because of the helical motion; as a result, cuttings transport performance may be improved. Hussain and Sharif also numerically showed the presence of the secondary flow for Herschel-Bulkley fluids in the eccentric annuli [62]. They concluded that cutting deposition in the narrow part of eccentric

annulus leads to an intensification in the existence of the secondary flow. The same result is deduced in this study because higher blockage height causes the main stream flow in the wider area where the secondary flow is more pronounced.

On the other hand, due to the shear thinning behavior of the non-Newtonian drilling fluid, viscosity is high in the center of the annulus (low-shear region), and inversely, it is lower near the walls (high-shear region). Increasing shear strain rate decreases the fluid viscosity. These phenomena can be seen in the Figure A-5 and Figure A-6 for concentric, and Figure B-5 and Figure B-6 for eccentric annular flow. Not only does low viscosity cause a reduction in the cuttings carrying capacity, but lower velocity also leads to destroy the turbulent fluctuations in the narrow section of the eccentric annulus; hole cleaning may become a challenge in the horizontal and deviated wells.

However, inner pipe rotation may contribute cuttings transport efficiently. Velocity values increase with rotation of the inner pipe in the smaller gaps. This behavior can be observed in Figure 4-16. In the figure, effect of the inner pipe rotation on the axial velocity profiles normalized with bulk velocity at the narrow part of the eccentric annulus is compared, and k-w SST turbulence model is selected for this comparison. Hence, increased velocity brings about proper hole cleaning, particularly in the horizontal and inclined wells. Furthermore, increasing rotary speed of the inner pipe also results in increase of the fluid viscosity in the narrow region of an eccentric annulus. Otherwise, increasing rotation speed causes increment in the annular pressure losses. This is also explained in a study conducted by Wan *et al.* [63].

In highly eccentric annulus, inertial effects become more dominant than shear thinning effects with increasing inner pipe rotation speed. Thereby, axial annular friction pressure gradient increases at higher rotation speeds. Nevertheless, inner pipe rotation does not have a significant impact on the velocity and turbulence structures in the concentric annulus (Figure A-1 to Figure A-6). Conversely, the effect of inner pipe rotation is more pronounced in the eccentric annulus. In addition, inhomogeneous turbulence structure and anisotropic eddy distribution were observed in the eccentric annulus flows with the rotation (Figure B-1 to Figure B-6). Neto *et al.* [64] investigated the rotating turbulent flows of Newtonian fluids using CFD with several turbulence models (k-ε Standard, k-ε RNG, k-ω Standard, k-ω SST, RSM linear Standard) based on RANS approach in concentric and eccentric annuli in order to compare the results with the

same experimental data that was used in this study [60, 61, 65]. Similar turbulence models also were used in this study for non-Newtonian drilling fluid. The same tendency for the velocity profiles was verified with that study [64].

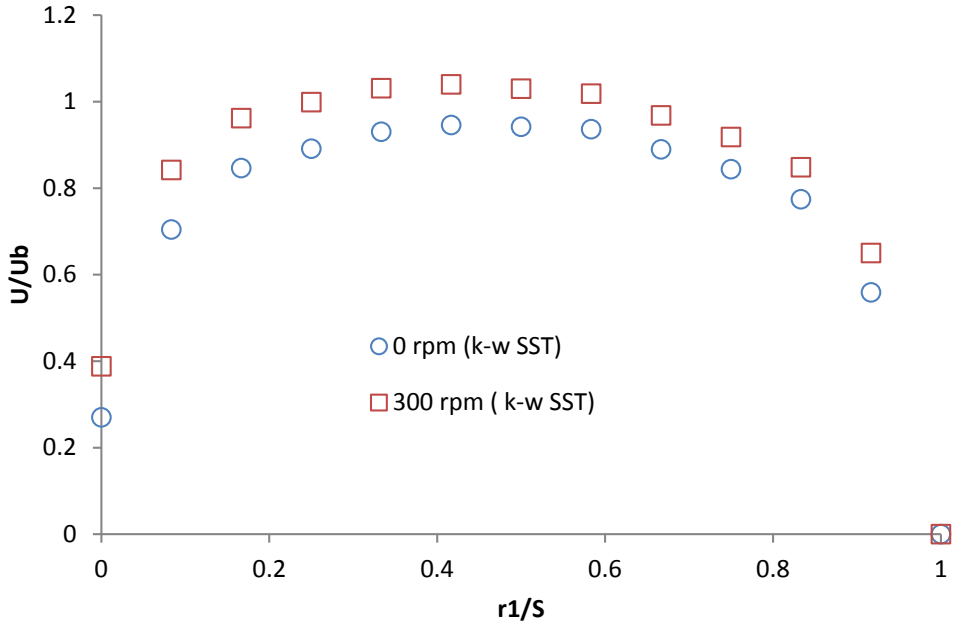

Figure 4-16: Comparison of axial velocity values normalized with bulk velocity with respect to the presence of the inner-pipe rotation for k-w SST turbulence model at Plane 1

Furthermore, LES and DNS of turbulent flows in concentric annulus were analyzed by Chung and Sung [45] and Chung *et al.* [42], respectively. Additionally, DNS of turbulent flows in eccentric annulus was studied by Ninokata *et al.* [46]. Simulated results by LES and DNS and experimental data [65] for axial velocities normalized by the bulk velocity showed a similar behavior with the current study. However, near wall behavior of LSE and DNS was better than URANS simulations. Since similar observations for velocity profiles were reported in the literature, and simulating LES and DNS of turbulent flows are computationally costly, the most computationally practical URANS approach was applied for the cuttings transport simulations. Although six different types of turbulent models were satisfied with the experiment, turbulent structures were totally different for each approach (Figure A-3&A-4 and Figure B-3&B-4).

Six types of URANS turbulence models differ in their computing of turbulent viscosity term, the shear stress transport (SST) k-ω model was applied in order to solve the continuous phase simulations in CFD-DEM coupling model. SST k-ω model is the composition of the k-ε in the free stream and k-ω in the near wall region [14]. Wall functions, which neglects the flow field in the buffer region and assumes an analytical solution in the viscous layer, are not carried out in SST k-ω model in order to solve the total flow field near the wall [14]. Low-Re corrections were also used in SST k-ω for the laminar-turbulent transition. Further details about the turbulence modeling can be found in the ANSYS FLUENT Theory Guide [14].

CHAPTER 5: ROLE OF PARTICLE COLLISION ON CUTTINGS TRANSPORT EFFICIENCY

Many numerical models neglect the inter-particle collisions; however, one of the most critical parameters during particle transport and deposition is particle-particle interaction. Given these realities, momentum and energy should be considered to exchange in the presence of the fact that each particle may have interaction with its adjacent particles or walls and its surrounding fluid. Indeed, considering the particle-particle collision is essential according to the Newton's second law of motion which states that the net force acting on a particle equals to the time rate of change of its linear momentum [66]. Accordingly, total kinetic energy before the collision will be different than total kinetic energy after the collision. Therefore, the kinetic energy is not conserved but it is transformed to other energy like particle deformation, friction, heat, etc. This type of collision is also called inelastic collision, and most likely to occur in drilled cuttings transport phenomenon.

In many numerical studies, the kinetic energy is assumed to be conserved; therefore, particle velocity is kept constant before and after the collision which is known as elastic collision. This is not realistic because the approach of Newton's first principle brings about different cuttings deposition rates and particle velocities contrary to what is observed in real physics. Newton's first law of motion indicates that the net force on a particle is zero, and it causes the velocity of a particle to be constant before and after the collision [66]. This is explained with the no momentum change. Applying the second law will dramatically affect the particulate process. Consequently, particle-fluid interaction considering drag and lift forces, particle-particle and particle-wall interactions resulting from collision forces should be studied closely to understand the particulate modeling. Numerical simulation of particle transport in different frameworks is discussed in detail in this chapter.

The two common methods used to predict cuttings trajectory and build into CFD are Eulerian and Lagrangian. The continuum phase is solved in Eulerian approach while the discrete phase is solved in the Lagrangian method. In the Eulerian-Eulerian formulation, particles act like a continuum phase. Particle velocity and concentration are computed applying mass and momentum conservation equations for each point of the numerical domain [14]. However, in the Eulerian-Lagrangian formulation, the particle trajectory calculations are taken into account [14].

This approach is mainly employed to estimate the overall particle dispersion pattern since particles act like a discrete phase. Discrete Phase Model (DPM) and Discrete Element Model (DEM) are both applied in Eulerian-Lagrangian approach in the ANSYS FLUENT ™ package. Although DPM and DEM models are aimed to simulate the particle trajectory and concentration in the numerical domain, there are significant differences between them. The DPM model is only applicable when the particle volume fraction is less than 10-12% [14]. Conversely, the DEM model considers particle-particle interactions.

In this study, particle trajectories are simulated by including the effect of particle collisions. This approach contributes to the solution of drilled cuttings transport in the complex geometries more accurately because it considers the behavior of the granular materials (particle dispersion and deposition) is totally controlled by the particle-particle interactions, particle-wall interactions as well as particle-fluid interactions. When particle volume fraction is less than 10-12%, the inter-particle collisions for dilute phase are neglected. However, collisions cannot be ignored in the dense phase because inter-particle interactions substantially change the cuttings transport performance in horizontal wells. On the contrary, the physics may be applied incorrectly by neglecting particle collision in a flow with a high volume fraction of the particles; therefore, profound understanding of these interactions is the key factor to develop a more robust particulate model. Commercial ANSYS FLUENT™ 15 CFD software has the capability of modeling the dense particulate flows allowing for the particle-particle interaction forces and taking into account the Newton's second law of motion in order to introduce the motion of individual particles in the fluid domain.

The continuum and discrete phases may have some interactions according to the degree of the coupling between them [11]. If the continuous phase motion influences the particle phase, this regime is called one-way coupling. In this regime, only the particles are affected by the carrier fluid; otherwise, particles do not have any effect on the carrier fluid. The fluid flow including dilute particle concentrations can be considered as one-way coupling particulate flow. In this type of coupling regime, a multiphase flow system containing a large number of particles cannot be modeled properly. Furthermore, when the particles influence the continuous and the continuous phase effects the particles, a two-way coupling regime is introduced. Even though the inter-particle collisions are neglected in this regime, discrete and continuum phases influence each other. Two-way coupling regime is valid for the intermediate particle concentrations.

Another important regime which plays a much more critical role on particulate modeling is four-way coupling.

In this study, particle-particle interactions are also taken into account along with the particle-fluid interactions. This approach is necessary for the dense particle concentrations because inevitably the particles will influence each other in such a dense domain, and these particles will most likely collide. These collisions can result from many reasons. One of the reasons for the inter-particle collisions is various particle size and shape in the fluid-solid multiphase flow domain. These physical changes in particles will directly affect the inter-particle velocity; therefore, different particle trajectories will occur due to the collisions. Another reason is that unsteady turbulence flows can lead to inter-particle collisions because the velocity resulting from the particle-particle interaction will change according to the turbulence intensity and eddy characteristics. Drill-pipe rotation also causes particle collision due to its orbital and lateral motion.

Consequently, the drilled cuttings trajectory in the complex geometries is essentially affected by these collisions to provide better predictions of the fluid flow field and particle motion. Drilled cuttings transport and deposition have been poorly understood because particle-particle collisions have not been included in the previous theoretical and numerical models. It would appear that there is no research considering the particle-particle interactions during cuttings transport in the oil industry. One of the novelties of this study is to contain the inter-particle collisions in order to develop a more accurate, physics based numerical model for the flow of particulate matter in a rotating system. Principally, cuttings always tend to collide with each other and the walls because of the whirling motion. Considering momentum and energy losses due to the inter-particle collisions will give more accurate results.

5.1 Discrete Element Method

DEM is a collision method used in DPM model in FLUENT in order to simulate dense particulate flows. As mentioned in the previous section, coupling between the continuous and discrete phase is determined by the cuttings concentration and physics of the problem. This brings about two-way coupling model including particle-particle interactions. In the Lagrangian formulation, particle motion in the carrier fluid is governed by solving a set of ODE along the

trajectory of individual Lagrangian particles to compute the change of particle location and the vector components of particle velocity. The DEM method has been used in many CFD applications for the past two decades. There are two types of DEM collisions in the literature: soft-sphere and hard-sphere approaches. Soft-sphere approach is the most commonly used method in DEM simulations, and developed by Cundall and Strack [67] for the granular dynamics simulations. In this approach, particles are allowed to slightly overlap. This is generally less than 0.5%. Hereby, particle deformations occur due to the collision. Contact forces resulting from elastic and plastic collisions and frictional forces between particles are calculated by these deformations [14]. Motion of individual particles is determined by implementing the Newton's laws of motion as discussed earlier. In soft-sphere approach, multiple particle contacts and collisions in a time are present. Otherwise, in hard-sphere approach, particles cannot penetrate each other during the collision and instantaneous contact at the time it is processed. In this study, soft-sphere method is used for particle tracking and characteristics for the discrete phase. For more information, ANSYS FLUENT User's Guide and Theory Guide can be referred to [14, 54].

5.1.1 Equations of Motion of Particles

The forces acting on a particle in a sedimentary bed can be illustrated in the Figure 1-2 [9] as discussed earlier in Chapter 1. The governing equations for the motion of the particle in a Lagrangian reference frame for the purpose of this study can be expressed in the Equation 5.1 and 5.2 [14].

$$m\frac{d\vec{v}}{dt} = \vec{F}_{drag} + \vec{F}_{pressure} + \vec{F}_{virtual\_mass} + \vec{F}_{Saffman's\_Lift} + \vec{F}_{gravitation} + \vec{F}_{other} \tag{5.1}$$

$$\frac{dx}{dt} = \vec{v} \tag{5.2}$$

where $\vec{F}_{drag}$ is the drag force per unit mass, $\vec{F}_{pressure}$ is the force caused by the pressure gradient, $\vec{F}_{virtual\_mass}$ is the virtual mass force required to accelerate the fluid surrounding the

particle, $\vec{F}_{Saffman's\_Lift}$ is the lift force due to shear, $\vec{F}_{gravitation}$ is the force of gravity on the particle and $\vec{F}_{other}$ is the additional force results from the particle collision with soft-sphere approach represented in the Figure 5-1.

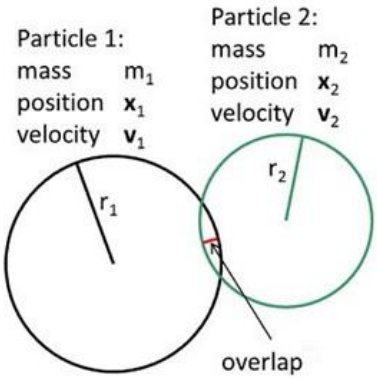

Figure 5-1: Particle deformation due to the overlap between pairs of sphere arising from collision [14]

Trajectory of particles is computed by integrating the force balance on a particle over time. In addition to these terms, forces arising from two-way turbulence coupling and rotation of the reference frame are also implemented in the force balance equation above. In the DEM method, there are three types of collision force laws: spring, spring-dashpot and friction. Selection of the appropriate properties and parameters play a significant role in order to produce accurate results. With this concern, a review of major applications and findings in DEM analyzed by Zhu *et al.* is referred to for information on cuttings transport behavior in horizontal wells [68].

In drilling operations, it is difficult to estimate the cuttings shape and size because cuttings are generated by breaking down different type of rocks and this causes uncertainties on the irregularity and non-sphericity of the cuttings. However, cuttings can be investigated from the surface equipment like shale shakers in the field operations. These observations can give some idea about the formation and cuttings characteristics. Hence, drilled cuttings are assumed to have low shape factors for estimation of non-spherical drag coefficient which is used in particle-fluid interaction forces.

Further information about the theory and applications for discrete element simulations can be obtained in the bibliography [11, 68].

5.1.2 Turbulent Dispersion of Particles

Discrete random walk model (DRW) is also applied in order to include the impacts of instantaneous turbulent velocity fluctuations on the particle motion. The surrounding fluid interacts with the cuttings, and this produces several particle-fluid interaction forces in addition to the buoyancy force. Particle-fluid interaction forces which are applied in this study are drag force, pressure gradient force, virtual mass force and Saffman's lift force [11]. Therefore, particle motion in the carrier fluid is affected by the particle-fluid interaction forces which should be considered properly and accurately. DRW is a stochastic tracking approach, and in this method, the turbulent dispersion of particles is determined by integrating the trajectory equations for individual particles, using the instantaneous fluid velocity, $u_i = \bar{u}_i + u'_i$, along the particle path during the integration [14]. ANSYS FLUENT is capable of including DRW when the turbulence flow is present. Enabling stochastic tracking approach enhances dispersion of the cuttings in the carrier fluid because of the turbulence.

5.1.3 CFD-DEM Coupling Scheme

As already mentioned, particle-particle interaction is included in numerical simulations in addition to particle-fluid interactions. This two-way coupling with the particle collision is achieved by alternately solving the continuous and discrete phase equations until each phase has no influence on the other and it converges. Figure 5-2 shows the multiphase flow modeling by DEM including CFD interactions [11]. At each time step, velocity properties and positions of individual particles, and volumetric fractions of each phases are computed and transferred to the equations used in the continuous phase. CFD updates properties given in the previous time step and uses the information from the DEM to calculate the particle-fluid interaction forces acting on individual particles. After updating the CFD properties, DEM interacts with continuous phase and estimate the motion of individual particles for the next time step. Detailed information about two-way coupling with particle collision can be obtained in the references [11, 14].

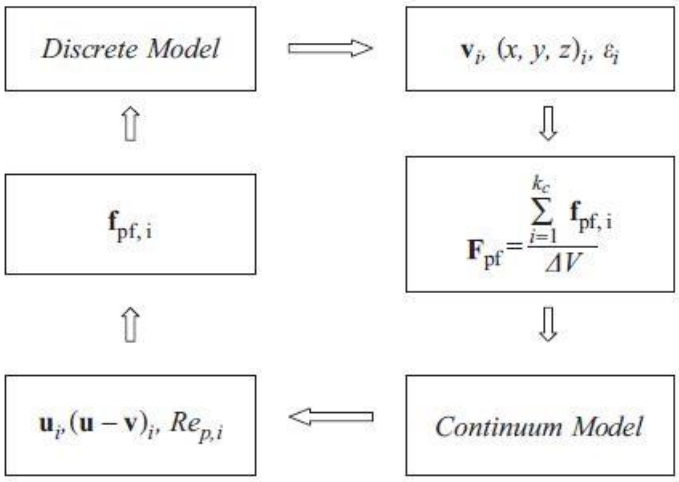

Figure 5-2: CFD-DEM coupling and heat, mass, and momentum exchange between CFD and DEM [11]

5.2 Comparison between DEM Model and Experimental Data

5.2.1 Predicting of Moving Bed Velocity in a Horizontal Annulus for Cuttings-Water Multiphase Flow using DEM Approach

Garcia-Hernandez *et al.* conducted an experimental study to determine the cuttings bed height and slip velocity in horizontal and deviated wells [38]. In this study, experimental data for horizontal well was used to predict the cuttings velocity in a moving layer using Eulerian-Lagrangian DPM method with DEM collisions. Results were compared with a previous CFD study in which one-way coupling of DPM method without particle collisions was implemented by Yilmaz [36]. In the experimental study, the carrier fluid is selected as a Newtonian fluid. The flow loop has an 8-in x 4.5-in annulus. Cuttings' diameters range between 3 mm to 5 mm. Average specific gravity of the particles is 2.6. Velocity values in the experiment were calculated for each data point using 5% uncertainty. Cuttings bed height was taken from the experimental observations and introduced into the simulations as a boundary condition because the goal of this part was to estimate the cuttings moving velocity. Figure 5-3 shows the comparison of cuttings moving layer velocities for the different approaches.

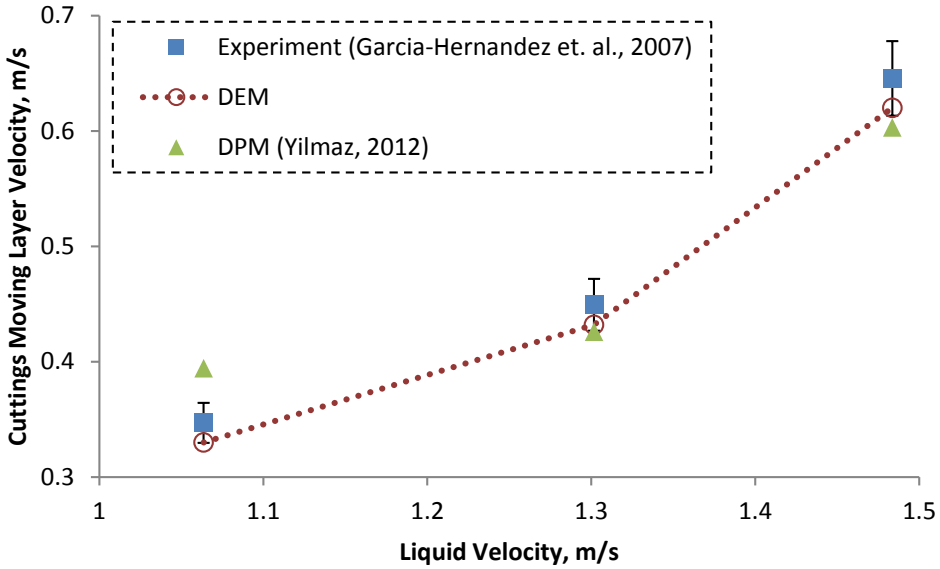

Figure 5-3: Comparison of model prediction of cuttings velocity in the moving layer

Relative errors between the experimental result and the DPM/DEM models were compared and summarized in the Table 5-1. As shown in the table, the errors were significantly decreased (below 5%) by implementing the DEM model. It was more than 5% on the study conducted by Yilmaz [36]. Further information about simulation details can be obtained in the bibliography [36]. It can be concluded that the DPM with particle collision model has satisfactory agreement with the experiment for cuttings transport problem.

Table 5-1: Comparison between the experimental results and model prediction for moving bed cuttings velocity

Flow Rate (GPM)	Cuttings Bed Height (in)	Liquid Velocity (m/s)	Cuttings Velocity (Experiment) (m/s)	Cuttings Velocity (DEM) (m/s)	Error with DPM Model (%)	Error with DEM Model (%)
200	3.44	1.064	0.347	0.330	13.64	4.89
300	2.4	1.302	0.449	0.432	5.19	3.86
400	1.7	1.484	0.646	0.620	6.59	3.96

5.2.2 Estimating Annular Pressure Drop and Cuttings Concentration in Eccentric Horizontal Annulus for Cuttings-Water Multiphase Flow with DEM

Two-phase flow experiments were conducted for estimating annular pressure losses and cuttings concentration in an eccentric horizontal annulus [19]. A 21 ft long annular test section with 2.91 inch O.D. casing and 1.85 I.D. pipe was used for the experiment. The inner pipe had a tendency to rotate up to 120 rpm. Eccentricity of the inner pipe was 0.623. For the test procedure, water was filled in the annulus and then the inner pipe was set to the desired rotary speed. Then, particles were injected to the annular section with respect to cutting rate of penetration. Once the stationary state was observed, the data was processed. The test matrix for the solid-water two phase flow used for the comparison study is summarized in Table 5-2.

Table 5-2: Validation of the model with the experimental data by Osguei [19] for predicting pressure losses and cuttings concentration in an eccentric horizontal annulus

Geometric Properties	
Outer Pipe Diameter, (D_o, in)	2.91
Inner Pipe Diameter, (D_{in}, in)	1.85
Eccentricity, e	0.623
Computational Length, (L, m)	2.0
Fluid Properties	
Fluid Velocity, (U_b, ft/s)	5-9
Inner Pipe Rotation, (rpm)	80
Power-Law Consistency Index , (Pa.s)	0.001
Power-Law Index	1
Density of the water, (ρ_f, kg/m^3)	998.5
Particle Properties	
Average Cuttings Size, (m)	0.00201
Cuttings Density, (ρ_p, kg/m^3)	2761.4
Rate of Penetration, (ROP, m/s)	0.00508

A mesh independence study was also carried out in order to optimize the grid sizes until the simulation results (annular pressure drop and cuttings concentration) were no longer dependent on the mesh size. For this purpose, the coarse mesh was created with an element size of 0.004 m and 61400 numbers of elements. For the medium mesh, the element size was decreased to 0.002 m corresponding with 159500 numbers of elements. Finally, the fine mesh was used with an element size of 0.001 m and 434800 numbers of elements.

The grid independence study was conducted for the water-solid two phase flow with a fluid velocity of 1.524 m/s, and inner-pipe rotation speed of 80 rpm. The simulations were performed using LSU HPC resources with 128 processors. Comparison between the annular pressure losses and cuttings concentration with respect to element size is shown in Figure 5-4 and Figure 5-5, respectively. In addition, simulated results are also compared with respect to mesh quality in the Table 5-3. According to the results, the optimum mesh size was determined as 0.002 m for the simulations.

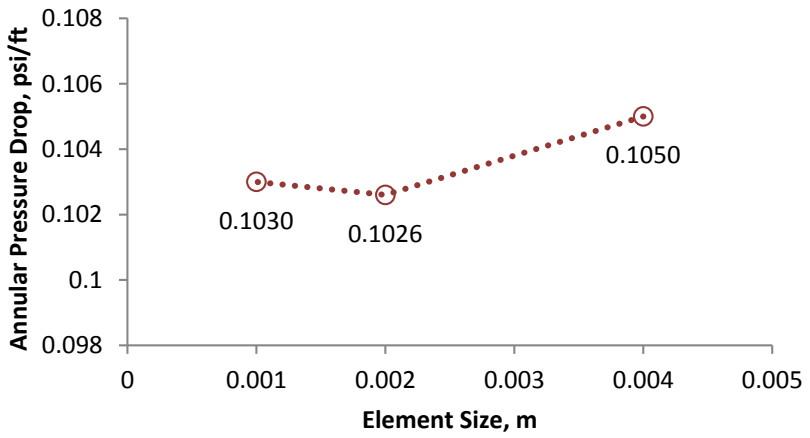

Figure 5-4: Grid independence study: Annular Pressure Drop vs. Elements Size

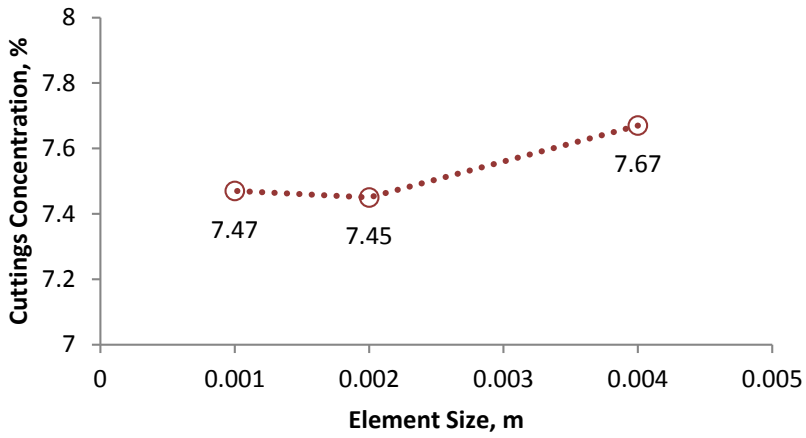

Figure 5-5: Grid independence study: Cuttings Concentration vs. Elements Size

Table 5-3: Grid independence study at ROP of 60 ft/h, rotary speed of 80 rpm

	Coarse Mesh (0.004 m)	Medium Mesh (0.002 m)	Fine Mesh (0.001 m)
ΔP/D, psi/ft	0.1050	0.1026	0.1030
Cc, %	7.67	7.45	7.47

After the grid size was determined, the simulation model was validated with the experimental study [19]. Figure 5-6 shows the annular pressure drop with superficial liquid velocity for an eccentric horizontal particle-fluid flow with 80 rpm inner pipe rotation and 60 ft/h ROP. On the other hand, cuttings concentration computed by DEM-CFD simulations was also compared with the experimental data as shown in the Figure 5-7. It is apparent that the simulated and experimental results have a satisfactory agreement for both predicting the annular pressure losses and cuttings concentration in the eccentric annulus. The maximum relative error with the experiment for the annular pressure losses was observed as 10.67%, and the minimum error was 3.92% as seen in the Table 5-4. Even though the relative error was obtained at more than 5% for most of the data point, DEM-CFD coupled simulation results demonstrated a similar pattern to the experimental data, in which increasing carrier fluid velocity leads to an increase in the annular pressure drop (Figure 5-6). Simulated results were also in good with the experiment for the cuttings concentration. Increasing superficial fluid velocity caused a reduction in the cuttings

concentration in the annular section (Figure 5-7). However, the error of each data point in the experiment was relatively high. The minimum and maximum errors were 4.34% and 13.73%, respectively (Table 5-4).

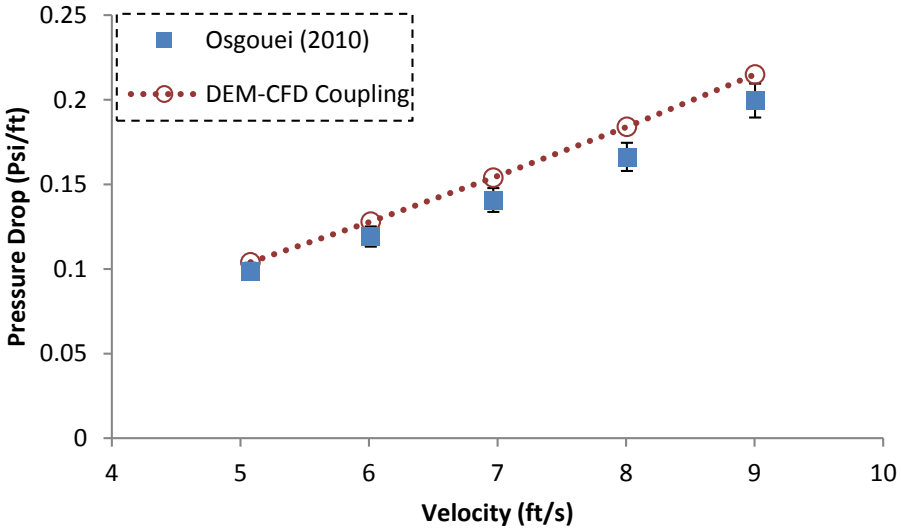

Figure 5-6: Comparison of annular pressure losses for cuttings-water multiphase flow in an eccentric horizontal annulus between the experimental and simulated data

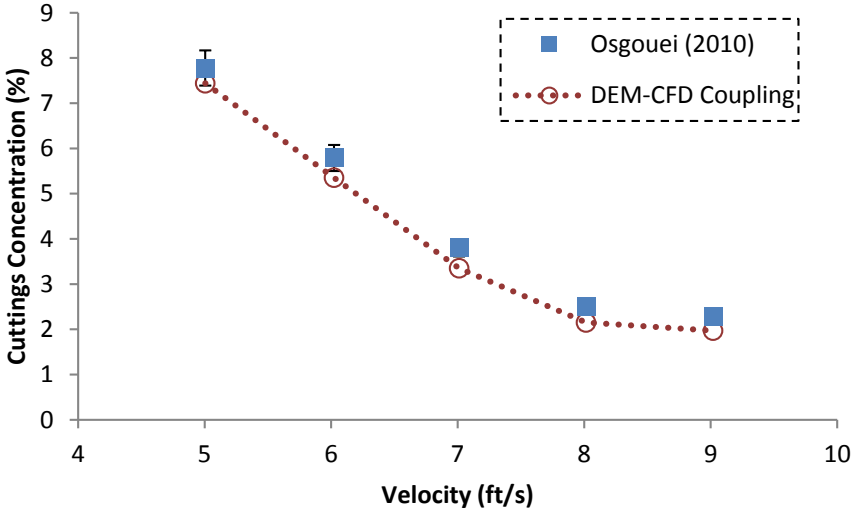

Figure 5-7: Comparison of cuttings concentration for cuttings-water multiphase flow in an eccentric horizontal annulus between the experimental and simulated data

Table 5-4: Summary of the experimental and simulated results and relative error analysis

Fluid Velocity (ft/s)	ΔP (Experiment) (psi/ft)	ΔP (DEM) (psi/ft)	Relative Error for ΔP (%)	C_c (Experiment) (%)	C_c (DEM) (%)	Relative Error for C_c (%)
5	0.098732	0.103	3.92	7.7775	7.44	4.34
6	0.119181	0.128	7.4	5.7885	5.35	5.58
7	0.140819	0.154	9.36	3.7994	3.35	11.84
8	0.166262	0.184	10.67	2.5003	2.15	14.01
9	0.199551	0.215	7.74	2.2836	1.97	13.73

To summarize, capability of CFD-DEM coupling model in unsteady particle tracking scheme for estimating the annular pressure losses and cuttings concentration in an eccentric horizontal well for the specified drilling condition, fluid and particle properties was presented with a good satisfactory with the experimental data [19]. Increasing fluid velocity resulted in a significant increment in the annular frictional pressure losses as seen in the Figure 5-6. Same trend was observed during the experiment; however, experimental results were slightly overestimated by the model. On the other hand, cutting concentration significantly decreased with increasing fluid velocity as seen in the Figure 5-7. The results indicated that increasing fluid velocity removed the cuttings for water as a carrier fluid. Nevertheless, there was no considerable change in the cuttings concentration at higher fluid velocities. Similar behavior of cuttings concentration with increasing fluid velocity was also obtained by the model. In this instance, simulation results underestimated the experimental data. To this end, the developed numerical model is successfully capable of simulating the cuttings transport process during eccentric horizontal annuli.

Whirling motion of the drill-pipe is discussed in the next chapter. The main purpose of this study was to implement dynamic motion of the drill-pipe into the coupled CFD-DEM model for improving the cuttings transport performance in eccentric horizontal wells.

CHAPTER 6: WHIRLING MOTION OF ROTATING DRILL-PIPE ON CUTTINGS TRANSPORT PERFORMANCE

Drill-string (generally consists of drill-pipe and bottom hole assembly in conventional drilling) helps to deliver the torque and dynamic motion taken by kelly or top drive to the drill bit. Also, transportation of the drilling fluid from the surface to drill bit is provided by the drill-string. During drilling, rotation of drill-string can behave unexpectedly because of the axial, lateral and torsional loads. These dynamic loads create vibrations on the drill-pipe; therefore, snaking and whirling motion of drill-string occurs after a certain rotary speed is reached [69-71].

Drill-pipe has relatively less wall thickness than drill-collars have; therefore, drill-pipe is most likely to be influenced by the dynamic vibrations. Interaction between the bit and formation also determines the type of the motion because the force acting on the drill string designates the position of it laterally. Moreover, in most of the directional and horizontal drilling operations, drill string is close to the bottom of the wellbore because of the gravity. In such cases, the drill string may touch the formation according to the eccentricity and this may result in a wash out problem. Likewise, it may touch the casing and lead to corrosion as well. As a consequence, these vibrations can damage the service life of the drill-pipe and down-hole equipment, and lead to fatigue failures and abrasive wear of tubular [69]. Hence, in drilling operations, these dynamic vibrations and their effects on drilling must be completely comprehended. However, this is another research, and there are several studies on drill-string vibrations.

Apart from dynamic vibrations, effect of whirling motion on cuttings transportation and deposition were analyzed in this study. In addition to axial drill-pipe rotation, it is also believed that whirling and drill-pipe vibrations can increase the efficiency of hole cleaning in extended reach wells due to its conveyor belt effect which causes transporting maximum amount of cuttings to the surface. In eccentric horizontal wells, this helical flow behavior transports cuttings, which are mostly deposited near the narrow part of annulus due to insufficient hole cleaning as a result of low fluid velocity, to the upper side of annulus in which the fluid velocity and transport efficiency is higher. Under these circumstances, hydro-mechanical effects maintain the continuous flow of drilled cuttings in the high velocity annular space of the hole, and sustain the conveyor belt effect for efficient cuttings transport to the surface [72].

Heisig *et al.* developed an analytical solution for lateral drill-string vibrations in extended reach wells [71]. They mainly investigated the snaking and whirling motion on hole cleaning efficiency. According to the results, it was concluded that lateral vibrations of the drill-pipe might contribute to improve cuttings transport in horizontal wells. In particular, the snaking type of motion was believed to suspend cuttings in the drilling fluid and remove cuttings bed formation. In addition, whirling also might improve hole cleaning performance by stirring up the stationary cuttings bed. They also indicated that the snaking mode shape of drill-pipe is a sinusoidal buckling, whereas whirling mode shape of drill-pipe is a helical buckling. These vibrations were considered to occur with dynamic loads and rotary speed up to 200 RPM in terms of hole cleaning aspects. It was also noted in the analytical model, when inner pipe rotary speed was continuously increased, large amplitudes observed after 120 rpm as shown in Figure 6-1. According to observations, snaking motion occurred when the inner pipe rotary speed was increased. However, dynamic behavior of the drill-pipe was completely different when the whirling motion was present because whirling motion of the drill-pipe continued even though the rotary speed was decreased.

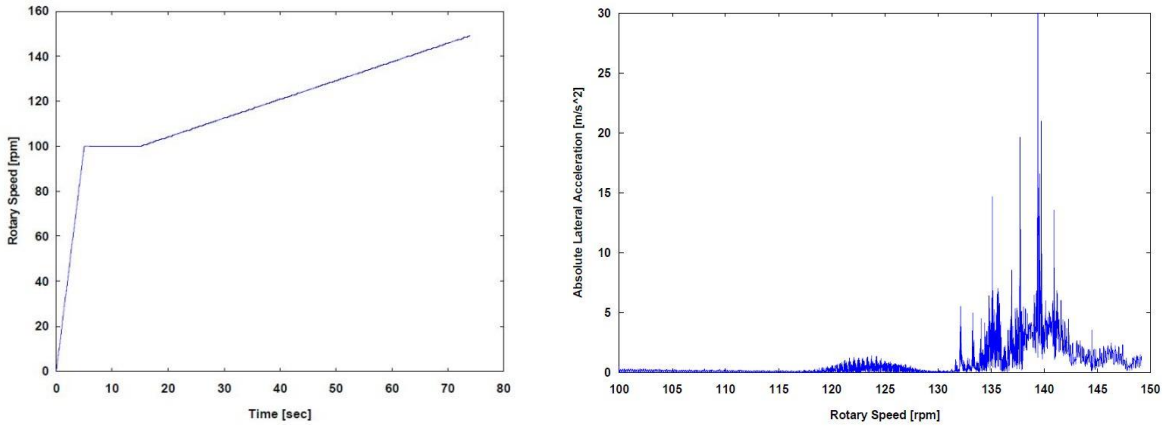

(a) (b)

Figure 6-1: Analytical results for the occurrence of dynamic motion of the drill-pipe a) inner-pipe rotary speed versus the time history, b) maximum lateral acceleration with respect to inner-pipe rotary speed [71]

In this study, whirling rotary was only considered for cuttings transport purposes. Any fatigue problem on string components and bit failure because of the whirling rotary were not taken into account in the numerical simulations. Based on the literature, it is believed that

whirling rotary would help enhance hole cleaning. However, there is no experimental and numerical research in which whirling motion of drill-pipe is considered. Some of researchers remark that a major contribution of hole cleaning comes from the dynamic behavior of the drill-string [16, 18]. On the other hand, because of the dynamic buckling of the drill string, variable eccentricity occurs. In this study, however, constant eccentricity is taken into account for whirling motion to make the mathematical equations simpler. In the forthcoming section, equations can be reached for the whirling motion. After that, numerical model was validated with another study [73].

6.1 Mathematical Derivation of Lateral Drill-pipe Motion in an Eccentric Wellbore

The phenomenon of whirling during drilling can be explained by drill-pipe that rotates around its own center and simultaneously the center of drill-pipe also rotates around the center of wellbore as shown in Figure 6-2, which is the description of the coordinate system to show 2D whirl motion of drill-pipe. Point O is the center of the drill-pipe and rotates counterclockwise around the Point O" which is center of the wellbore. On the other hand, axial rotation of drill-pipe occurs in the clockwise direction. In Figure 6-2, it is highlighted that drill-pipe contacts the wall of the wellbore on Point P with the full eccentricity.

Based on the 2D schematic, the equation of the position vectors (6.1 & 6.2) are written as follows:

$$x = \varepsilon\, cos(\Omega t) + r_p cos(\omega t) \tag{6.1}$$

$$y = \varepsilon sin(\Omega t) + r_p sin(\omega t) \tag{6.2}$$

It can be seen from the Equation 6.1 & 6.2, position of a significant point changes regarding to drill-pipe rotation and whirl motion of the drill-pipe around the center of the wellbore. Since the derivative of the position vectors with respect to time gives velocity vectors, the equation of velocity for each direction is derived as follows:

$$V_x = \frac{dx}{dt} = \frac{d}{dt}\Big(\varepsilon \cos(\Omega t) + r_p cos(\omega t)\Big) = -\varepsilon\Omega sin(\Omega t) - r_p \omega sin(\omega t) \tag{6.3}$$

$$V_y = \frac{dy}{dt} = \frac{d}{dt}\left(\varepsilon sin(\Omega t) + r_p sin(\omega t)\right) = \varepsilon\Omega cos(\Omega t) + r_p \omega cos(\omega t) \tag{6.4}$$

Equation 6.3 and 6.4 represent the rate at which any particular point on the inner pipe changes its position. The direction of the velocity vector is the same as the direction that the point P is moving. In particular, it is determined by the rotating rate and whirling rate.

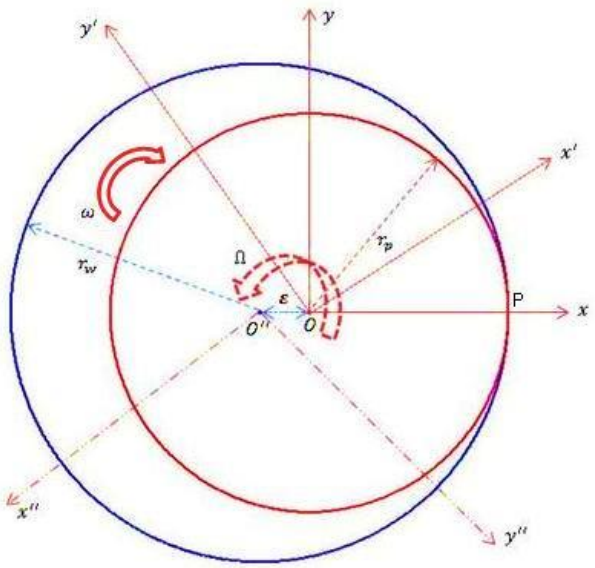

Figure 6-2: Whirling schematic of inner pipe in an eccentric annulus

where,

O_{xy} = Fixed reference frame centered in the wellbore

$O_{x'y'}$ = Rotating reference frame with speed $\boldsymbol{\omega}$ and its origin located on the axis of the drill-pipe

$O''_{x''y''}$ = Rotating reference frame with speed $\boldsymbol{\Omega}$ and its origin located at the center of the wellbore

ω = Rotating speed of the drill-pipe with respect to O_{xy}, rad/s

Ω = Whirling speed of the drill-pipe $O''_{x''y''}$, rad/s

ϵ = Whirling radius resulting from the displacement of the drill-pipe center ($O'' - O$), m

r_w = Wellbore radius, m

r_p = Drill-pipe radius, m

P = Point P for inner pipe whirling trajectory

6.2 Verification of Whirling Motion

Using these equations of whirling motion of the drill-pipe, a MATLAB code was developed in order to predict the trajectory of Point P (demonstrated in the Figure 6-2) with inner pipe rotation and whirling motion of the inner pipe for verification. Data was obtained from a Ph.D. study conducted by Shyu [73]. In his study, eccentricity was considered as 0.875 inches. Radius of drill-pipe and wellbore was recorded as 3.5 and 4.375 inches respectively.

Shyu also considered different whirling conditions which can be faced during drilling, and summarized these scenarios in Table 6-1. In the table, in addition to rotating rate and whirling rate, slip velocity was also taken into account in order to see the slip effect on the whirling motion. This effect comes from the relative contact velocity with the wall, and mathematical expression is presented in the Equation 6.5 [73]:

$$v = \varepsilon \, x \, \Omega + r_p \, x \, \omega \tag{6.5}$$

Table 6-1: Various types of drill-pipe rotation with whirling motion [73]

Case	Rotating Rate, Hz	Whirling Rate, Hz	Absolute Slip Velocity, ft/s
1- Backward Whirl with Slip	-2.2	9.9	0.5
2- Backward Whirl, no Slip	-2.2	8.8	0
3- Backward Whirl, Forward Slip	-2.2	2.2	3.02
4- No Whirl, Pure Rotation	-2.2	0	4.03
5- Forward Whirl with Slip	-2.2	-1.1	4.53
6- Synchronous Whirl with Slip	-2.2	-2.2	5.04
7- Forward Whirl with Forward Slip	-2.2	-3.3	5.54

According to geometric details and different cases, MATLAB code was successfully validated with the study conducted by Shyu [73]. In order to clarify the calculation of slip velocity, case number 1 is examined in detail.

Hence, slip velocity in terms of ft/s is calculated with respect to Equation 6.5 :

$$V_{slip} = 0.875\ in * \frac{ft}{12 * in} * 9.9 * 2 * \pi - 3.5\ in * \frac{ft}{12 * in} * 2.2 * 2 * \pi = 0.5\ ft/s$$

Slip velocities for the other cases were estimated similarly by using Equation 3.18 and given in Table 6-1. The minus sign determines the clockwise rotation while the plus sign indicates the counterclockwise rotation. MATLAB results were successfully compared for each case and shown in Figure 6-3 through Figure 6-9. Two schematics (previous study versus present study) are compared in the same line for each scenario. In the figures for the current study, the red circle represents the drill-pipe, the blue circle symbolizes the wellbore and the black dashed line presents the trace of Point P with whirling rotary. Different whirling velocities exemplify discrepant trajectories as seen in the particular figures.

Furthermore, numbers in Table 6-1 have a physical meaning of zero tangential velocity (case 2) that leads to no wear on the drill-pipe. Otherwise, case 6 has a high tangential velocity with no bending fatigue and results in abrasively wearing out the drill-pipe [73]. These kinds of physical significances were not considered for an effective hole cleaning performance. The main objective of this part was to validate the code and improve it for cuttings transport in eccentric horizontal annulus in order to sustain the conveyor belt effect for an effective hole cleaning. With respect to this purpose, a user defined function (UDF) in C programming language was developed for mesh motion and implemented in ANSYS FLUENT 15 to consider the effects of whirling rotary of drill-pipe on cuttings transport performance.

The impact of pipe rotation with whirl motion on cuttings transport performance in eccentric horizontal wellbores was systematically investigated for each case and results were discussed comprehensively in Results and Discussion part in Chapter 7.

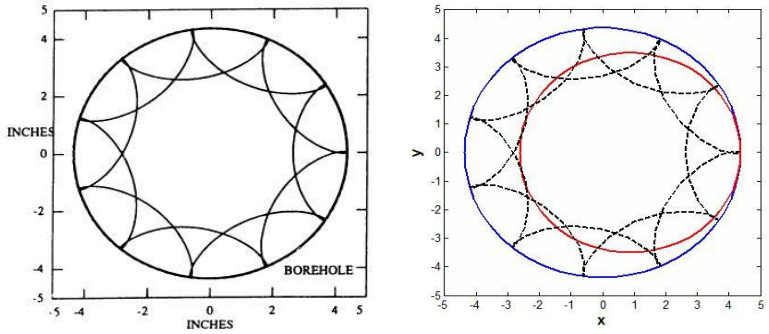

Previous study, 1989 Current study, 2014

Figure 6-3: Backward Whirl with Slip, Rotation Speed -2.2 Hz, Whirling Speed 9.9 Hz

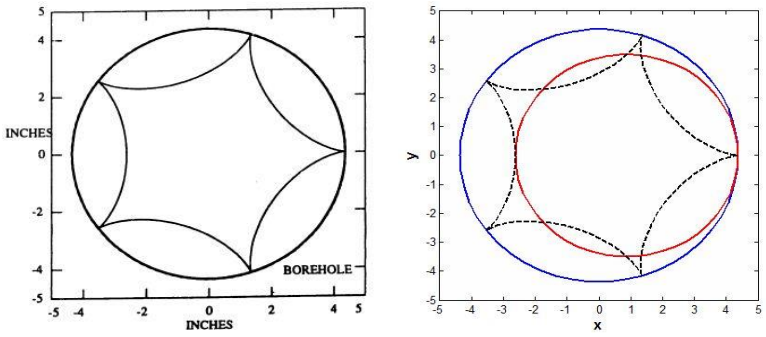

Previous study, 1989 Current study, 2014

Figure 6-4: Backward Whirl, No Slip, Rotation Speed -2.2 Hz, Whirling Speed 8.8 Hz

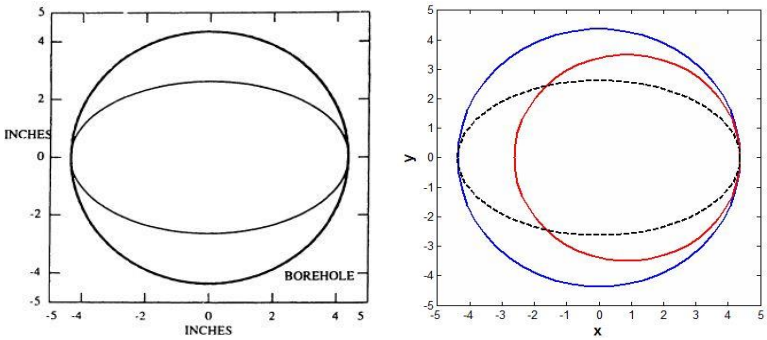

Previous study, 1989 Current study, 2014

Figure 6-5: Backward Whirl with Forward Slip, Rotation Speed -2.2 Hz, Whirling Speed 2.2 Hz

The trajectory of Point P with different slip at backward whirl was illustrated in the Figure 6-3, Figure 6-4, and Figure 6-5. It means that the direction of whirling motion is opposite to the direction of drill-pipe rotation itself. Moreover, tangential velocities of Point P showed differences for each case. Moreover, backward whirl with no slip lead to no tangential velocity as seen in Figure 6-5. In Figure 6-6, drill-pipe only rotated around center of itself; whirling motion did not occur for this case because whirling rotary speed was equal to zero.

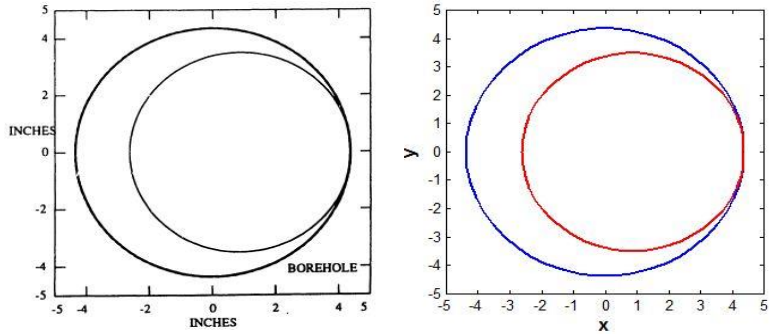

Previous study, 1989 Current study, 2014

Figure 6-6: No Whirl, Pure Rotation, Rotation Speed -2.2 Hz, Whirling Speed 0 Hz

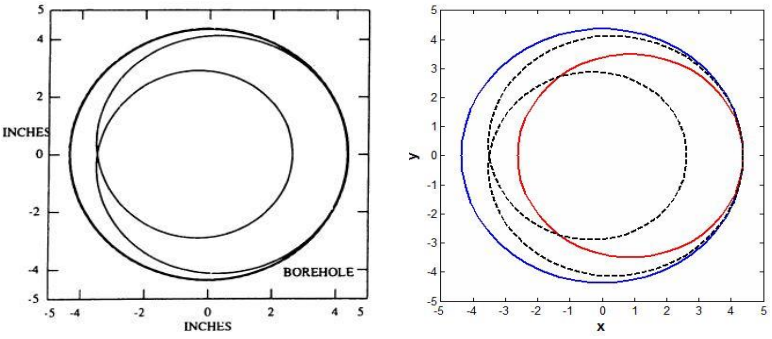

Previous study, 1989 Current study, 2014

Figure 6-7: Forward Whirl with Slip, Rotation Speed -2.2 Hz, Whirling Speed -1.1 Hz

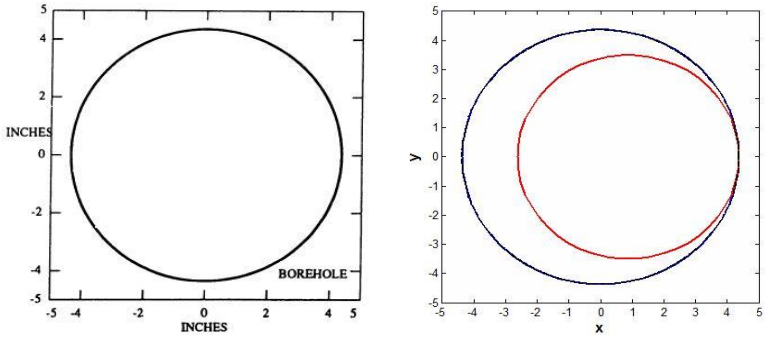

Previous study, 1989 Current study, 2014

Figure 6-8: Synchronous Whirl with Slip, Rotation Speed -2.2 Hz, Whirling Speed -2.2 Hz

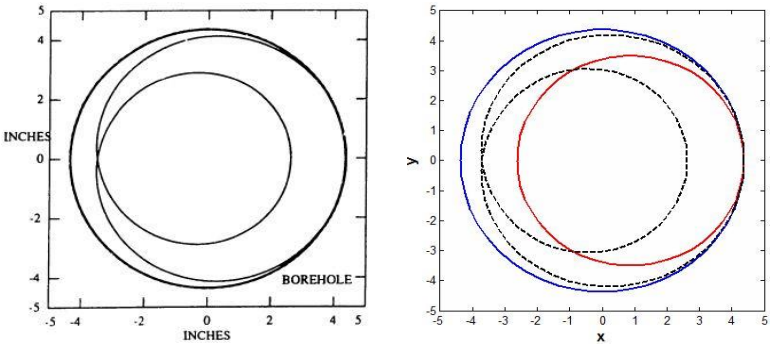

Previous study, 1989 Current study, 2014

Figure 6-9: Forward Whirl with Forward Slip, Rotation Speed -2.2 Hz, Whirling Speed -3.3 Hz

Forward whirl motion was presented in the Figure 6-7, Figure 6-8, and Figure 6-9; because the direction of drill-pipe rotation was the same with the direction of whirling rotation of drill-pipe. Additionally, trajectory of Point P traced exactly the path through the wellbore since the rotation speed and whirling speed were similar. Detailed information about the motions can be obtained from the bibliography [73].

Up to this point, modeling of turbulence flow, DEM method and orbital motion of drill-pipe were discussed in detail, and validation/verification cases were provided successfully. Now, a combination of these three approaches is firstly employed for the main purpose of the research to improve wellbore hole cleaning efficiency. It should be noted that it is assumed there is no slip/friction between the inner pipe and wellbore in the numerical simulations.

CHAPTER 7: COUPLED CFD-DEM SIMULATIONS OF WHIRLING MOTION ON HOLE CLEANING PERFORMANCE

7.1 Materials and Methods

ANSYS FLUENT^{TM} 15.0 CFD software was adopted to investigate the inner pipe rotation effect on cuttings transport performance in this study. The carrier flow containing discrete particles were modeled using Discrete Particle Model including particle interactions (DEM). Particles are tracked in the Lagrangian fashion in this approach. In the continuous phase flow, mass and momentum conservation equations were solved with the proper boundary and initial conditions. Detailed information about the theory of each model can be reached in the previous parts of this study (Chapter 4 & 5).

In this section, the computational domain between the stationary wellbore and rotating drill-pipe is demonstrated as an eccentric horizontal annulus, as presented in the Figure 7-1. The discretized annulus represents a virtual flow system which consists of the inner pipe diameter of 1.85 in and outer pipe diameter of 2.91 in. Computational length for the cuttings transport simulations is determined to be 6.56 ft in order to eliminate the ends effect and provide the fully developed flow regime. Hence, increasing annular length requires more computational effort. An unstructured hexahedral mesh of 1.6 x 10^5 elements, approximately corresponding to 14, 114, 100 nodes in the radial, azimuthal, and axial directions, respectively, were used for the simulations, as shown in the Figure 7-1. In order to solve the flow structure accurately in the near wall region, inflation layers were also generated near both the inner and outer pipes. The optimum element size was determined to be 0.002 m after conducting a mesh independence study discussed in Chapter 5 for the validation case of the experimental study carried out by Osgouei [19].

A velocity inlet boundary condition was used in order to define the drilling fluid flow rate at the inlet while a pressure outlet boundary condition with a static (zero gauge) pressure was specified at the outlet. The no-slip boundary condition was enforced at both the inner and outer pipe walls for the wall boundary conditions. Specified boundary conditions for this study are demonstrated in the Figure 7-1.

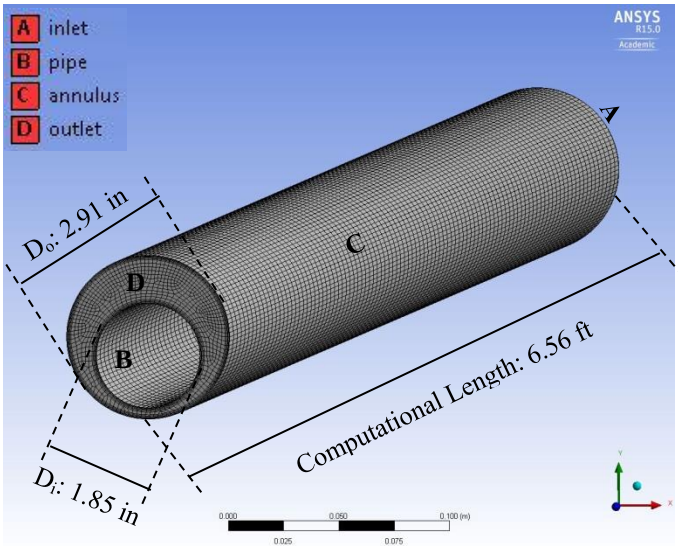

Figure 7-1: 3D section of computational grid for the eccentric horizontal annulus

The numerical calculations were implemented using the pressure discretization scheme following the Second-Order routine. For the pressure-velocity coupling the SIMPLE algorithm was employed. Since the drilling fluid charging rate is varied to involve the laminar, transient and fully turbulent regions, the shear stress SST k-ω turbulence model was conducted for the turbulent flow simulations. The flow regime was determined laminar for the fluid velocity of 3 ft/s; transient for 4 and 5 ft/s, and fully turbulent for 6 and 7 ft/s based on the Reynolds Number of the particular fluid. The equations of mass, momentum, turbulent kinetic energy and turbulent dissipation rate were discretized using the QUICK scheme. The solution converged when the convergence criteria of 10^{-4} residual error was reached for all multiphase flow simulations.

Particles were randomly injected from the inlet boundary corresponding to "A" section illustrated in the Figure 7-1. Injection file for each simulation was generated by a simple MATLAB script to ensure non-uniform distribution of particles in the inlet surface with changing location of the drill-pipe due to the orbital motion. After generated particle injection file, it was implemented in Fluent for coupled CFD-DEM simulations. A format of each line is mentioned in section 25.3.12 of Fluent 14 User's Guide [54]. It should be noted that particle injection locations are fixed by the x, y, z coordinates specified in the injection file. They are not updated as the mesh is moving. In fact, this is one of the reasons to use a file injection.

The overall process for file injection is as follows:

1) Injection file was generated such that all seed points cover the entire cross section of the outer diameter. This means that some seed points may fall inside the inner pipe diameter. At each injection event, Fluent automatically discards the parcels which are injected outside the domain. Since the cross section keeps changing, some seed points may fall within the domain at an instance and fall outside the domain at another. However, the mean injected mass flow rate would reach a steady value over a long period of time.

2) Appropriate number of seed points was computed with respect to drilling rate. Hence, particle injection rate was determined with respect to rate of penetration, and computed as 0.10534 kg/s for ROP of 105 ft/hr.

3) Mass flow rate was calculated so that the chosen time step size results in the desired "parcel diameter". Specifically for DEM, as mentioned earlier, the collisions are between "parcels" and not "particles". Hence, for DEM simulations, one particle per parcel was used in this study for physical description of the DEM method.

4) A high value for "end time" was used for injection so that parcels being injected at every injection event were visible. Particle injections ended when the number of particles stopped changing in the numerical setup as the steady state condition was reached.

As discussed earlier, the current model setup was validated with the experimental study carried out by Osgouei [19] for annular pressure drop and cuttings concentration in an eccentric horizontal well, and reported in Chapter 5. After satisfactory agreement with the experimental data was achieved, the numerical setup was adopted for the main scope of this study so that the effect of inner-pipe rotation on cuttings transport performance in eccentric horizontal wells would be investigated. Table 7-1 summarizes the rheological properties and drilling parameters for the current model setup.

Table 7-1: Coupled CFD-DEM simulation data for cuttings transport simulations

Rheological Properties & Drilling Parameter	Power-Law Drilling Fluid	Unit
	Continuous Phase	
Fluid Density	8.345	ppg
Flow Behavior Index, n	0.51	
Viscosity Consistency, K	0.092	lb s^n /100 ft^2
Fluid Velocity	3, 4, 5, 6, 7	ft/s
Inner Pipe Rotation	0, 80, 120, 200	rpm
Diameter Ratio, κ	0.7	
Eccentricity, e	0.623	
ROP	105	ft/h
	Discrete Phase	
Cutting Density	23.045	ppg
Average Cutting Size	0.079	in

In order to define performance measures on cuttings transport, annular frictional pressure losses, cuttings concentrations and average cuttings transport velocities with respect to the average fluid velocities are determined for different inner pipe rotary speeds. Cuttings concentrations are calculated with regards to the number of particles in the annulus after the steady-state condition is reached. Ratio between the volume of particles and total volume of the annulus designates the cuttings concentration in the virtual flow system. In addition, cuttings transport velocity is defined the velocity of a particle in the axial direction. Particle transport velocity is calculated based on the forces acting on an individual particle in the flow direction.

For the post-processing analysis, the annuli were divided into 8 sectors, and certain calculations for cuttings concentration were computed for each sector, as shown in the Figure 7-2. It is assumed that this configuration represents the rear view in which sectors are divided

through the outlet boundary. In the analysis, cardinal directions – east, north, west, and south – (going counterclockwise) were also used to simplify the expression of particle location. In other words, 0°, 90°, 180°, and 270° represent the east, north, west, and south respectively as seen in the Figure 7-2. In order to specify the sectors, angular distance of any particle to the center of the wellbore is calculated, and the angle is determined based on the distance and local coordinates of the particle. For instance, cuttings are placed in sector 1 if the angle is between 0° and 45°. Concept of the Figure 7-2 is used to analyze the data for determining the position of individual particles.

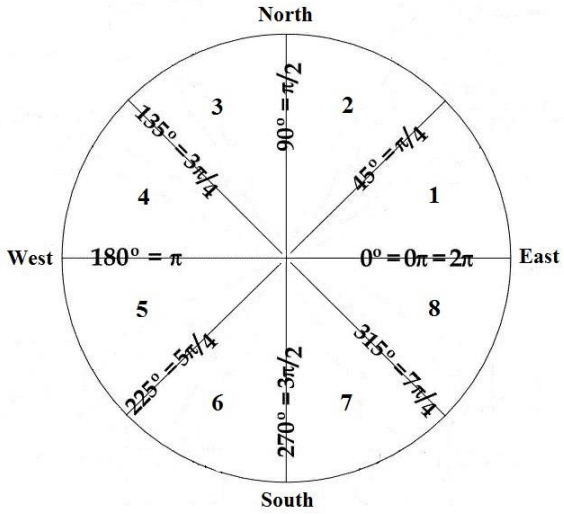

Figure 7-2: Annulus is composed of a series of sector division for particle data analysis

In order to analyze the effect of inner pipe rotation on cuttings transport performance, a step wise approach was implemented.

- First, inner pipe rotation speed was changed from 0 to 200 rpm with various fluid velocities between 3 ft/s to 7 ft/s, including laminar, transient and fully turbulent flow regimes. Other drilling parameters were kept constant, and the whirling motion was not included in this part. It was aimed at quantitatively investigating the influence of drill-pipe rotation itself on annular pressure losses, cuttings concentration and average cuttings transport velocity by case studies.

- Second, with respect to the main scope of the work, whirling motion was taken into account. Drill-pipe rotary speed was kept constant at 80 rpm, and whirling speed and direction were changed in order to examine the importance of whirling rotation on hole cleaning. Backward and forward whirl was adopted at different whirling speeds: whirling speed was either less than or more than the inner pipe rotary speed. Whirling speed of 120 rpm was determined based on the knowledge gained from the literature [71]. In order to see the effects of different whirling speed and direction on cuttings transport performance, other whirling speeds were set for the calculations. Backward and forward whirl was determined in regards to the direction of the rotation. For the synchronous whirl, inner pipe rotary speed and rotary direction was determined similar to the inner pipe rotary speed and direction.

Current simulation data for the parametric study to observe the effect of various whirling cases on the particle behavior in an eccentric horizontal well is summarized in Table 7-2. Inner-pipe only rotates around its own axis in Case #1; whirling motion is not applied here. Nevertheless, different types of whirling motion are implemented in Case #2-4 by keeping the inner-pipe rotary speed and direction constant as already discussed.

Table 7-2: Different scenarios for whirling motion of rotating drill-pipe

#	Case	Fluid Velocity, ft/s	Rotation Speed, RPM	Whirling Speed, RPM
1	No Whirl, Pure Rotation	3, 4, 5, 6, 7	0, 80, 120, 200	0
2	Backward Whirl	3, 4, 6	80	-40 -120
3	Forward Whirl	3, 4, 6	80	-40 -120
4	Synchronous Whirl	3, 4, 6	80	80

7.2 Results and Discussion

7.2.1 No Whirl, Pure Rotation

Drill-pipe rotation is provided by defining the inner pipe as a rotationally moving wall in the current model, and it is forced to rotate only on its own axis in the clockwise direction while the outer pipe is stationary. In an eccentric horizontal well, it is believed that orbital motion of drill-pipe around the wall of the wellbore is observed during drilling; however, dynamic behavior of drill string causing whirling motion is ignored initially. It can be assumed that centralizers were used to restrict the inner pipe to rotate around its own axis.

Annular frictional pressure losses increase with increasing rotary speed as seen in Figure 7-3. At higher flow rates, effect of inner pipe rotation on pressure drop is more pronounced. In addition to pipe rotation, it was also observed that fluid velocity plays a significant role on frictional pressure losses at any rotary speed. During drilling, bottom-hole pressure is directly related to annular pressure losses. In consequence, fluid velocity significantly alters bottom-hole pressure (BHP) at any rotation speed. This behavior can be explained with the formation of Taylor vortices during the rotation because of the centrifugal forces and shear instabilities [74]. Rotation of drill-pipe generates unstable flow which leads to an increase in annular pressure losses.

Drill-pipe rotation, however, had a negative effect on pressure drop at the lower fluid velocity, in which the flow regime was laminar as shown in the Figure 7-3. This situation explains that drill-pipe rotation increases the shear rate and reduces the viscosity due to the shear thinning behavior of the drilling fluid. Therefore, annular frictional pressure reduces with increasing pipe rotation because shear thinning is more predominant than inertial effects. This phenomenon is completely different in turbulent flows as indicated earlier. Flow is destabilized with the inner pipe rotation, and some additional energy is contributed to the flow structure. This “turbulent like” flow causes an increase in pressure drop while rotating drill-pipe because inertial effects become more dominant than shear thinning in this case [75].

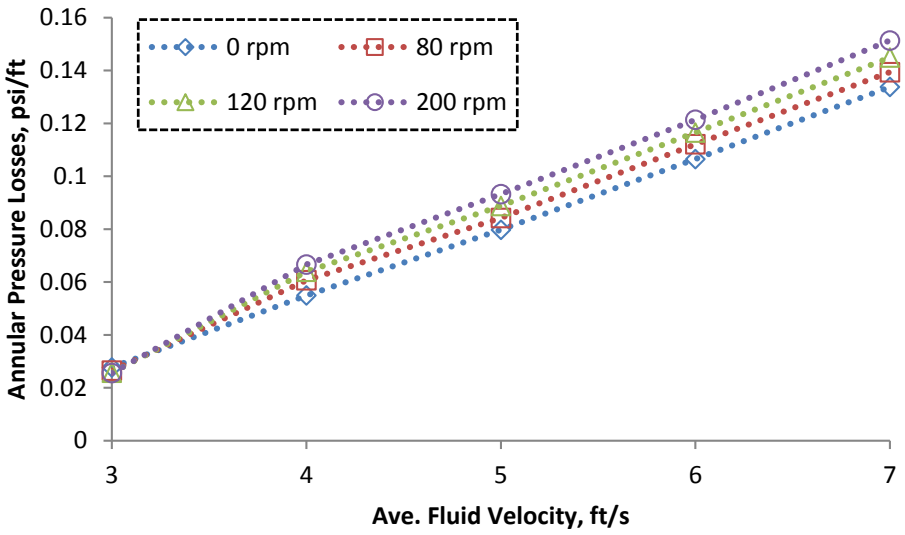

Figure 7-3: Annular pressure losses as function of fluid velocity and pipe rotation without particle injection

With respect to the purpose of this study, cuttings were injected continuously according to the penetration rate. As seen in the Figure 7-4, not only does an increasing fluid velocity lead to significant increment in the annular pressure drop, but frictional losses also increase at higher rotary speeds when the flow is transient and fully turbulent. Hence, it was observed that the presence of cuttings resulted in higher annular frictional losses. This result is expected because cuttings increase the drag force and skin friction in the fluid-solid multiphase flow system. Furthermore, cuttings tend to deposit on the lower side of the annulus in eccentric horizontal wells because of gravity. When the axial flow is present, energy coming from the pump is consumed by the accumulated cuttings so that they could accelerate.

Also, momentum and energy are dissipated with particle-particle and particle-wall collisions. Therefore, additional increase in pressure drop occurs due to the contribution of the cuttings. Increasing pressure losses adversely impact the formation pressure; thereby, drilling parameters which cause an increase in pressure drop must be controlled during drilling. In particular, high drill-pipe rotation may result in an increase in equivalent circulating density (ECD) because of the high annular pressure losses. This can be prevented by adjusting the pumping rate and drilling fluid density. This is a complex situation because reducing fluid velocity would result in increasing cuttings concentration as seen in the Figure 7-5. Thereby, an optimization is needed for safe drilling and effective hole cleaning.

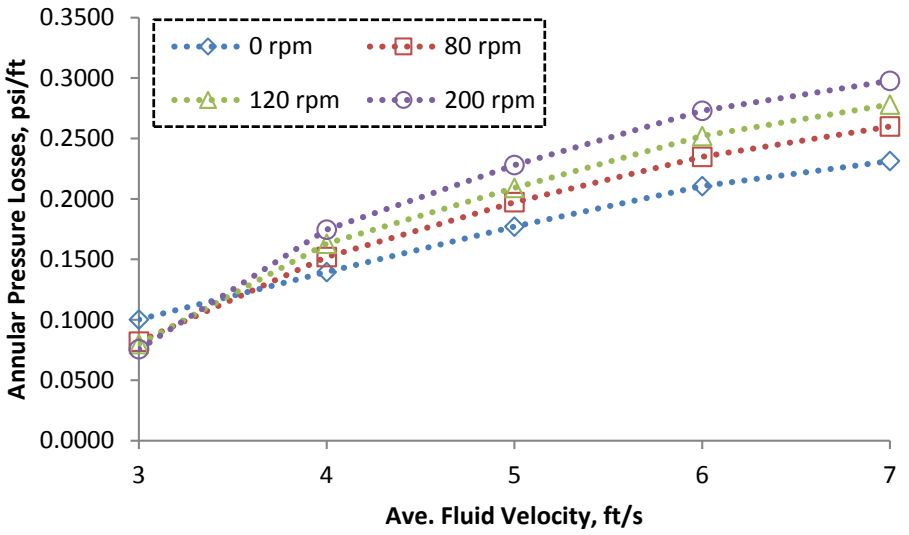

Figure 7-4: Annular pressure losses as function of fluid velocity and pipe rotation with particle injection rate of 0.105 kg/s

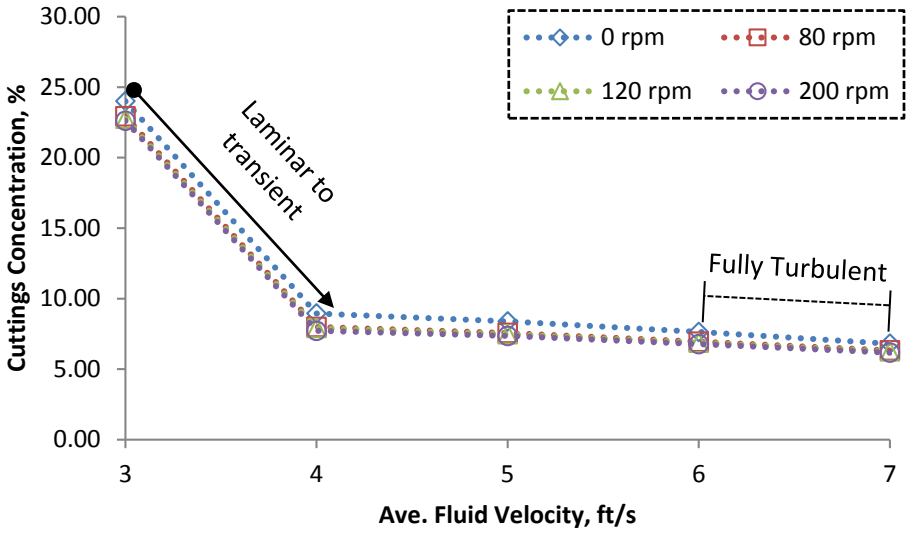

Figure 7-5: Cuttings concentration as function of fluid velocity and drill-pipe rotation

Fluid velocity is a major factor on cuttings transport. At lower flow rates, cuttings concentration is dramatically higher than in higher flow rates. It should be noted that cuttings are carried sufficiently when the flow becomes turbulent as indicated in Figure 7-5. Beyond that, increasing fluid velocity may be restricted by various factors during drilling such as, maximum allowed ECD, and availability of hydraulic power. Additionally, at high flow rates, the cuttings

concentration decreases slightly with increasing flow rate. On the contrary, it is emphasized that drill-pipe rotation does not have a significant influence on the cuttings concentration at any flow rate. Reduction in cuttings concentration is more apparent when drill-pipe rotary speed changes from 0 rpm to 80 rpm. After 80 rpm rotary speed, there is no remarkable effect of drill-pipe rotation on the cuttings volume fraction. This behavior can be seen in Figure 7-6.

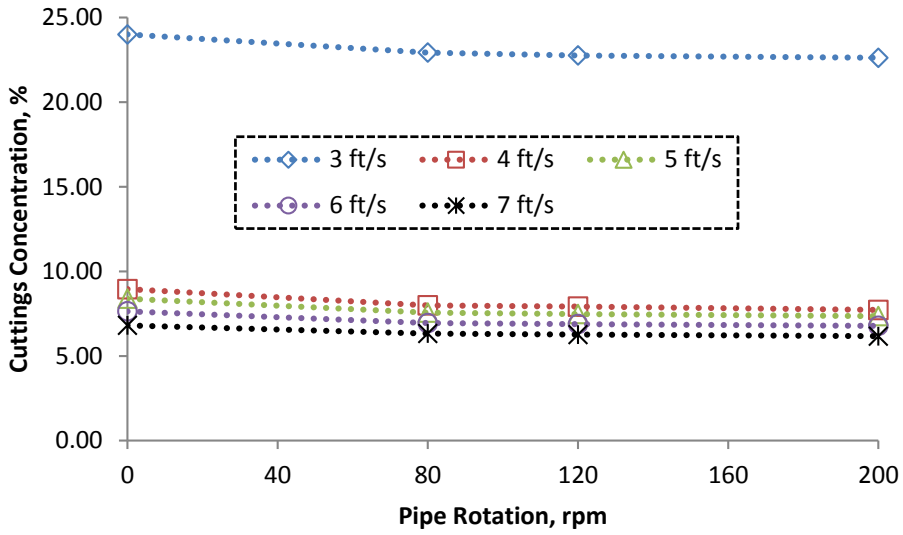

Figure 7-6: Variation of cuttings concentration with rotational speed at various fluid velocities

It is also noted that increasing fluid velocity shows the same pattern for average cuttings transport velocity as seen in the Figure 7-7. To clarify, increasing pumping rate increases the cuttings transport efficiency. The more significant increments in the average cuttings transport velocity are observed where the flow regime changes from laminar to transient. Furthermore, rotation of drill-pipe increases the average cuttings transport velocity especially at higher flow rates, while effect of rotary speed on transport velocity can be neglected at lower flow rates. The effect of drill-pipe rotation on the average cuttings transport velocity is found to be more important when the rotary speed varies between 0 - 80 rpm. There is no significant changes on the average cuttings transport velocity after rotary speed of 120 rpm.

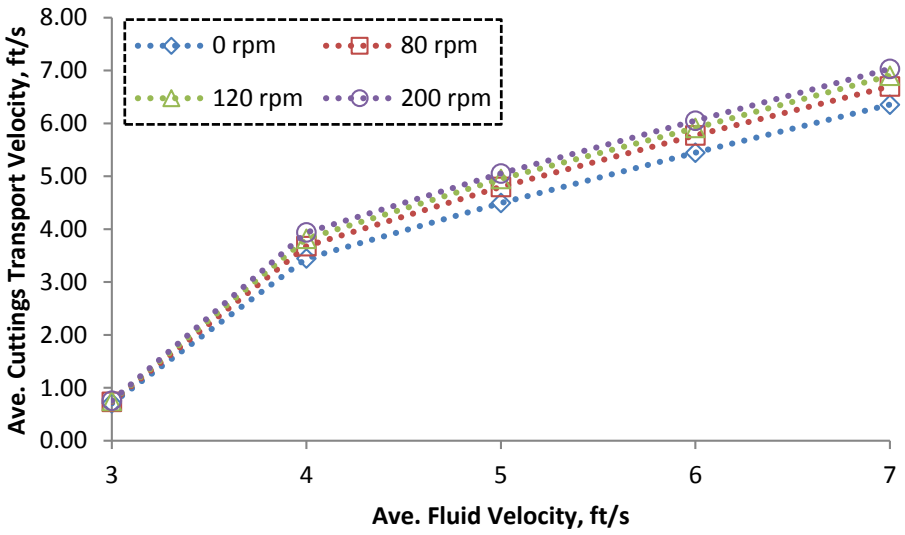

Figure 7-7: Variation of cuttings transport velocity with rotational speed and flow rate

Another important observation on the effect of inner pipe rotation on cuttings transport for different flow regimes can be demonstrated in Figure 7-8 through Figure 7-12. Cuttings are mostly deposited on the lower side of the annulus at a fluid velocity of 3 ft/s where the flow is laminar. Due to the eccentricity, fluid velocity is insufficient to carry cuttings through the narrow part. This results in high cuttings accumulation in the small gaps at lower fluid velocities. In sector 2 and 3, there is only a small amount of particles in the suspension regime. With increasing rotary speed, cuttings tend to move tangentially with respect to the direction of the rotation. As pointed out in the Figure 7-8, the number of particles increases in the sectors 3, 4, 5 and 6 due to the rotation, while the number of particles decreases in the sectors 7 and 8. Rotary speed does not significantly alter the number of particles in sector 7, as can be observed from the particular figure.

Furthermore, at high fluid velocities, it is indicated that cuttings become more dominant in the suspension region. However, cuttings deposit in the narrow part of the annulus when the fluid velocity is low and the drill-pipe does not rotate. On the contrary, increasing flow rate creates a better hole cleaning as a result of the turbulent flow behavior. Therefore, cuttings are mostly suspended, and a proper hole cleaning is achieved at higher fluid velocities in these circumstances. Increasing rotary speed also shows similar pattern at higher velocities as seen in the Figure 7-9 through Figure 7-12.

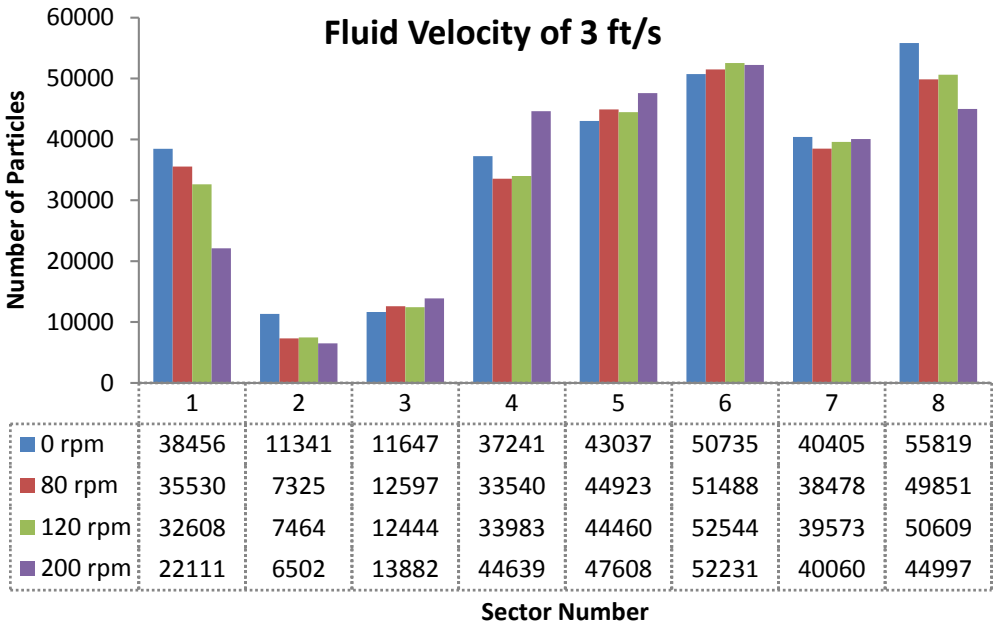

	1	2	3	4	5	6	7	8
0 rpm	38456	11341	11647	37241	43037	50735	40405	55819
80 rpm	35530	7325	12597	33540	44923	51488	38478	49851
120 rpm	32608	7464	12444	33983	44460	52544	39573	50609
200 rpm	22111	6502	13882	44639	47608	52231	40060	44997

Figure 7-8: Particle distribution along sectors at fluid velocity of 3 ft/s with rotational speed 0 to 200 rpm

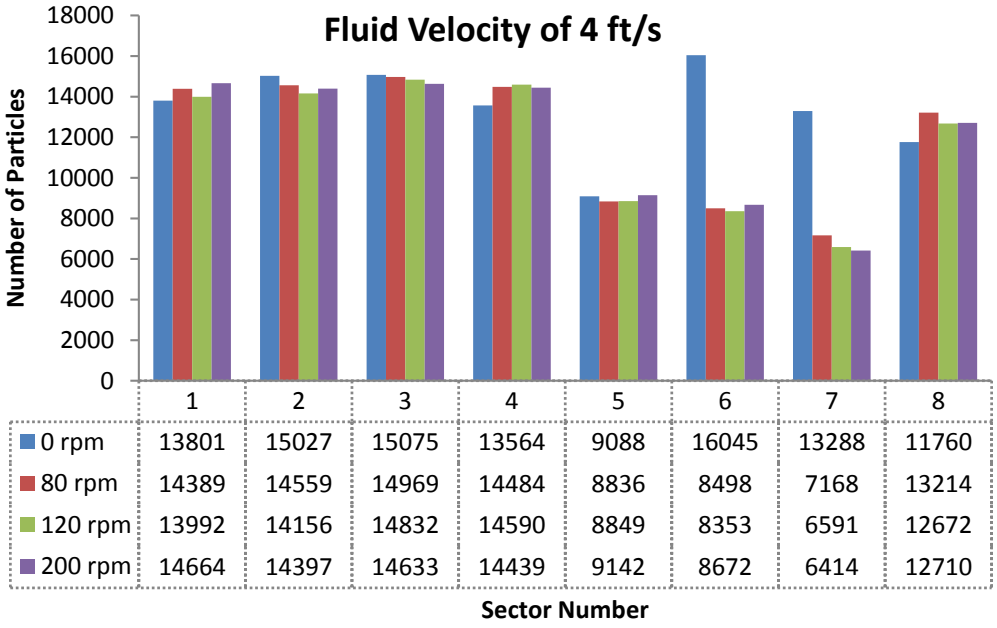

	1	2	3	4	5	6	7	8
0 rpm	13801	15027	15075	13564	9088	16045	13288	11760
80 rpm	14389	14559	14969	14484	8836	8498	7168	13214
120 rpm	13992	14156	14832	14590	8849	8353	6591	12672
200 rpm	14664	14397	14633	14439	9142	8672	6414	12710

Figure 7-9: Particle distribution along sectors at fluid velocity of 4 ft/s with rotational speed 0 to 200 rpm

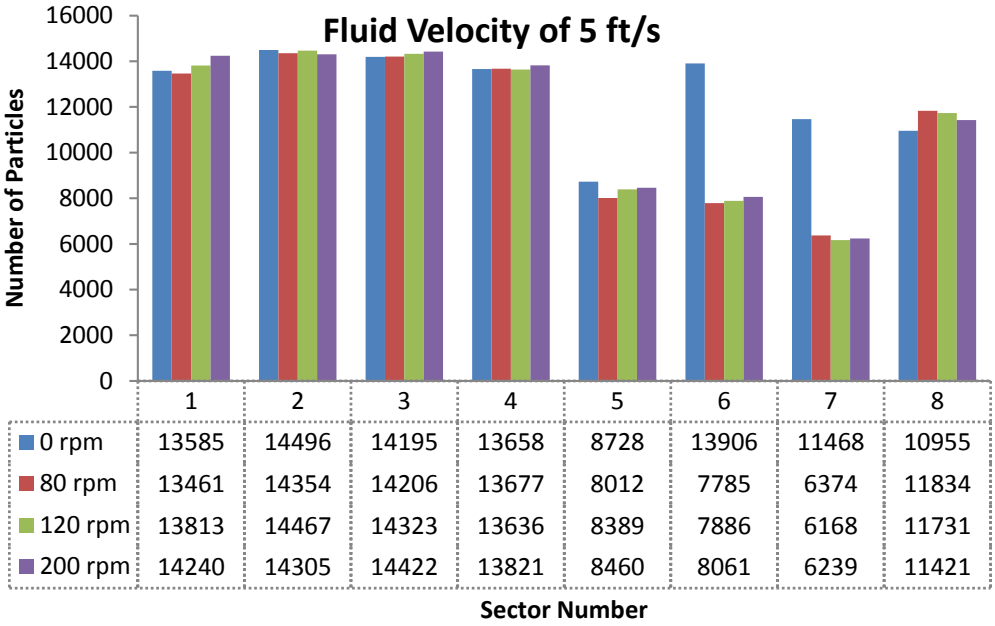

Figure 7-10: Particle distribution along sectors at fluid velocity of 5 ft/s with rotational speed 0 to 200 rpm

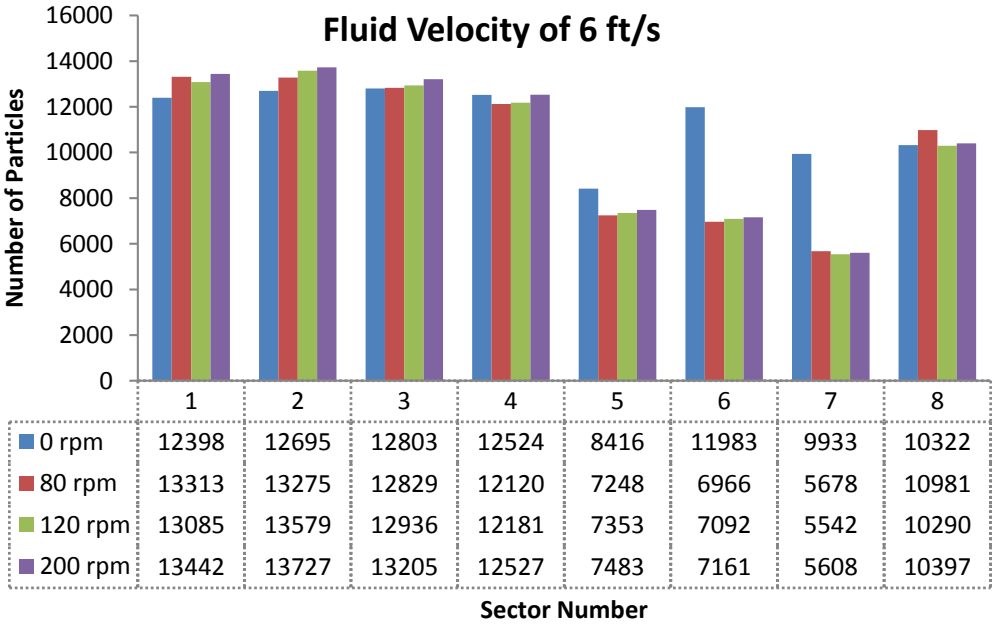

Figure 7-11: Particle distribution along sectors at fluid velocity of 6 ft/s with rotational speed 0 to 200 rpm

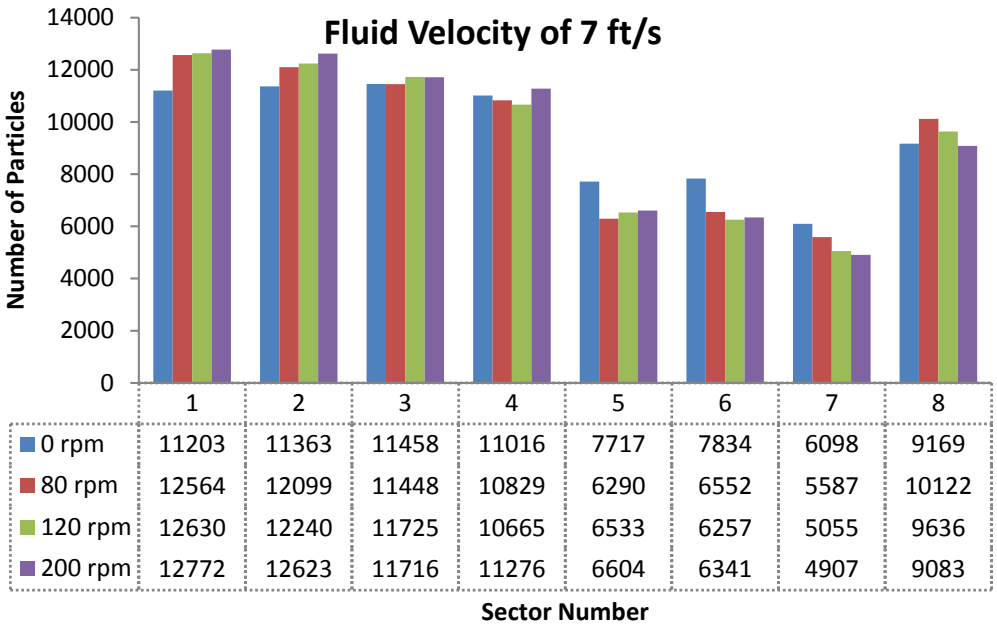

	1	2	3	4	5	6	7	8
0 rpm	11203	11363	11458	11016	7717	7834	6098	9169
80 rpm	12564	12099	11448	10829	6290	6552	5587	10122
120 rpm	12630	12240	11725	10665	6533	6257	5055	9636
200 rpm	12772	12623	11716	11276	6604	6341	4907	9083

Figure 7-12: Particle distribution along sectors at fluid velocity of 7 ft/s with rotational speed 0 to 200 rpm

Trajectory of cuttings and streamlines of fluid velocities in the eccentric annulus were also investigated in this study, as illustrated in the Figure 7-13 through Figure 7-16. Effect of rotary speed and flow rate on cuttings transport can be better understood by analysis of these demonstrations. First, it is important to emphasize that stationary cuttings bed occurs in the narrow part of the eccentric annulus at low flow rates. Particularly, a fluid velocity of 3 ft/s is the worst scenario for a proper hole cleaning among the cases, because cuttings dramatically settle down and block the well. Increasing flow rates prevents the cuttings bed formation and contributes to cuttings transport. Otherwise, effect of drill-pipe rotation on cuttings removal is not as significant as regarding the cutting concentration. Furthermore, tangential velocity of the inner pipe is observed near the drill-pipe with the rotation. Due to the shear thinning behavior of the drilling fluid, drilled cuttings are tangentially dragged by the viscous forces. This slightly increases the cuttings transport with rotation because cuttings close to the drill-pipe are dragged into the suspension with rotation. However, inadequate tangential velocity leads to insufficient hole cleaning as a result of inability to carry cuttings into the main fluid flow stream. Hence, those cuttings tend to deposit and form a stationary bed in the lower part of the annulus.

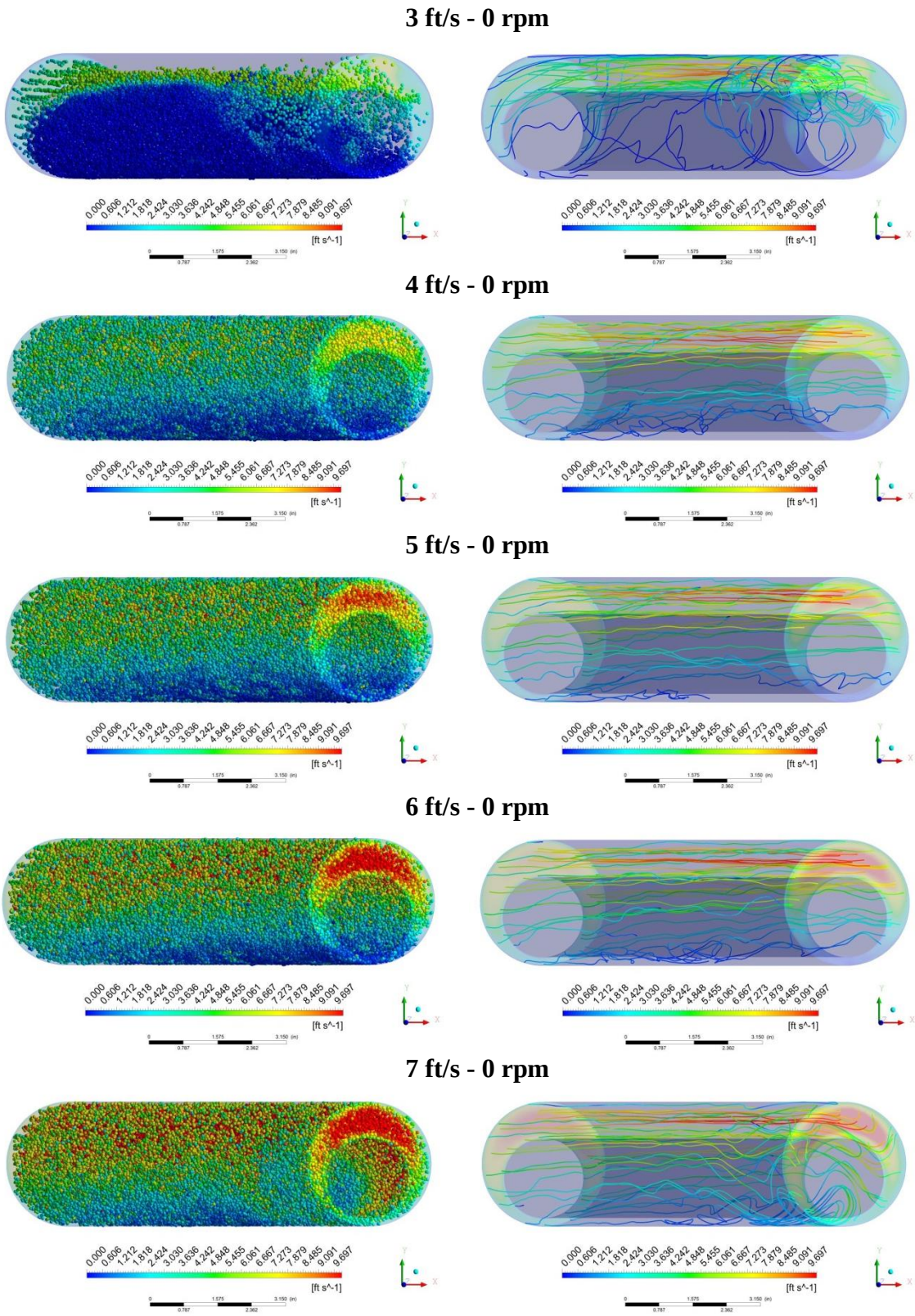

Figure 7-13: Trajectory of particles and 3D streamlines of fluid velocity for varying fluid velocity at rotary speed of 0 rpm

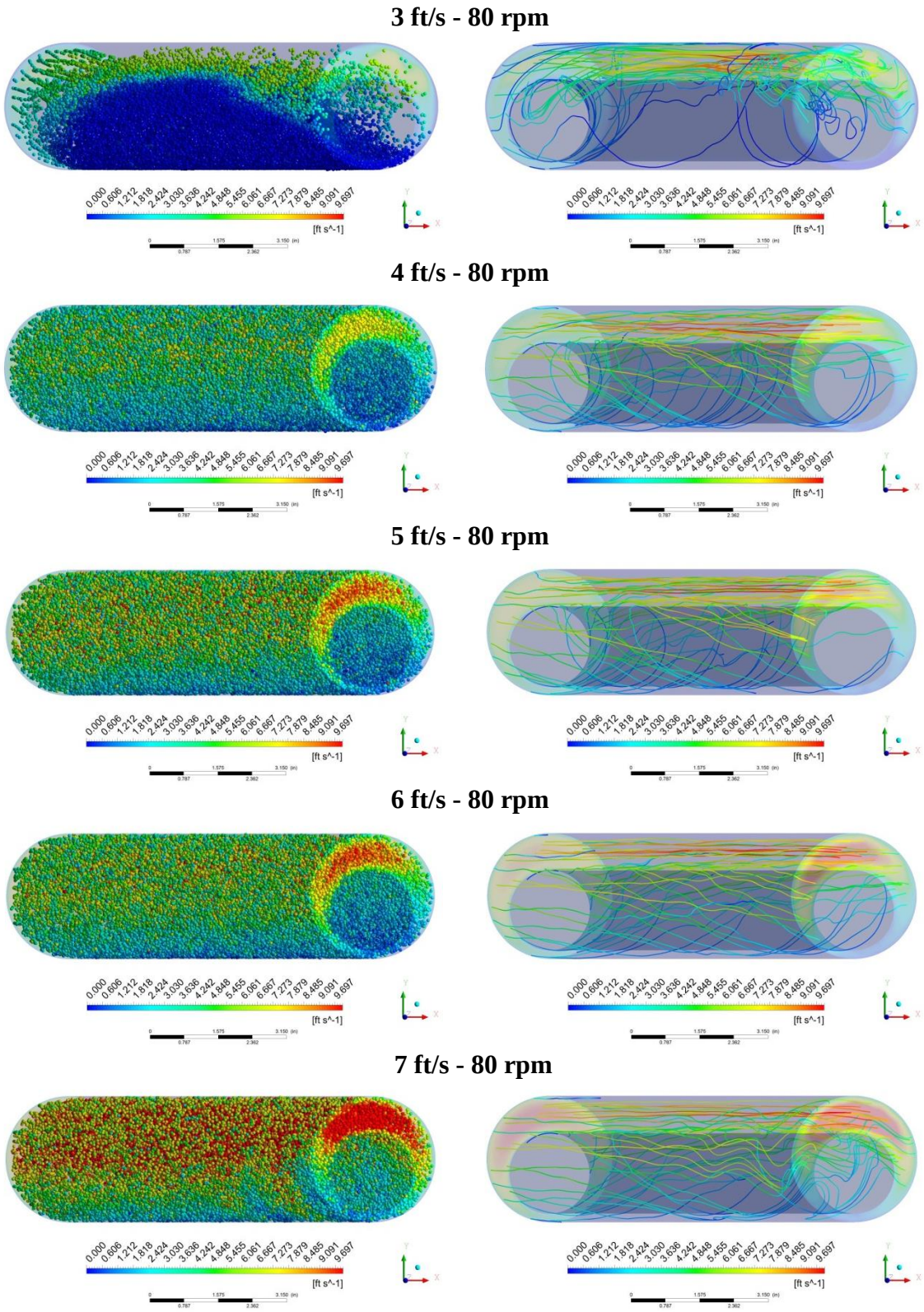

Figure 7-14: Trajectory of particles and 3D streamlines of fluid velocity for varying fluid velocity at rotary speed of 80 rpm

3 ft/s - 120 rpm

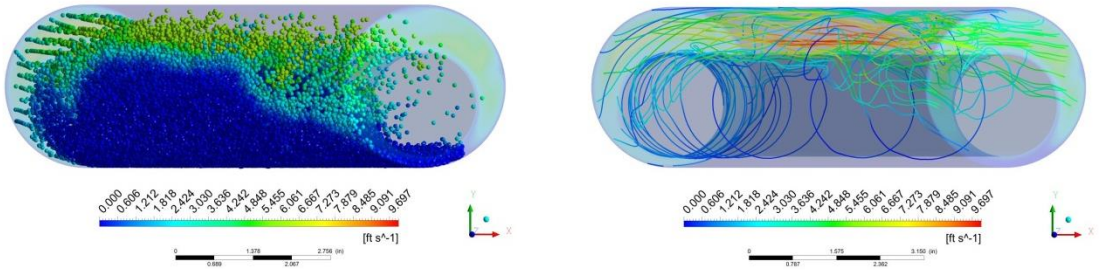

4 ft/s - 120 rpm

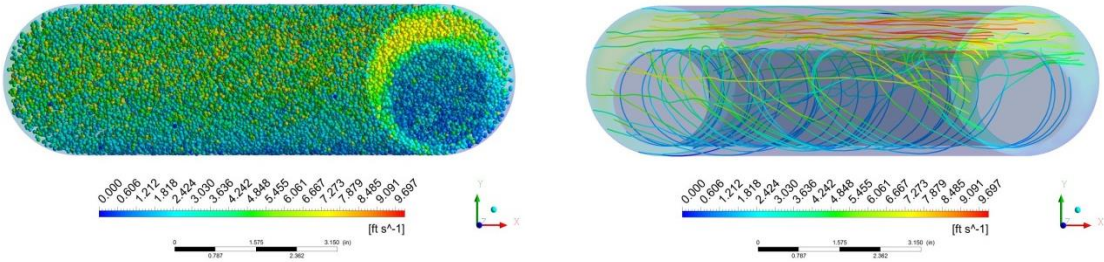

5 ft/s - 120 rpm

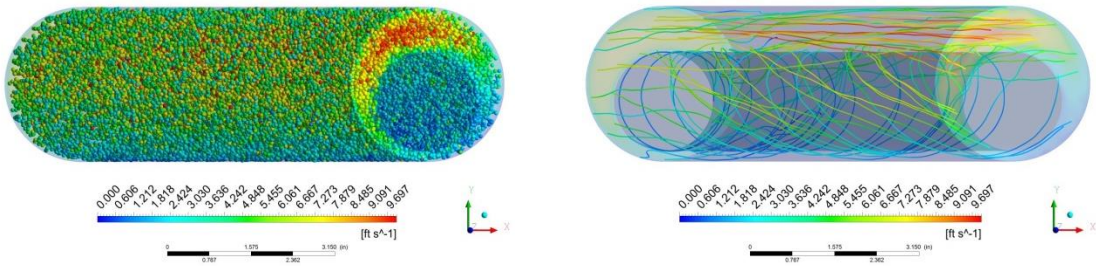

6 ft/s - 120 rpm

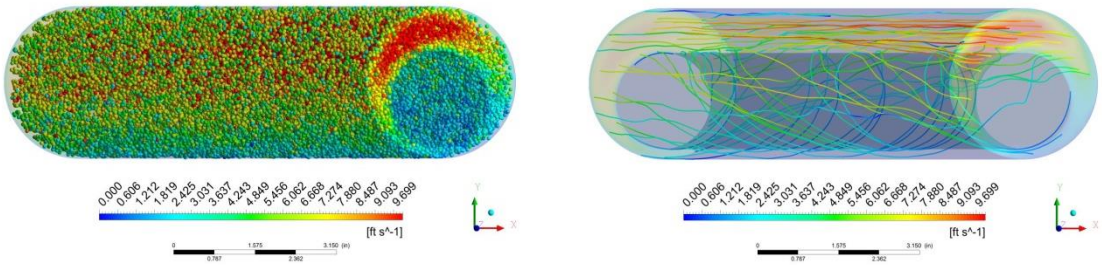

7 ft/s - 120 rpm

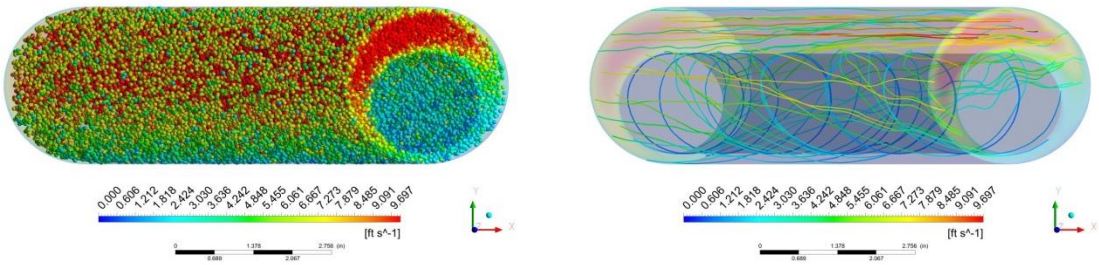

Figure 7-15: Trajectory of particles and 3D streamlines of fluid velocity for varying fluid velocity at rotary speed of 120 rpm

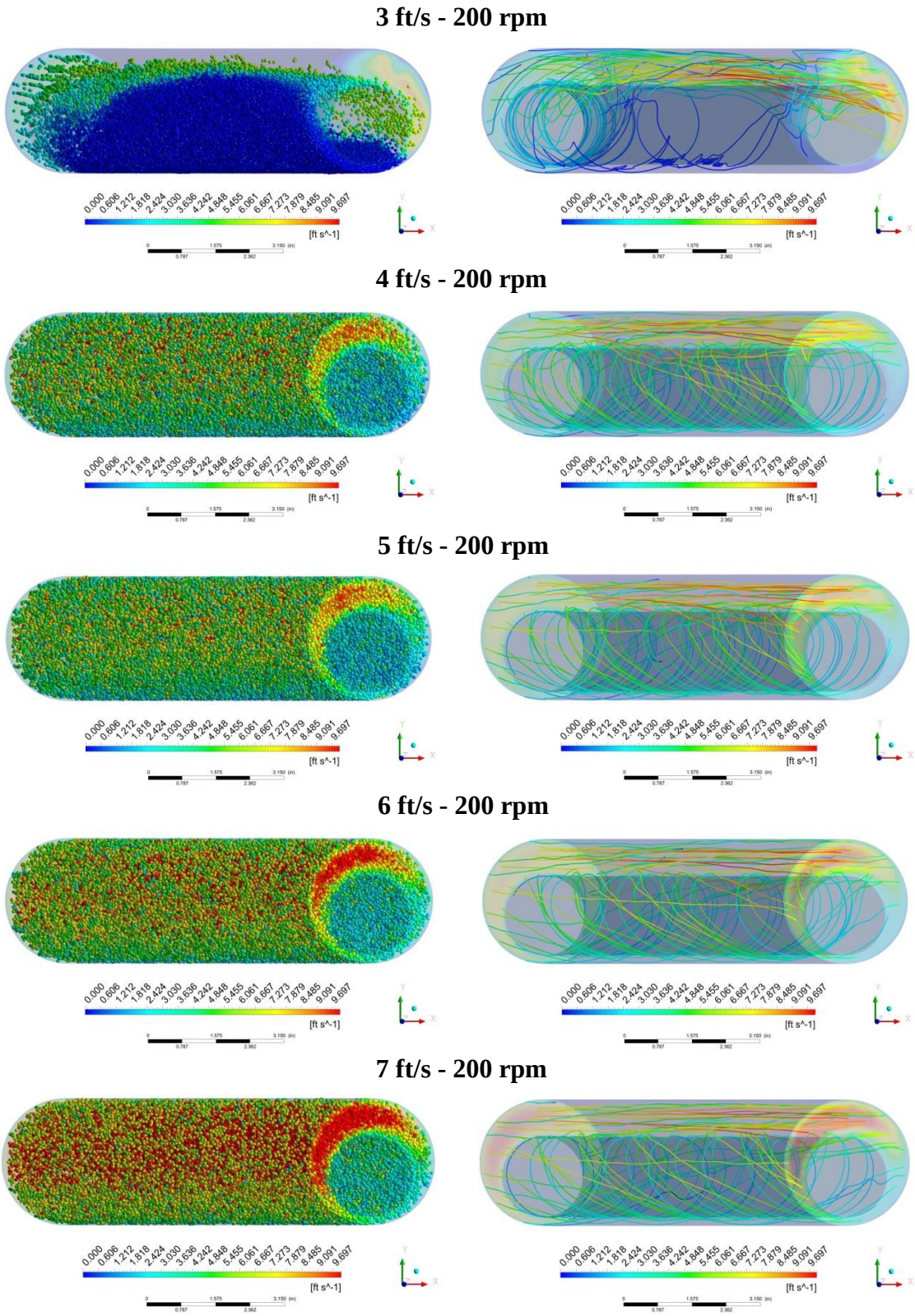

Figure 7-16: Trajectory of particles and 3D streamlines of fluid velocity for varying fluid velocity at rotary speed of 200 rpm

According to these results, drill-pipe rotation does not have significant effect on cuttings concentration if it rotates on its own axis. Fluid velocity is found to be one of the major parameters that have a critical role on cuttings concentration and average cuttings transport velocity in this study. Cuttings tend to sway tangentially from one side to another side due to drill-pipe rotation. This can be explained in more detail as inner pipe rotation creates a rotating zone close to the drill-pipe. The narrow part of the annulus is affected by the rotation while the larger one is not. Axial velocity is more dominant than the tangential velocity in the larger section of the annulus. Therefore, the location of the cuttings in the smaller gaps migrates towards the larger area as a result of fixed rotation. This phenomenon does not causes significant improvement of hole cleaning. However, it is believed that drill-pipe rotation has a crucial impact on hole cleaning in inclined and horizontal wells. Due to the eccentricity and dynamic behavior of the drill string, the inner pipe makes an orbital motion, and it generates a whirling motion which increases cuttings transport efficiency. Whirling motion improves the hole cleaning performance considering that mechanical agitation of the drill-pipe sweeps the cuttings from the narrow section of the annulus into the larger area in which the fluid velocity is higher. In addition, whirling generates helical motion that enhances the motion of the particles and reduces cuttings concentration.

In the following parts, different types of whirling motion with a constant pipe rotary speed are studied for cuttings transport performance. Whirling motion is assumed to occur under some conditions: dynamic loads and eccentricity as already discussed in the Chapter 6.

It is believed that one of the major contributors to provide an effective hole cleaning is originated from the dynamic behavior of drill-pipe in which snaking and/or whirling motion is produced. Backward whirl (Sign convention -), where the whirling motion has a counterclockwise direction while the drill-pipe rotates clockwise is investigated here. Whirling motion and drill-pipe rotation is towards the same direction in the forward whirl (Sign convention +). If the drill-pipe rotary speed and direction is equal to whirling rotary speed and direction, synchronous whirl is present. Inner pipe rotary speed and fluid velocity are kept constant at 80 rpm. Different flow regimes were also considered for any mode of whirling; therefore, 3ft/s, 4 ft/s and 6 ft/s of fluid velocities were used in order to analyze the effect of flow rates on orbital motion of drill-pipe. More parameters such as fluid rheology, eccentricity, inclination, and cuttings size and shape could be investigated on cuttings transport performance;

however, running of the numerical simulations are computationally expensive. For instance, a run for the backward whirl with 40 rpm whirling speed takes approximately 30 hours with 128 processors by using LSU HPC resources. Hence, only different types of whirling motion and speed could be analyzed on hole cleaning efficiency in this study.

In the first case, whirling speed was taken 40 rpm which is half of the drill-pipe rotary speed. In the second case, whirling speed was assumed to be 120 rpm which is 1.5 times faster than the inner pipe rotary speed. Orbital movement may change during the drilling depending on the dynamic buckling of the drill-pipe and eccentricity. Therefore, whirling speed may be less or faster than the fixed inner pipe rotary speed. Simulations are performed until the drill-pipe makes 4 whole cycles; therefore, the residence time of the cuttings may be different for any simulation. Numerical simulations are aimed at predicting the annular friction pressure losses, cuttings concentration and average cuttings transport velocities after a certain number of whirling motions around the center of borehole is carried out due to the eccentricity.

Drill string motion at different whirling types was also investigated before analyzing the data. Trajectory of drill-pipe was provided by selecting a point on the drill-pipe, and its motion was traced during the rotation. Snapshots of backward, forward and synchronous whirl after 4 whole cycles are depicted in Figure 7-17. For the backward whirl, lateral deflection is more pronounced when the whirling speed is 120 rpm and drill string rotary speed is 80 rpm. In other words, backward whirl motion fills the space more than forward and synchronous whirling motions. However, the frequency of the drill-pipe motion is greater for 4 whole cycles when the whirling speed is 40 rpm and the drill string rotary speed is 80 rpm because the drill-pipe rotates more than whirling motion. Moreover, the trajectory pattern of the drill-pipe for the forward whirl is observed to be similar even though the whirling speed is either 40 rpm or 120 rpm while the drill-pipe rotary speed remains at 80 rpm. However, the number of completed patterns for the 40 rpm scenario is more than what is completed for the 120 rpm within the same time frame. Whirling speed is more dominant when the whirling speed is more than the rotary speed. At synchronous whirl, lateral deflection in the trajectory is at a minimum as seen in the Figure 7-17.

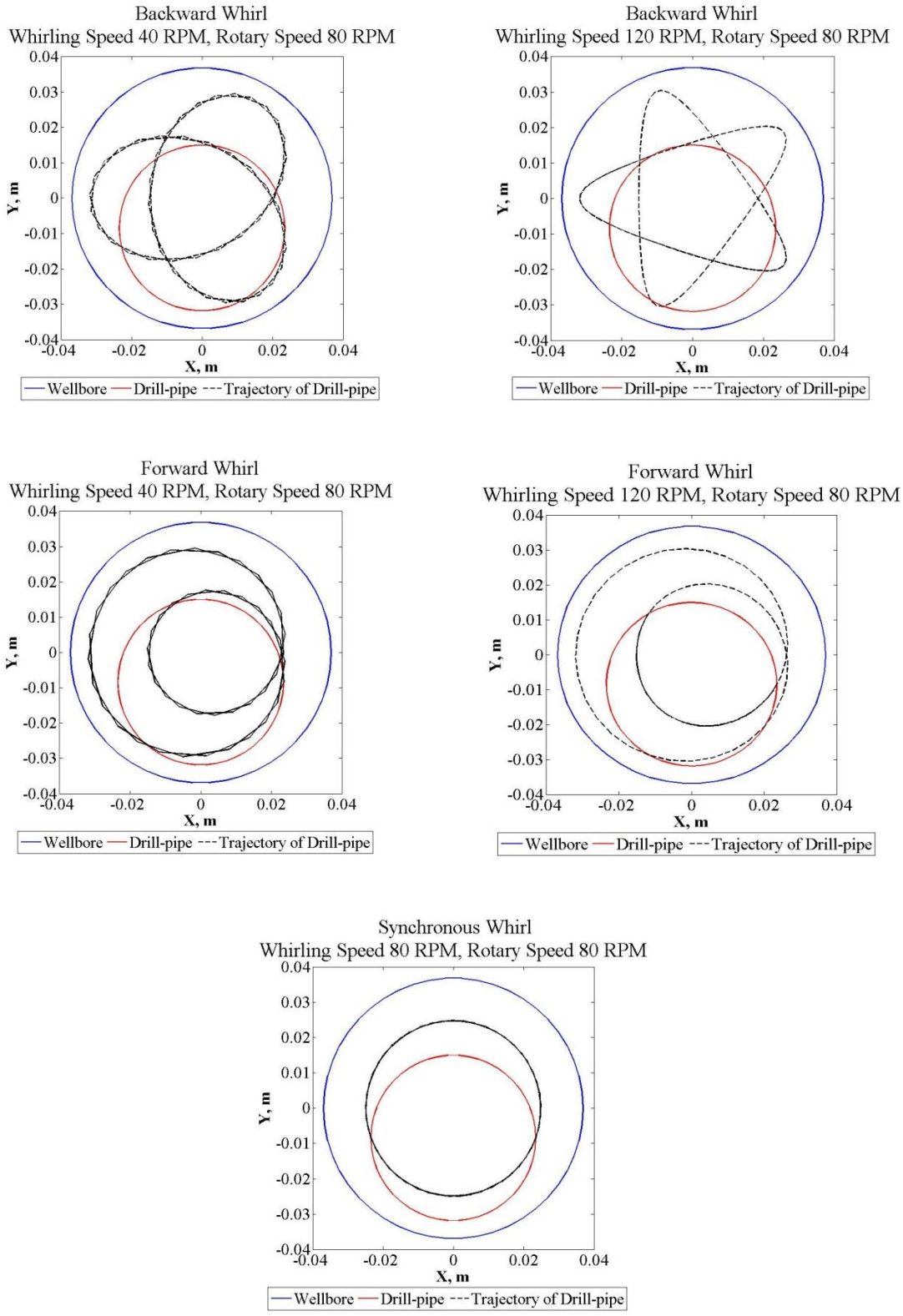

Figure 7-17: Snapshot of drill-pipe trajectory for 4 whole cycles at different mode of whirling of the drill-pipe in an eccentric horizontal well

In this study, plastering effect was also investigated both qualitatively and quantitatively. This is a different research topic but some observations were obtained during whirling rotary, and thefore a simple methodology was employed to investigate the occurrence of the plastering effect. For this purpose, a virtual region was created at a radial distance of the particle diameter from the wellbore.

As seen in Figure 7-18, number of particles in the virtual region was determined by calculating the volume of $\pi({r_w}^2 - (r_w - d_p)^2)$ along with the wellbore length at any drill-pipe location, where d_p is the particle diameter. If the number of particles along the virtual region did not decrease with the orbital motion of the drill-pipe, some cuttings were assumed to be smeared to the borehole as a result of continuous trowelling of the whirling rotary. Despite the whirling rotation speed, some particles could not be swept by the drilling fluid; instead, they were pushed away from the drill-pipe through the wellbore. Existence of the plastering effect quantitatively was determined based on this assumption. However, it is known that there are several factors affecting the plastering effect: diameter ratio between the drill-pipe and wellbore, cuttings size, rotary type and rotary speed. Karimi *et al.* qualitatively studied the plastering effect of casing drilling [76]. They emphasized that the plastering effect is a mechanism that can be predicted from the field observations, no analytical and/or numerical approaches have been done; therefore, the proposed assumption is properly made for evaluating the plastering effect.

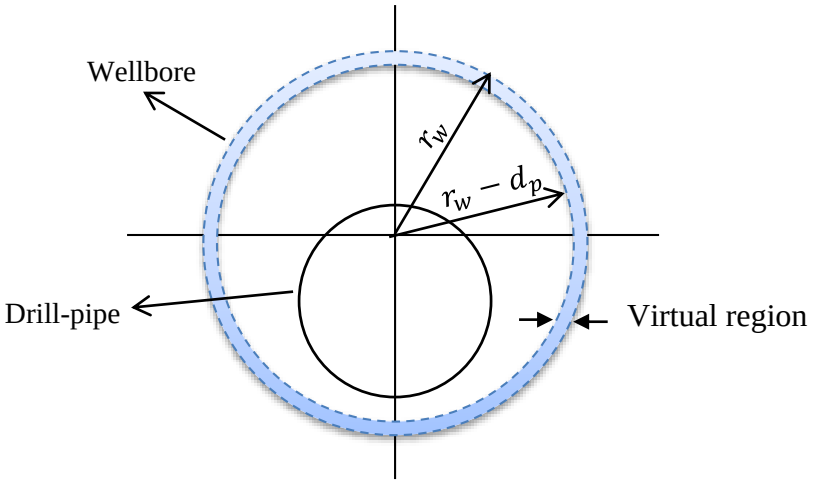

Figure 7-18: Wellbore cross-section for predicting presence of the plastering effect

7.2.2 Backward Whirling [Whirling Speed: (-) 40 rpm, Rotary Speed: (+) 80 rpm]

In this part, backward whirl with whirling speed of 40 rpm is analyzed in detail. Trajectory of drilled cuttings and streamlines of fluid velocities for this particular whirling motion are demonstrated in the Figure 7-19 through Figure 7-21. In the laminar flow regime, cuttings tend to deposit at the narrow part of the annulus when the drill-pipe is located at the direction of south. With backward whirling, the accumulated particles are stirred up and partially transported when the drill-pipe is at the direction of east, as seen in the Figure 7-19. However, cuttings bed deposition is observed again once the drill-pipe reaches its original place. This transport behavior is explained that axial fluid velocity is not enough to carry cuttings at the narrow part.

In the transient flow regime, same pattern is observed with the laminar flow regime as depicted in Figure 7-20. Cuttings deposition is also present at the narrow part of the annulus while rotation. In order to enhance cuttings transport efficiency, the drilling fluid velocity is needed to be increased.

Hole cleaning performance is obviously improved with the particular whirling motion at the turbulent flow regime as seen in Figure 7-21. Increasing fluid velocity results in an increase in the lift force and fluctuation of the drilling fluid due to the propagation of the turbulence. Furthermore, backward whirling also contributes to the suspension of the cuttings. However, some particles are smeared at the bottom and cannot be transported into the main flow stream as a result of the moment of inertia because of the resistance of the any particular cutting to change its velocity and position in its state of motion.

It seems that inner pipe rotary speed and direction forces the particles not to carry into the main flow stream. It should be remembered that whirling motion is counterclockwise while the drill-pipe rotates clockwise; therefore, particles are squeezed and smeared with the particular whirling motion.

3 ft/s - Drill-pipe at 270°

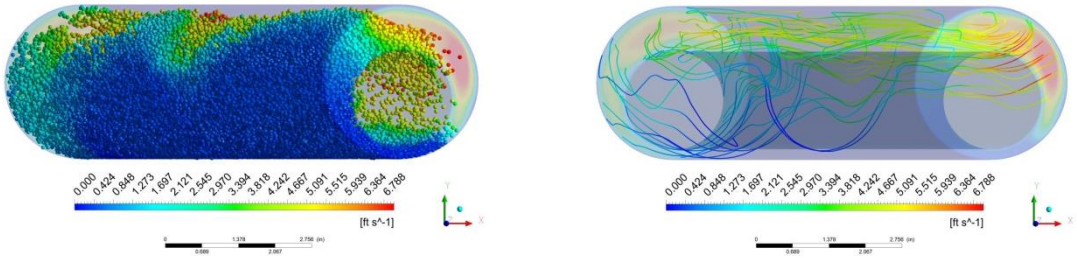

3 ft/s - Drill-pipe at 180°

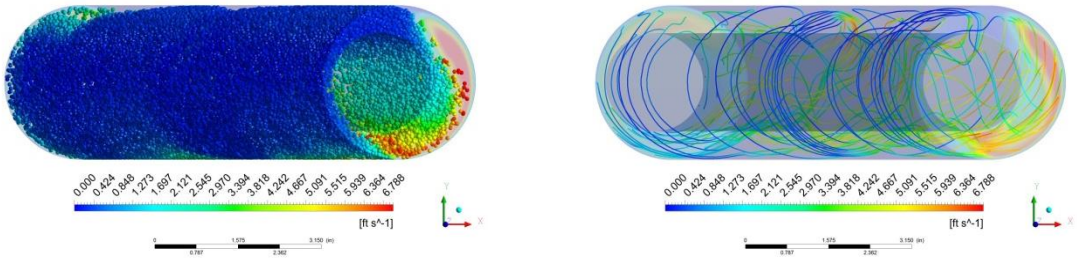

3 ft/s - Drill-pipe at 90°

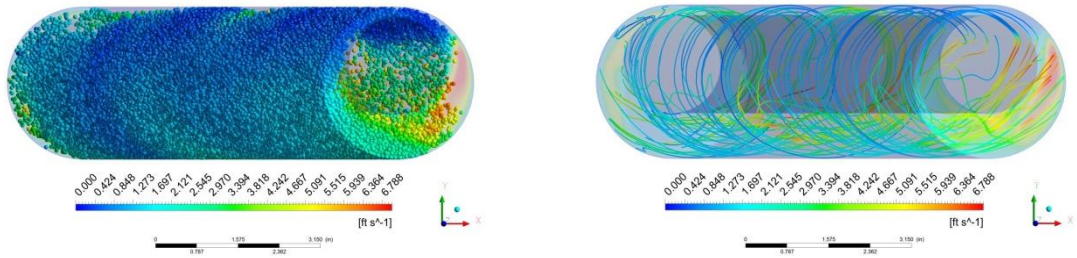

3 ft/s - Drill-pipe at 0°

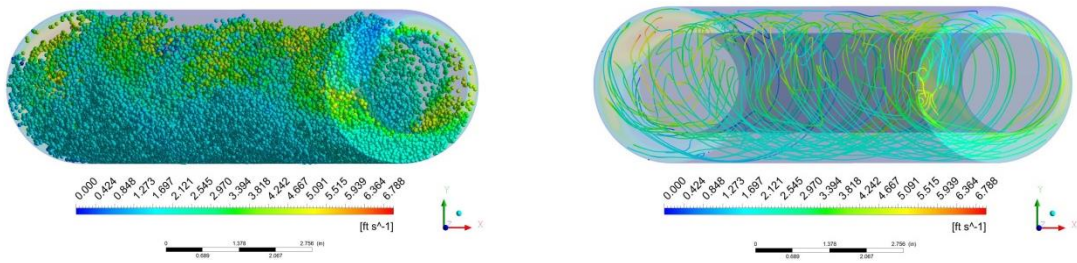

3 ft/s - Drill-pipe at 270° (1 whole cycle completed)

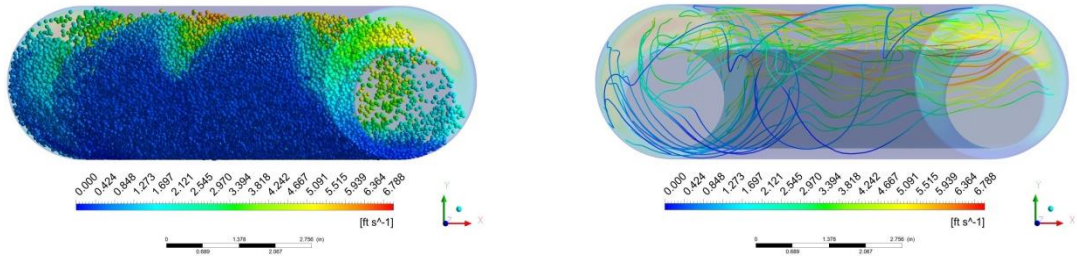

Figure 7-19: Trajectory of particles and 3D streamlines of fluid velocity for backward whirling [whirling speed: (-) 40 rpm, rotary speed: (+) 80 rpm] at 3 ft/s of fluid velocity

4 ft/s - Drill-pipe at 270°

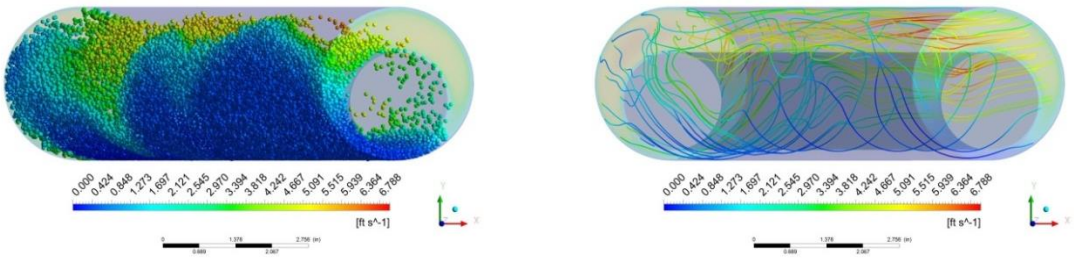

4 ft/s - Drill-pipe at 180°

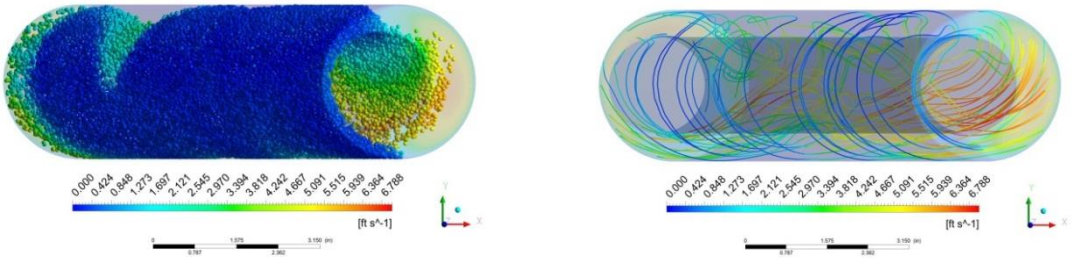

4 ft/s - Drill-pipe at 90°

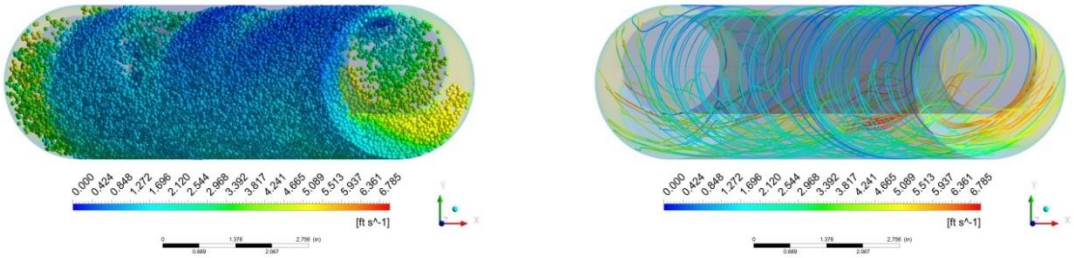

4 ft/s - Drill-pipe at 0°

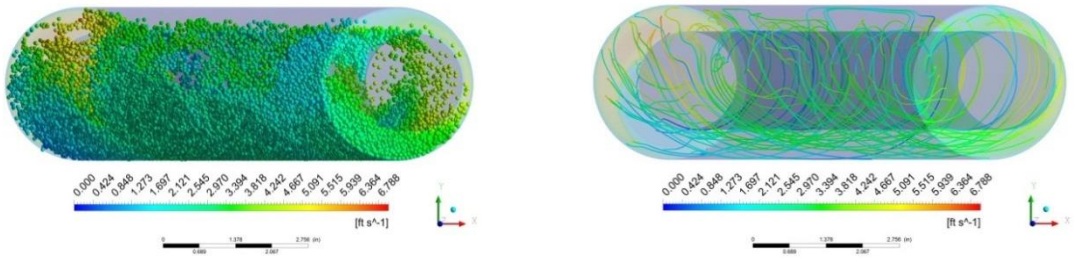

4 ft/s - Drill-pipe at 270° (1 whole cycle completed)

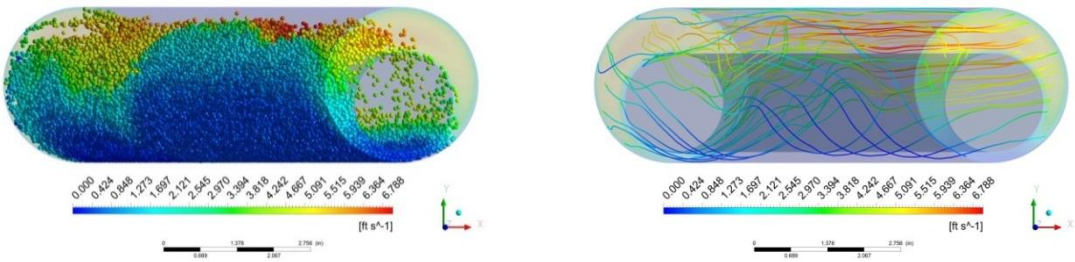

Figure 7-20: Trajectory of particles and 3D streamlines of fluid velocity for backward whirling [whirling speed: (-) 40 rpm, rotary speed: (+) 80 rpm] at 4 ft/s of fluid velocity

6 ft/s - Drill-pipe at 270°

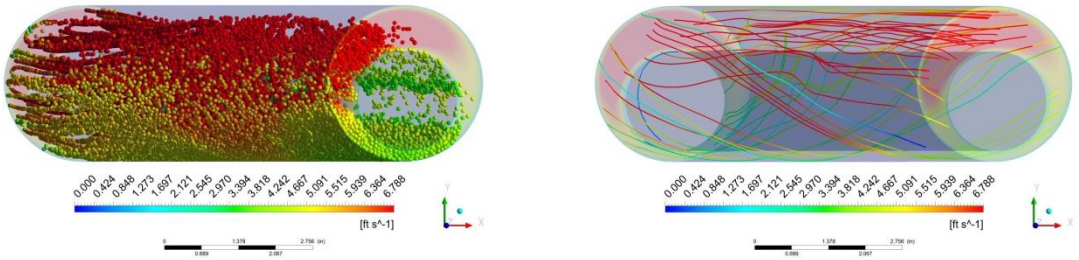

6 ft/s - Drill-pipe at 180°

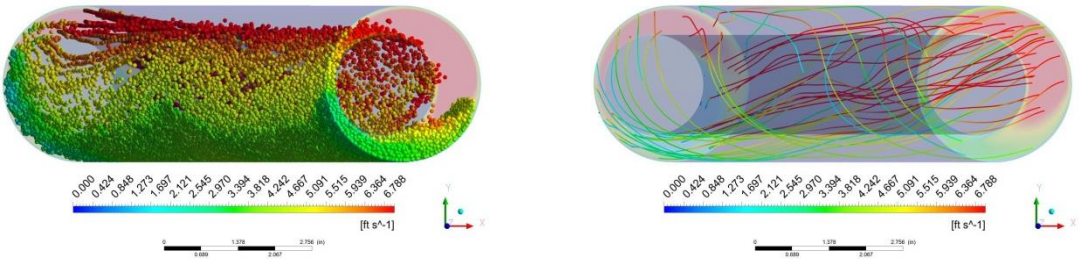

6 ft/s - Drill-pipe at 90°

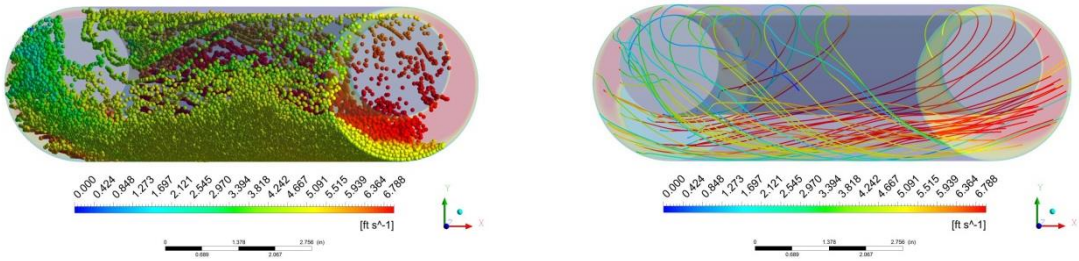

6 ft/s - Drill-pipe at 0°

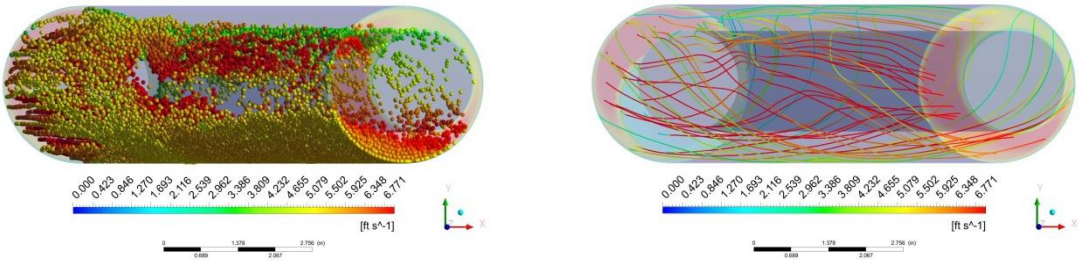

6 ft/s - Drill-pipe at 270° (1 whole cycle completed)

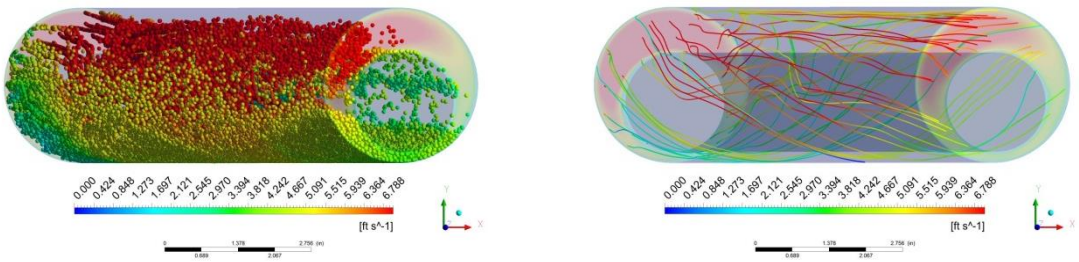

Figure 7-21: Trajectory of particles and 3D streamlines of fluid velocity for backward whirling [whirling speed: (-) 40 rpm, rotary speed: (+) 80 rpm] at 6 ft/s of fluid velocity

Additionally, it is observed that some cuttings are smeared to the wellbore in the larger section of the annulus when the drill-pipe is at the direction of north. This is explained with the presence of the plastering effect. Furthermore, distribution of cuttings increases near the wellbore when the drill-pipe moves from the direction of west to north as shown in Figure 7-22. After the drill-pipe takes its original location, it is concluded that backward whirling at 40 rpm does not sweep all the particles, particularly, those at which near to the wellbore.

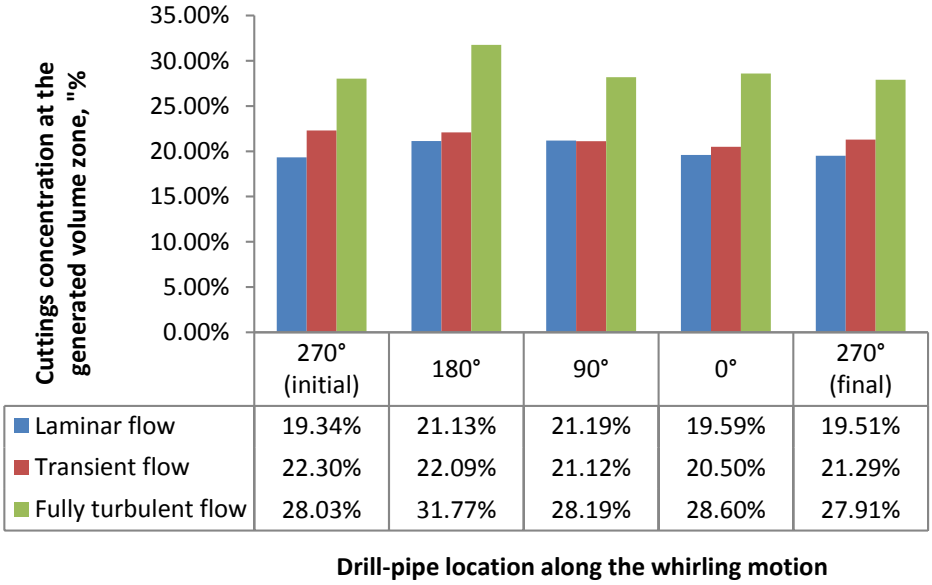

	270° (initial)	180°	90°	0°	270° (final)
Laminar flow	19.34%	21.13%	21.19%	19.59%	19.51%
Transient flow	22.30%	22.09%	21.12%	20.50%	21.29%
Fully turbulent flow	28.03%	31.77%	28.19%	28.60%	27.91%

Figure 7-22: Cuttings distribution along the whirling rotary at the virtual region at backward whirl at 40 rpm

7.2.3 Backward Whirling [Whirling Speed: (-) 120 rpm, Rotary Speed: (+) 80 rpm]

In this part, backward whirl with whirling speed at 120 rpm is investigated. It can be observed from Figure 7-23 through Figure 7-25; cuttings are swayed towards the wellbore at high whirling speed at any flow regime. Noticeable reduction in the stationary cuttings bed is observed although the flow regime is laminar because the centrifugal forces become more dominant due to the high whirling rotation. Furthermore, trowelling effect of the particular whirling rotary is more pronounced when whirling rotary speed is 120 rpm; therefore, probability of occurrence of the plastering effect or smearing is high.

3 ft/s - Drill-pipe at 270°

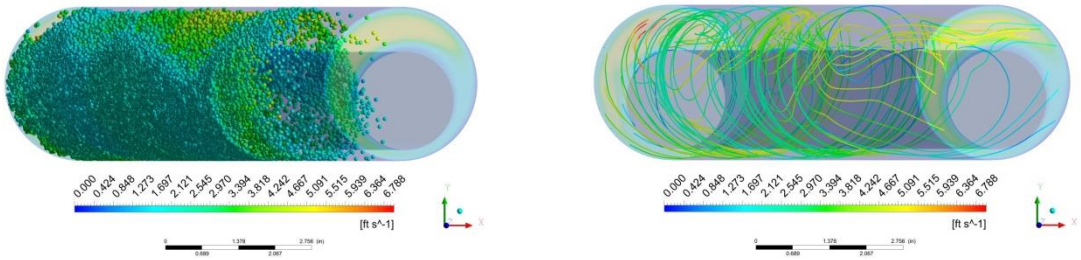

3 ft/s - Drill-pipe at 180°

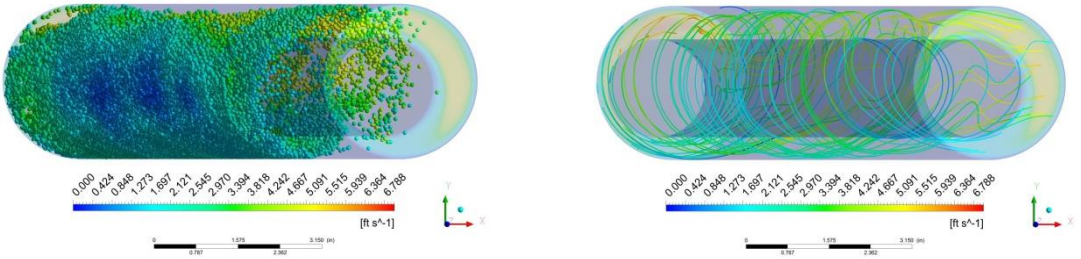

3 ft/s - Drill-pipe at 90°

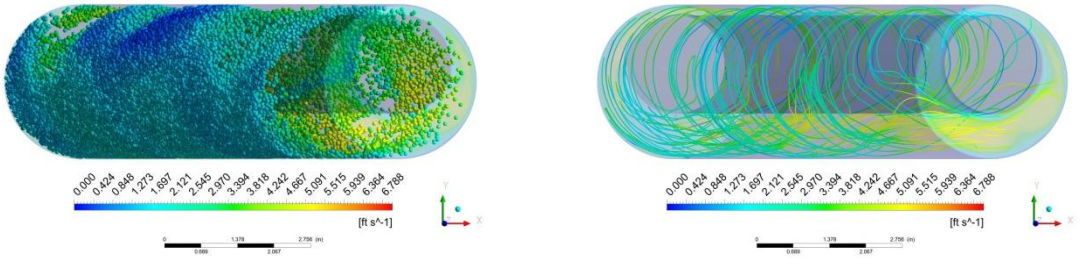

3 ft/s - Drill-pipe at 0°

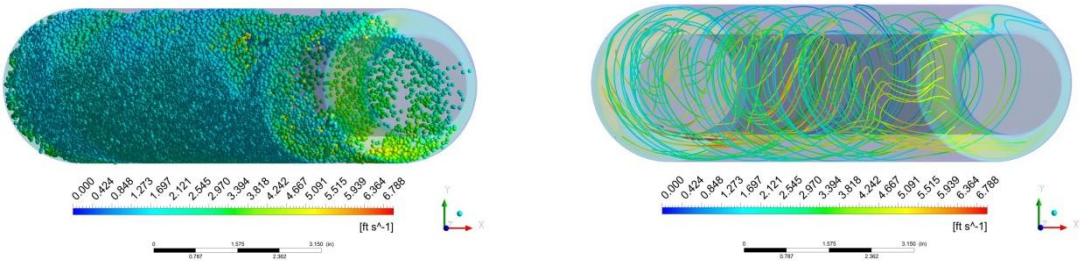

3 ft/s - Drill-pipe at 270° (1 whole cycle completed)

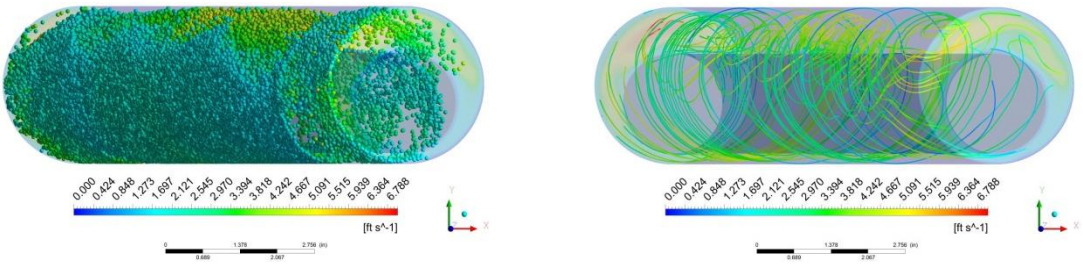

Figure 7-23: Trajectory of particles and 3D streamlines of fluid velocity for backward whirling [whirling speed: (-) 120 rpm, rotary speed: (+) 80 rpm] at 3 ft/s of fluid velocity

4 ft/s - Drill-pipe at 270°

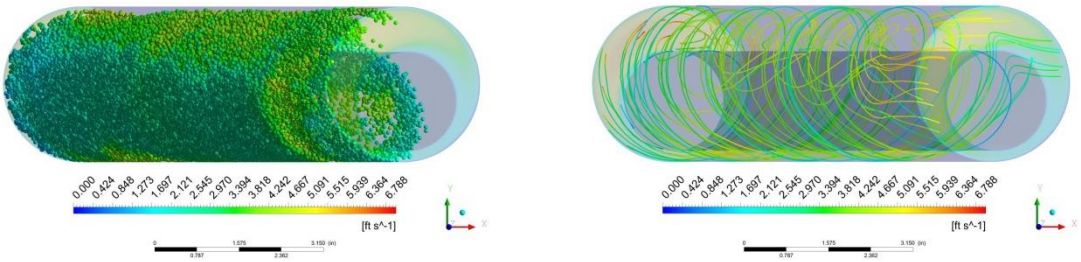

4 ft/s - Drill-pipe at 180°

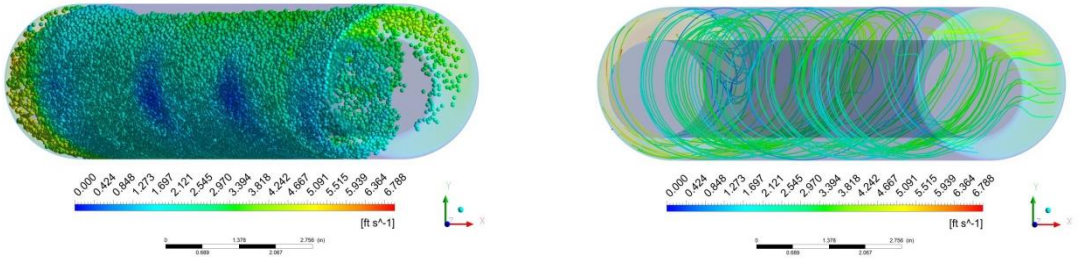

4 ft/s - Drill-pipe at 90°

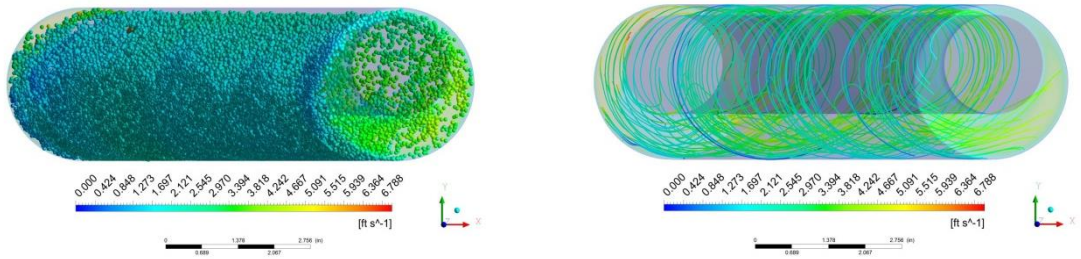

4 ft/s - Drill-pipe at 0°

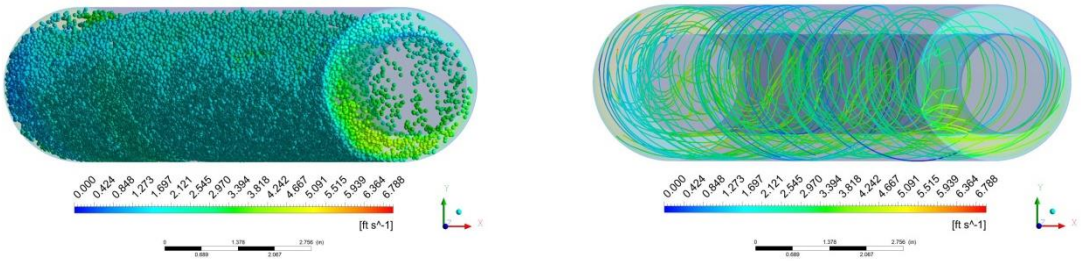

4 ft/s - Drill-pipe at 270° (1 whole cycle completed)

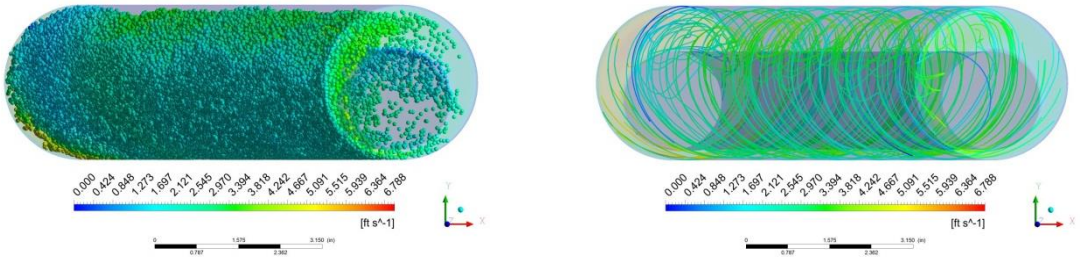

Figure 7-24: Trajectory of particles and 3D streamlines of fluid velocity for backward whirling [whirling speed: (-) 120 rpm, rotary speed: (+) 80 rpm] at 4 ft/s of fluid velocity

6 ft/s - Drill-pipe at 270°

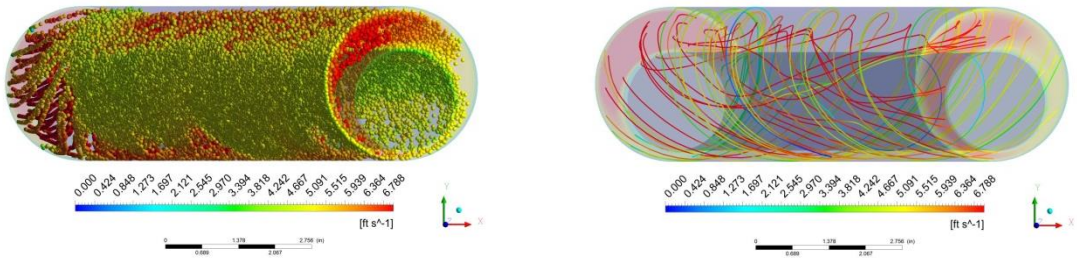

6 ft/s - Drill-pipe at 180°

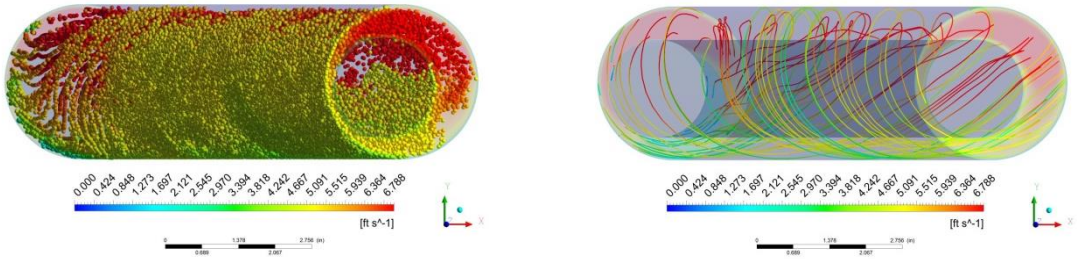

6 ft/s - Drill-pipe at 90°

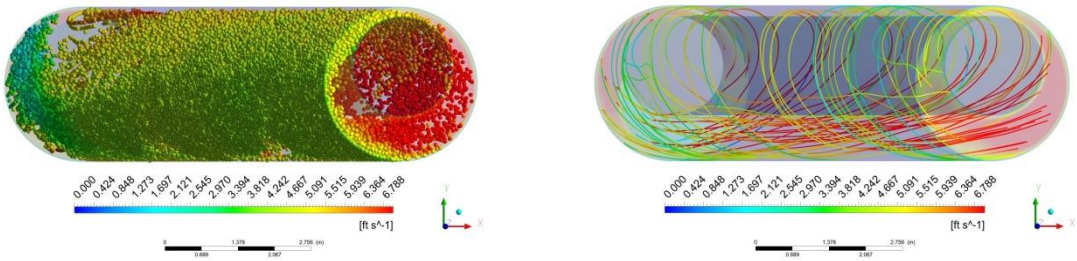

6 ft/s - Drill-pipe at 0°

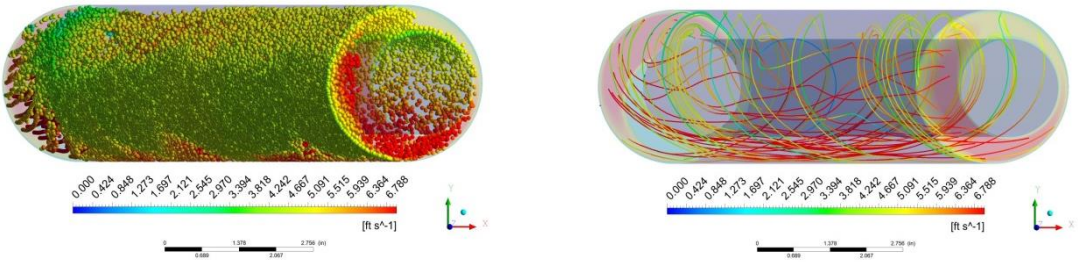

6 ft/s - Drill-pipe at 270° (1 whole cycle completed)

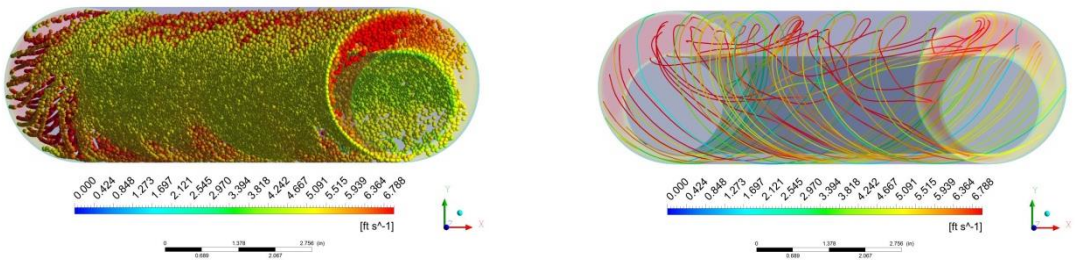

Figure 7-25: Trajectory of particles and 3D streamlines of fluid velocity for backward whirling [whirling speed: (-) 120 rpm, rotary speed: (+) 80 rpm] at 6 ft/s of fluid velocity

Moreover, the number of cuttings along with the whirling motion shows fluctuation for any flow regime as demonstrated in Figure 7-26. It is observed from the figure that increasing fluid velocity results in an increment in the numbers of cuttings. However, when the drill-pipe is at the direction of east, some cuttings could not be stirred up with the whirling motion, and a cuttings layer is produced as a consequence of the smearing effect.

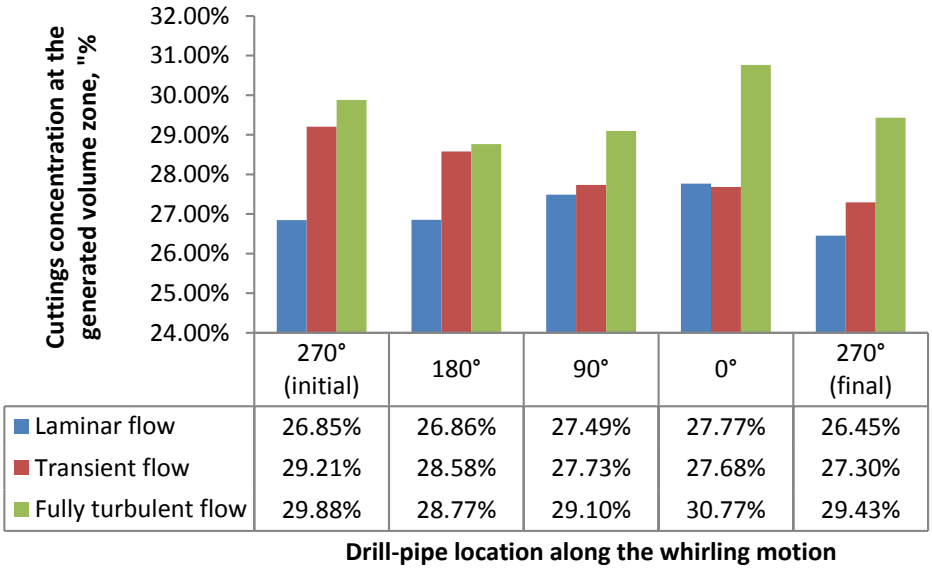

	270° (initial)	180°	90°	0°	270° (final)
Laminar flow	26.85%	26.86%	27.49%	27.77%	26.45%
Transient flow	29.21%	28.58%	27.73%	27.68%	27.30%
Fully turbulent flow	29.88%	28.77%	29.10%	30.77%	29.43%

Figure 7-26: Cuttings distribution along the whirling rotary at the virtual region at backward whirl at 120 rpm

7.2.4 Forward Whirling [Whirling Speed: (+) 40 rpm, Rotary Speed: (+) 80 rpm]

Forward whirl with whirling speed at 40 rpm is analyzed in this part. Drill-pipe and whirling rotation is both clockwise in the forward whirling motion. DEM particles and streamlines for the fluid velocities at different flow regimes are demonstrated in the Figure 7-27 to Figure 7-29. When the drill-pipe radially moves upward (from south to north), the particles tend to move to the bottom of the annulus. Conversely, the cuttings are transported into the main flow region when the whirling motion of the drill-pipe is taken place from to the bottom. In all flow regimes, cuttings are mainly transported with the backward whirling.

3 ft/s - Drill-pipe at 270°

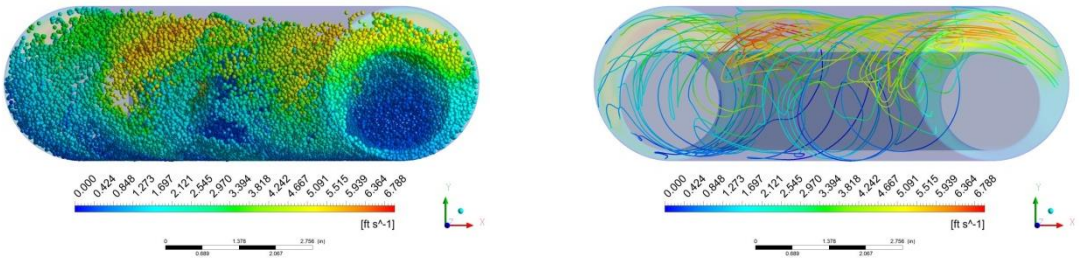

3 ft/s - Drill-pipe at 0°

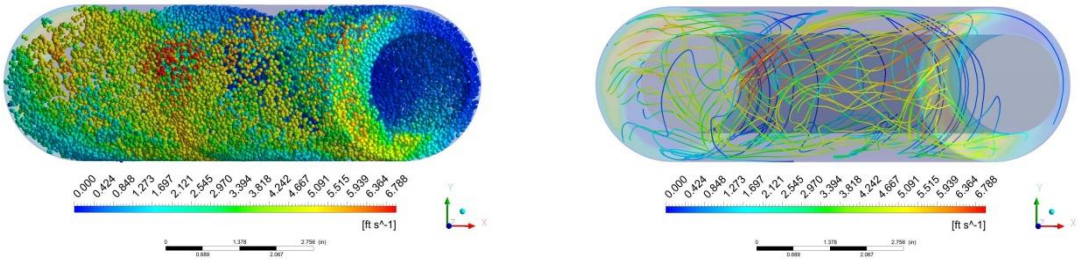

3 ft/s - Drill-pipe at 90°

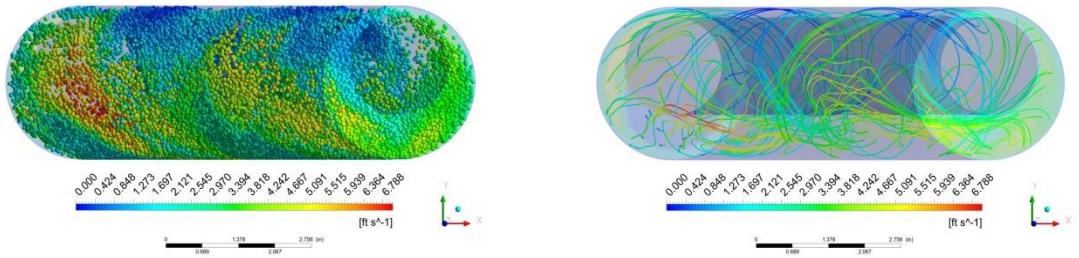

3 ft/s - Drill-pipe at 180°

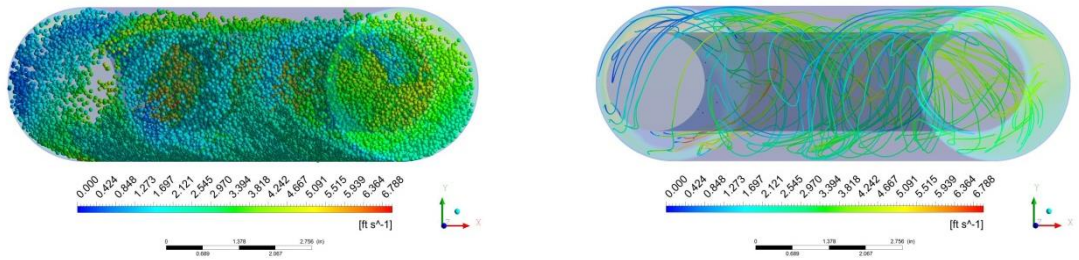

3 ft/s - Drill-pipe at 270° (1 whole cycle completed)

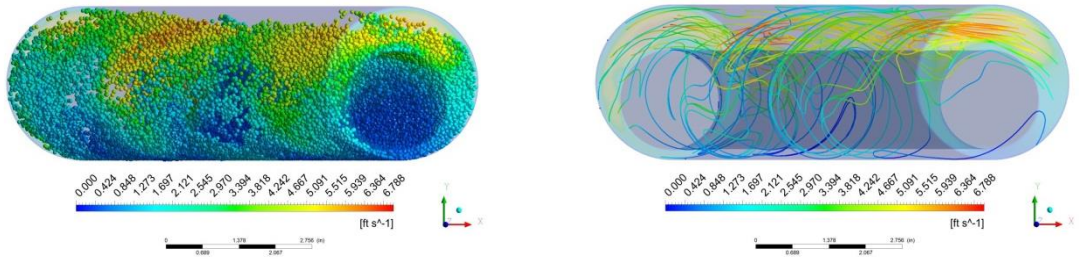

Figure 7-27: Trajectory of particles and 3D streamlines of fluid velocity for forward whirling [whirling speed: (+) 40 rpm, rotary speed: (+) 80 rpm] at 3 ft/s of fluid velocity

4 ft/s - Drill-pipe at 270°

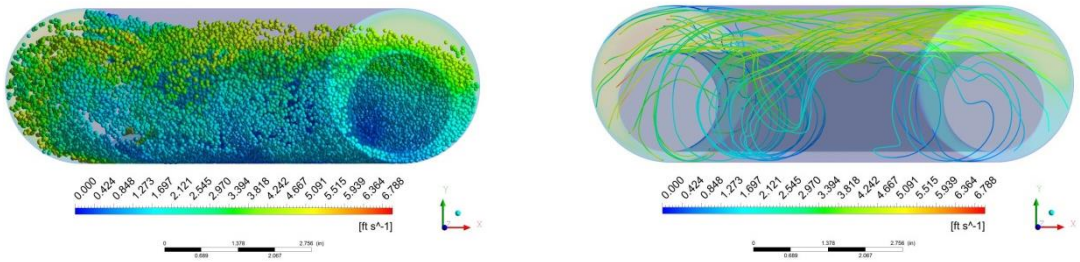

4 ft/s - Drill-pipe at 0°

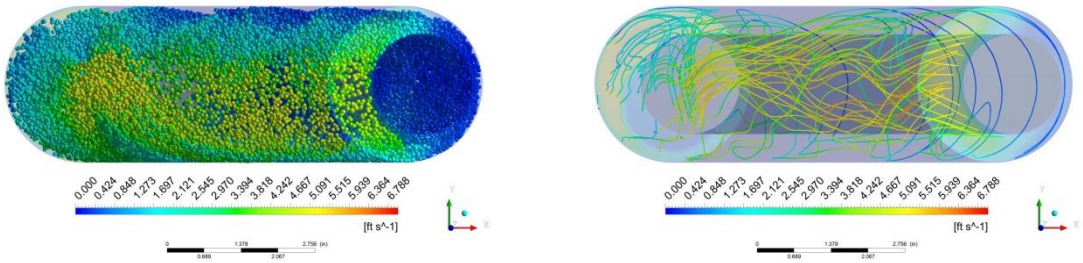

4 ft/s - Drill-pipe at 90°

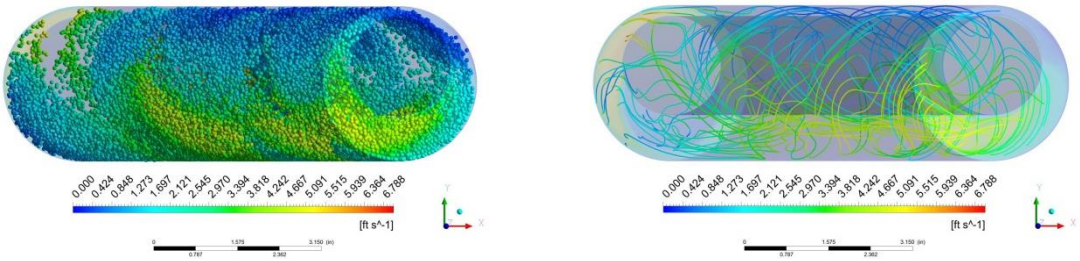

4 ft/s - Drill-pipe at 180°

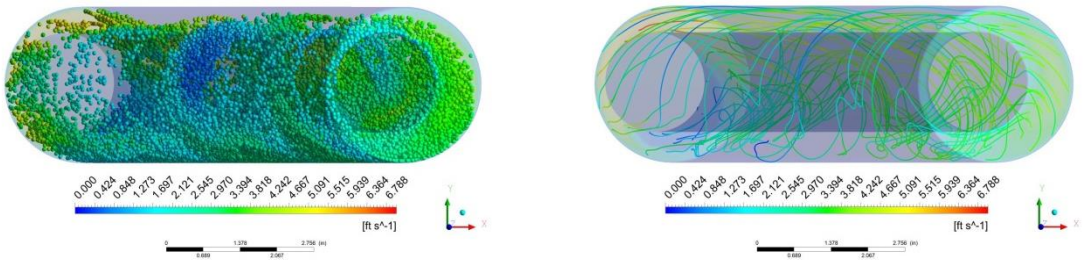

4 ft/s - Drill-pipe at 270° (1 whole cycle completed)

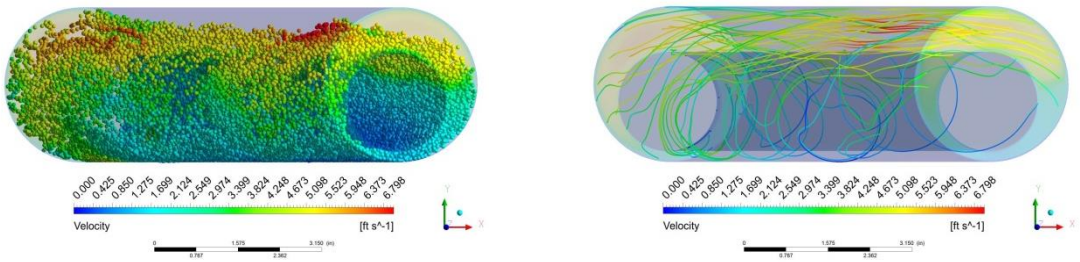

Figure 7-28: Trajectory of particles and 3D streamlines of fluid velocity for forward whirling [whirling speed: (+) 40 rpm, rotary speed: (+) 80 rpm] at 4 ft/s of fluid velocity

6 ft/s - Drill-pipe at 270°

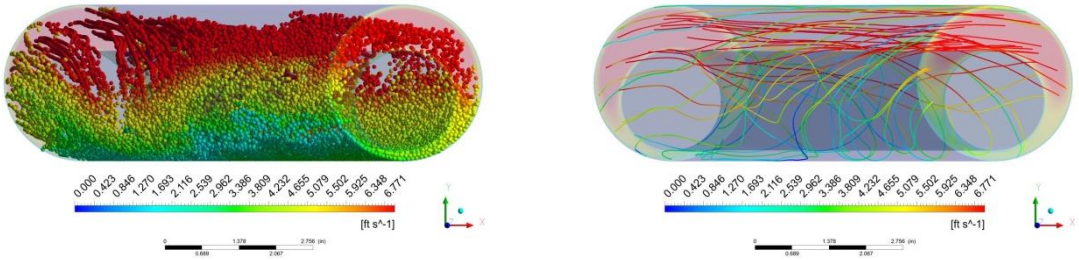

6 ft/s - Drill-pipe at 0°

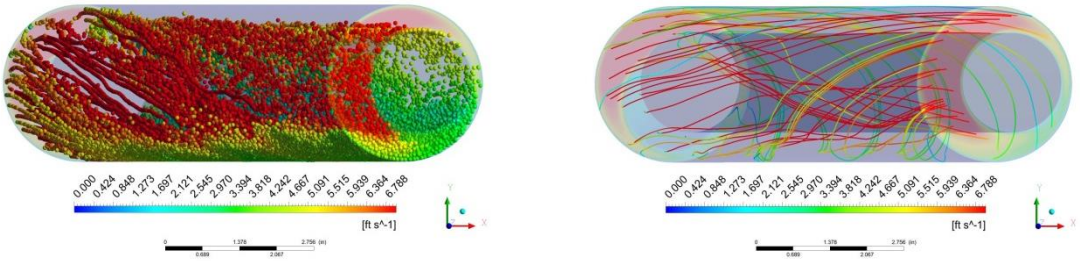

6 ft/s - Drill-pipe at 90°

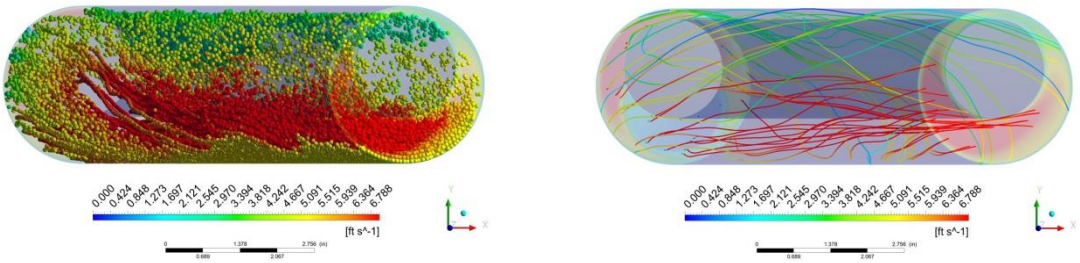

6 ft/s - Drill-pipe at 180°

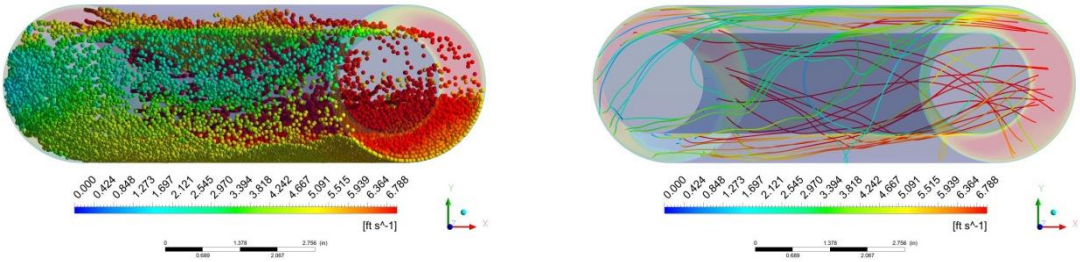

6 ft/s - Drill-pipe at 270° (1 whole cycle completed)

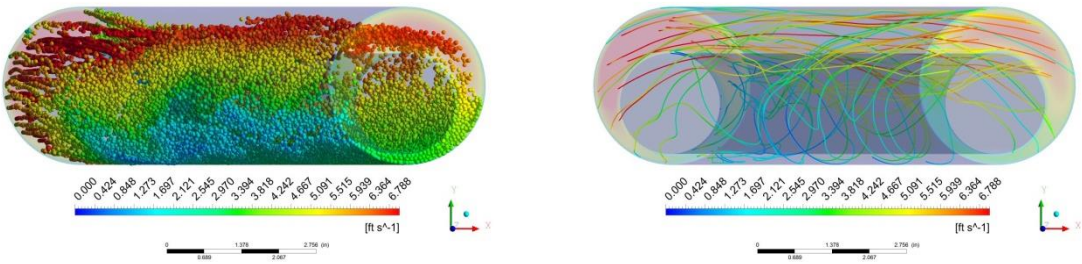

Figure 7-29: Trajectory of particles and 3D streamlines of fluid velocity for forward whirling [whirling speed: (+) 40 rpm, rotary speed: (+) 80 rpm] at 6 ft/s of fluid velocity

Cuttings concentration at the virtual region increases at high fluid velocities as seen in Figure 7-30. This is different what it is observed in the backward whirling. The plastering effect is mechanism that the cuttings are smeared through the wellbore; however, here, a moving layer occurs, and the axial velocity of those particles at the moving layer changes with respect to the location of the drill-pipe. This observation is made only the flow regime is fully turbulent. Otherwise, the particles are efficiently swept because of the backward whirling at the laminar and transient flow regimes.

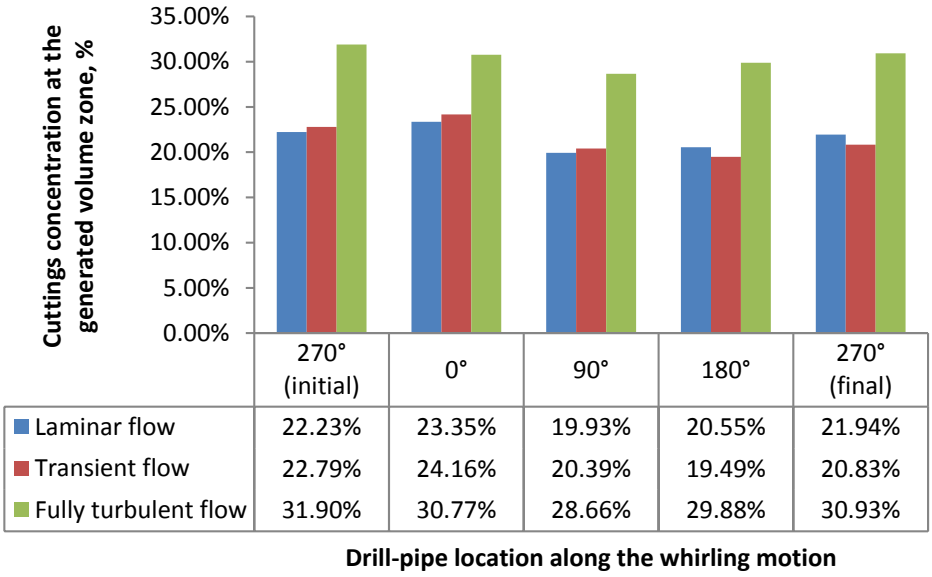

	270° (initial)	0°	90°	180°	270° (final)
Laminar flow	22.23%	23.35%	19.93%	20.55%	21.94%
Transient flow	22.79%	24.16%	20.39%	19.49%	20.83%
Fully turbulent flow	31.90%	30.77%	28.66%	29.88%	30.93%

Figure 7-30: Cuttings distribution along the whirling rotary at the virtual region at forward whirl at 40 rpm

7.2.5 Forward Whirling [Whirling Speed: (+) 120 rpm, Rotary Speed: (+) 80 rpm]

An effective hole cleaning is achieved when the forward whirling with 120 rpm rotary speed is present for all flow regimes. In other words, cuttings transport performance is significantly improved by increasing whirling speed. Particle trajectories can be observed from Figure 7-31 to Figure 7-33. In addition, there is no any presence of cuttings build-up at the particular whirling motion even though the fluid velocity is low as seen from the figures below.

3 ft/s - Drill-pipe at 270°

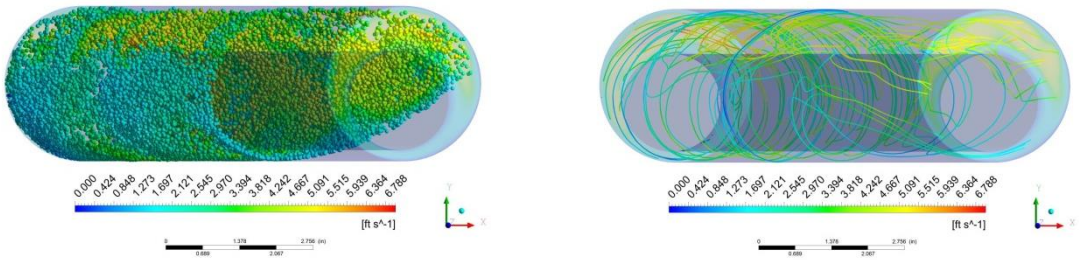

3 ft/s - Drill-pipe at 0°

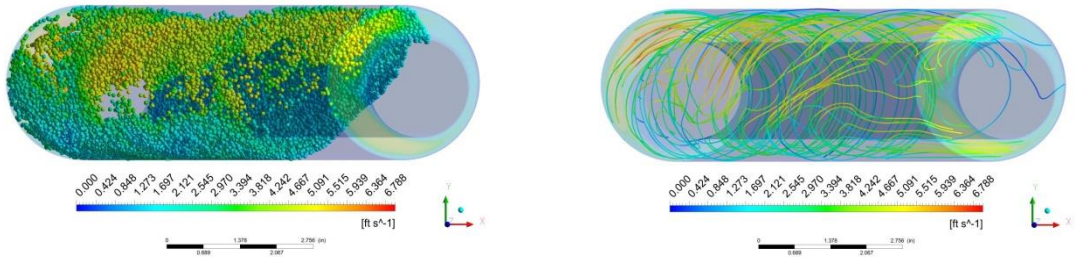

3 ft/s - Drill-pipe at 90°

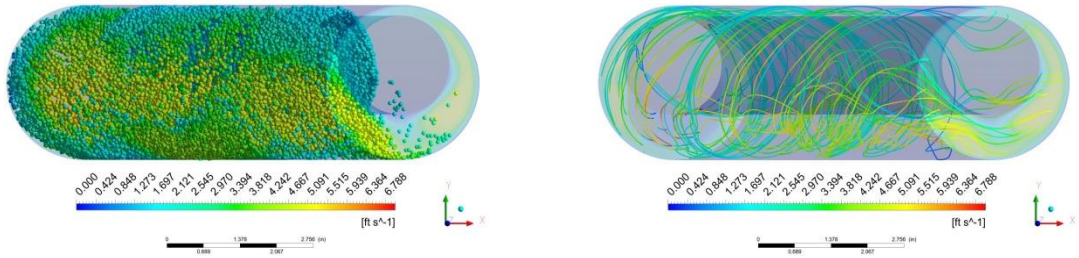

3 ft/s - Drill-pipe at 180°

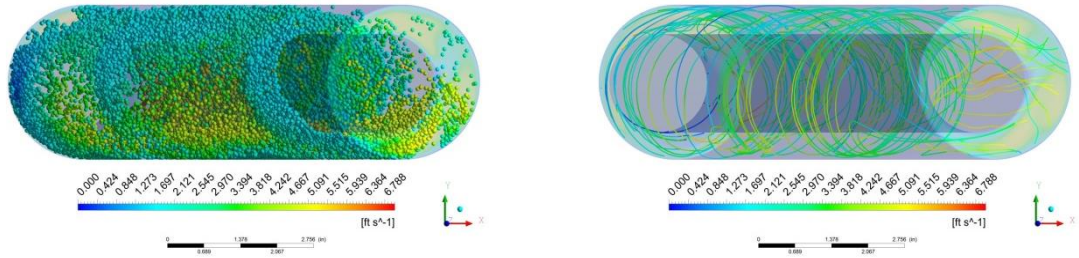

3 ft/s - Drill-pipe at 270° (1 whole cycle completed)

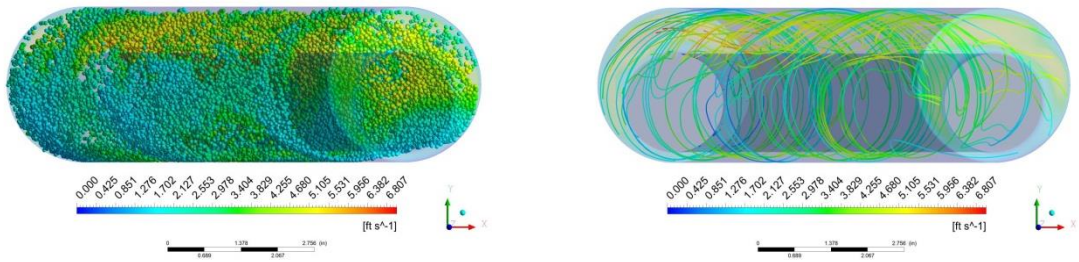

Figure 7-31: Trajectory of particles and 3D streamlines of fluid velocity for forward whirling [whirling speed: (+) 120 rpm, rotary speed: (+) 80 rpm] at 3 ft/s of fluid velocity

4 ft/s - Drill-pipe at 270°

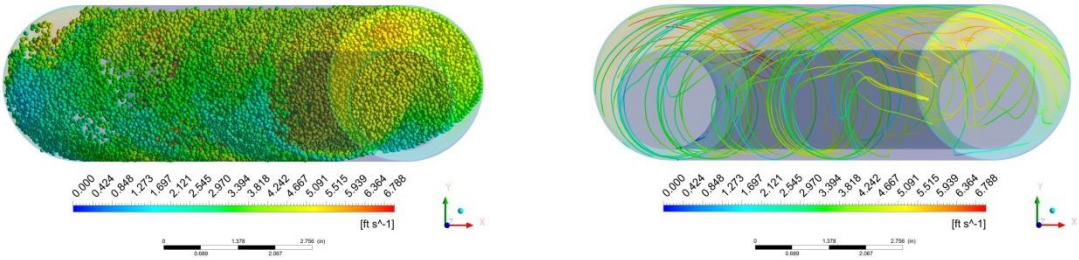

4 ft/s - Drill-pipe at 0°

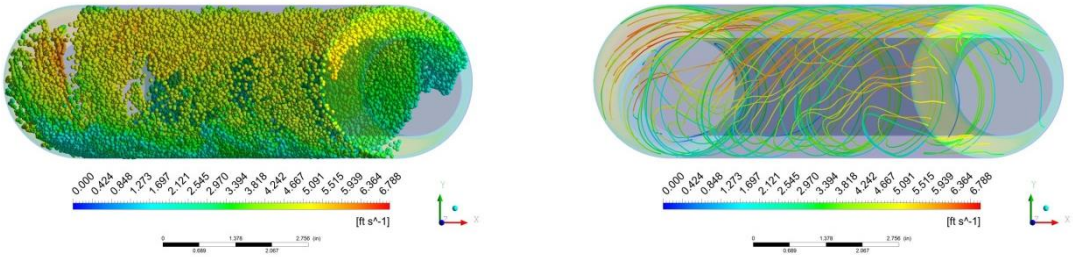

4 ft/s - Drill-pipe at 90°

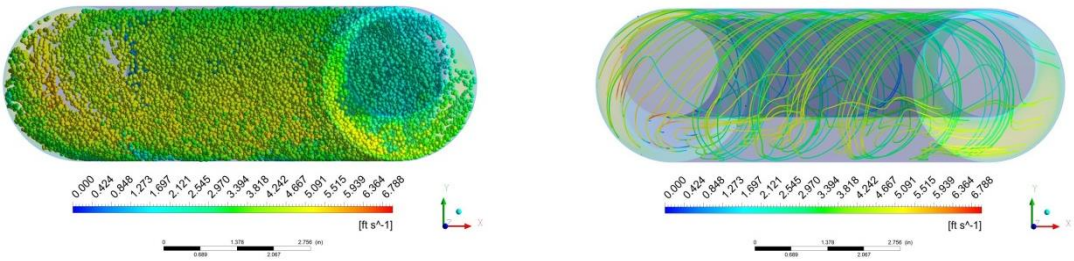

4 ft/s - Drill-pipe at 180°

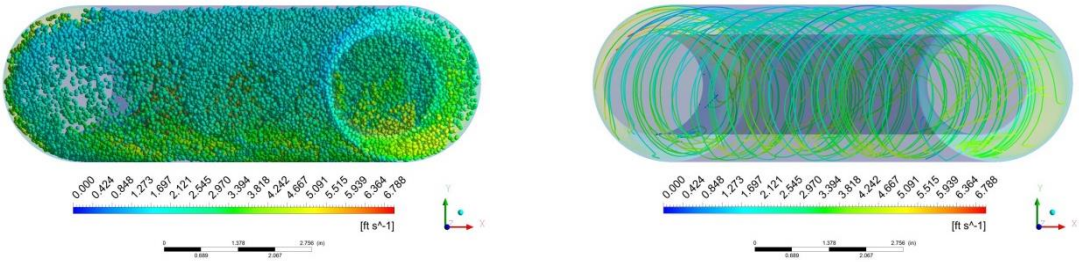

4 ft/s - Drill-pipe at 270° (1 whole cycle completed)

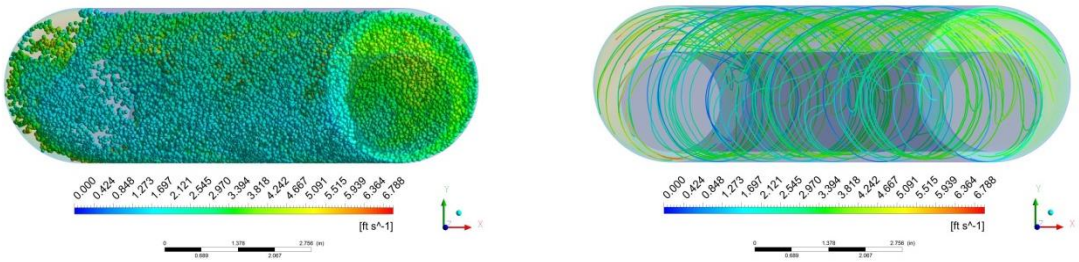

Figure 7-32: Trajectory of particles and 3D streamlines of fluid velocity for forward whirling [whirling speed: (+) 120 rpm, rotary speed: (+) 80 rpm] at 4 ft/s of fluid velocity

6 ft/s - Drill-pipe at 270°

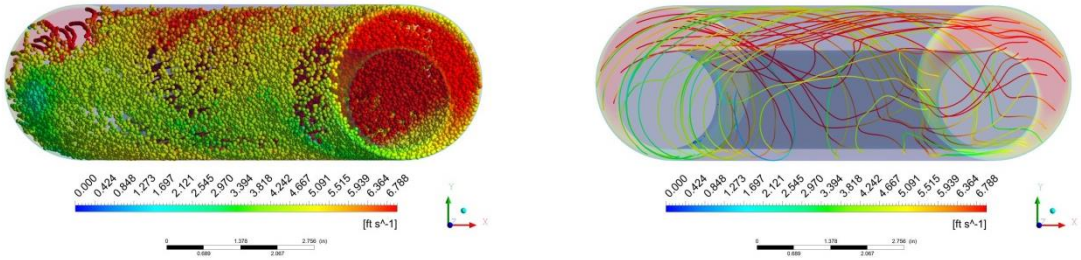

6 ft/s - Drill-pipe at 0°

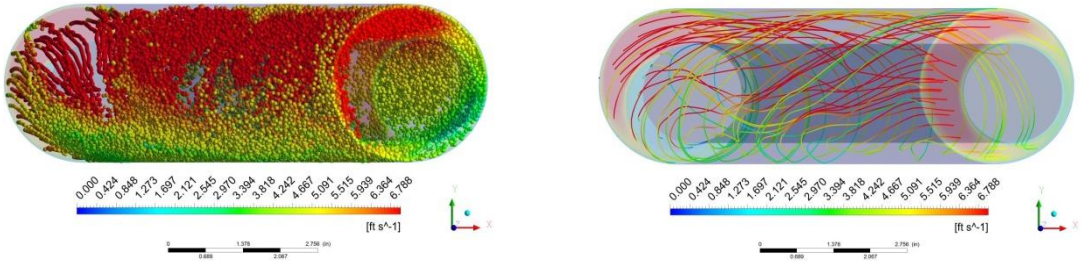

6 ft/s - Drill-pipe at 90°

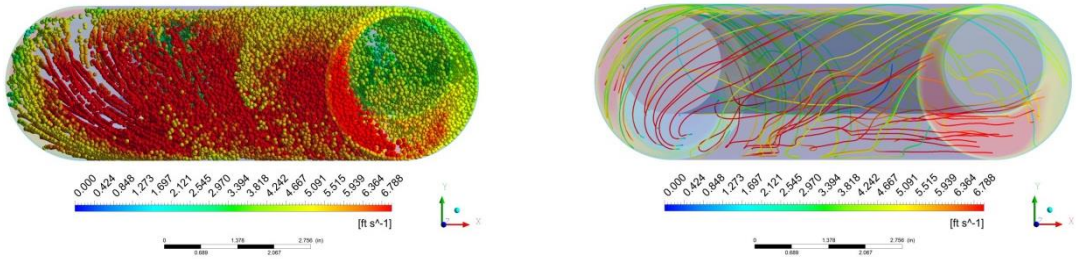

6 ft/s - Drill-pipe at 180°

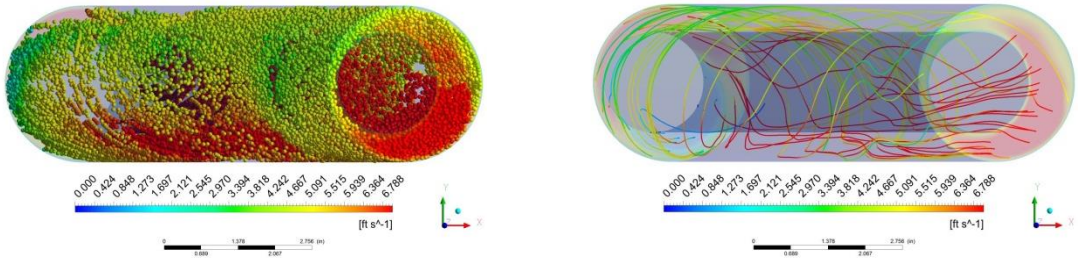

6 ft/s - Drill-pipe at 270° (1 whole cycle completed)

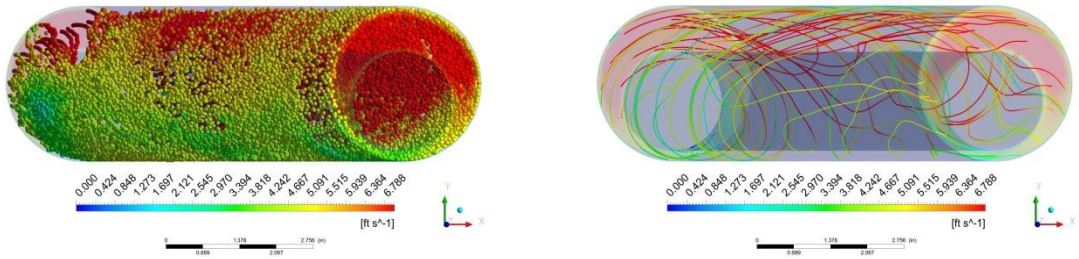

Figure 7-33: Trajectory of particles and 3D streamlines of fluid velocity for forward whirling [whirling speed: (+) 120 rpm, rotary speed: (+) 80 rpm] at 6 ft/s of fluid velocity

Furthermore, cuttings concentration at the virtual region decreases with whirling rotation, and starts increasing again during one complete revolution of the drill-pipe. This behavior can be clearly seen in Figure 7-34. High whirling rotary speed for that the drill-pipe rotary direction is same as the whirl direction improves the cuttings transport efficiency by sweeping the particles during the revolution. However, when the flow regime is laminar, cuttings could just reach to the end of the wellbore because tangential velocity of the fluid is more pronounced than the axial velocity of the fluid.

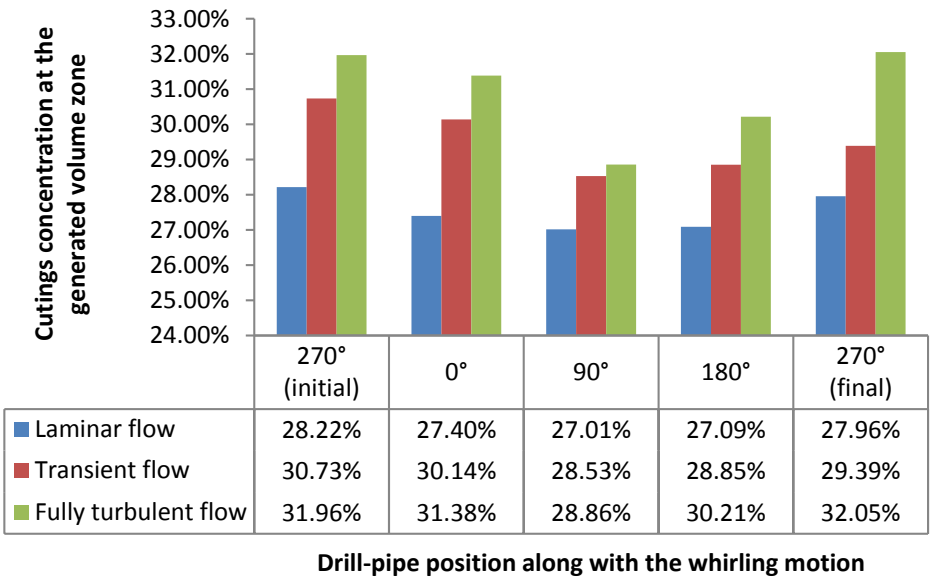

	270° (initial)	0°	90°	180°	270° (final)
Laminar flow	28.22%	27.40%	27.01%	27.09%	27.96%
Transient flow	30.73%	30.14%	28.53%	28.85%	29.39%
Fully turbulent flow	31.96%	31.38%	28.86%	30.21%	32.05%

Figure 7-34: Cuttings distribution along the whirling rotary at the virtual region at forward whirl at 120 rpm

7.2.6 Synchronous Whirl [Whirling Speed: (+) 80 rpm, Rotary Speed: (+) 80 rpm]

When the drill-pipe rotation direction and speed is the same as whirling direction and speed, synchronous whirl is present. Trajectory of DEM particles and streamlines of fluid velocities for this particular whirling motion are shown in the Figure 7-35 through Figure 7-37. In these circumstances, cuttings are barely deposited at the narrow part of the annulus during the revolution at the laminar flow regime. This deposition does not stay permanently at which the fluid velocity is low because whirling motion stirs up the cuttings. They are swayed one side to another by the whirling rotary, without having any consequences of the smearing effect.

3 ft/s - Drill-pipe at 270°

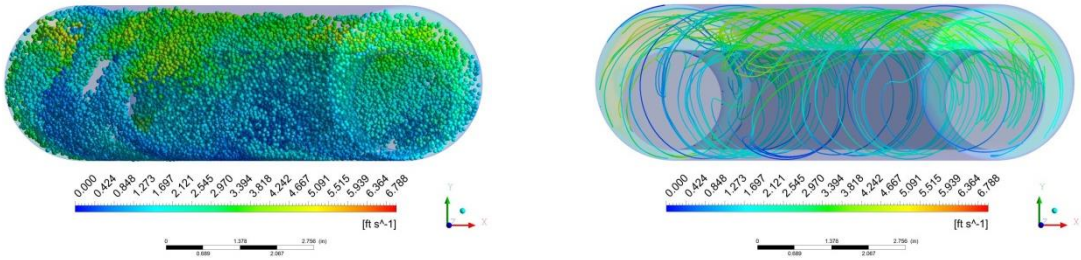

3 ft/s - Drill-pipe at 0°

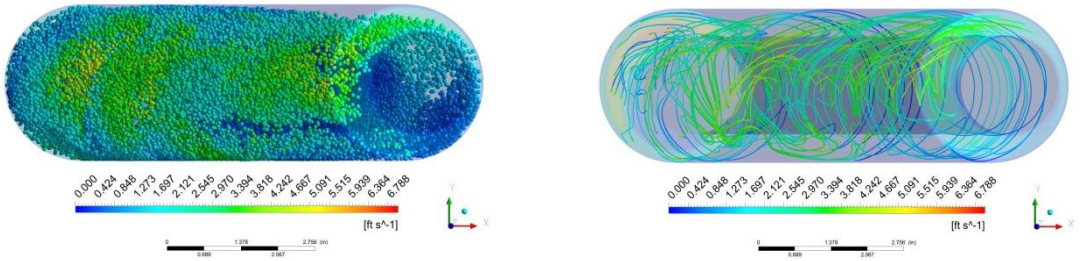

3 ft/s - Drill-pipe at 90°

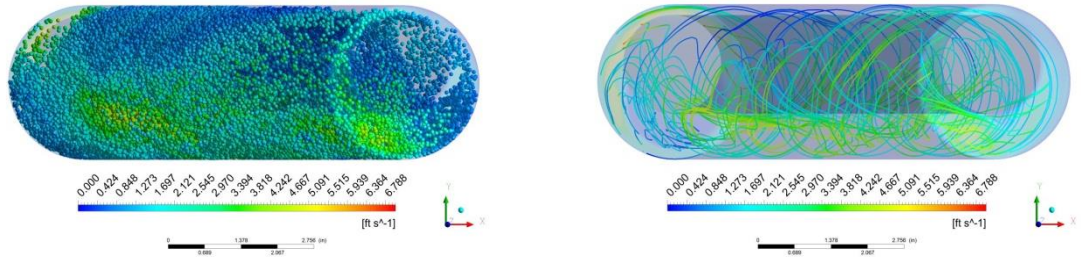

3 ft/s - Drill-pipe at 180°

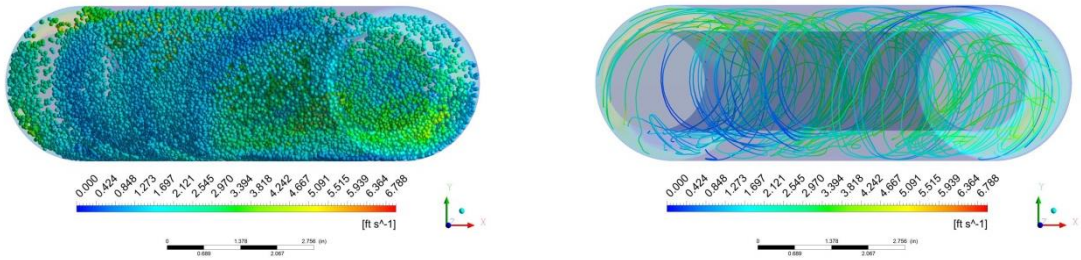

3 ft/s - Drill-pipe at 270° (1 whole cycle completed)

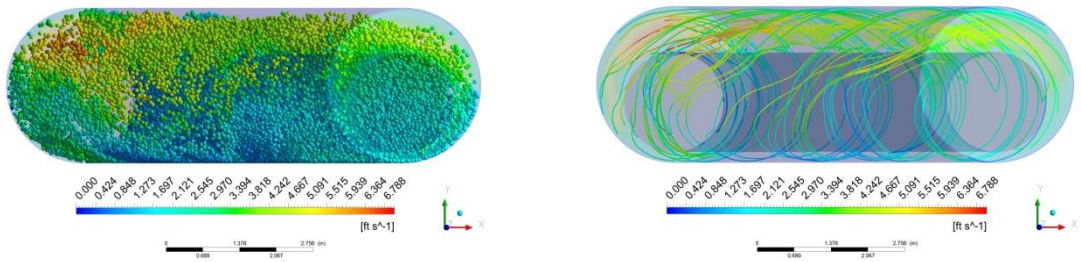

Figure 7-35: Trajectory of particles and 3D streamlines of fluid velocity for synchronous whirling [whirling speed: (+) 80 rpm, rotary speed: (+) 80 rpm] at 3 ft/s of fluid velocity

4 ft/s - Drill-pipe at 270°

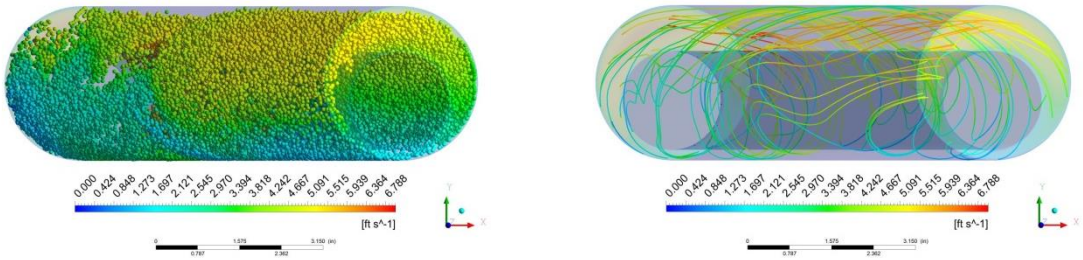

4 ft/s - Drill-pipe at 0°

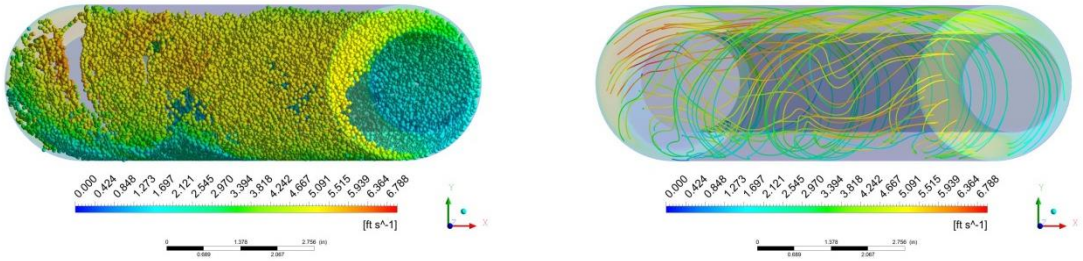

4 ft/s - Drill-pipe at 90°

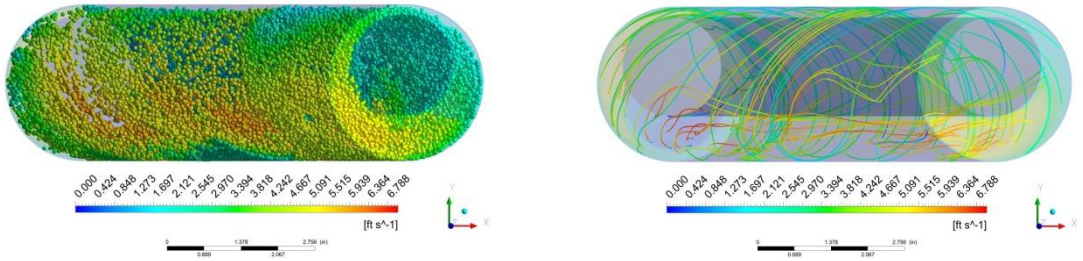

4 ft/s - Drill-pipe at 180°

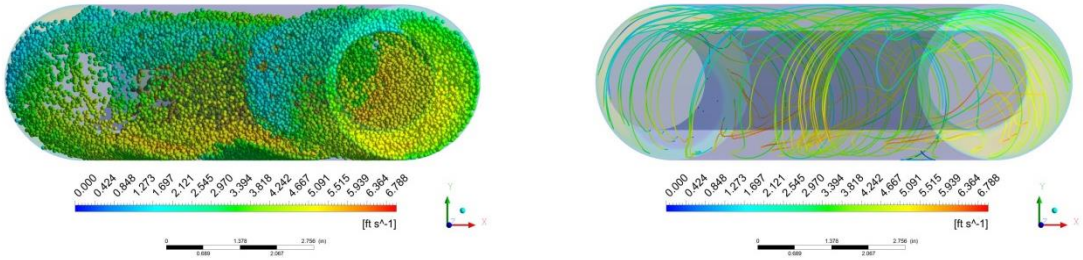

4 ft/s - Drill-pipe at 270° (1 whole cycle completed)

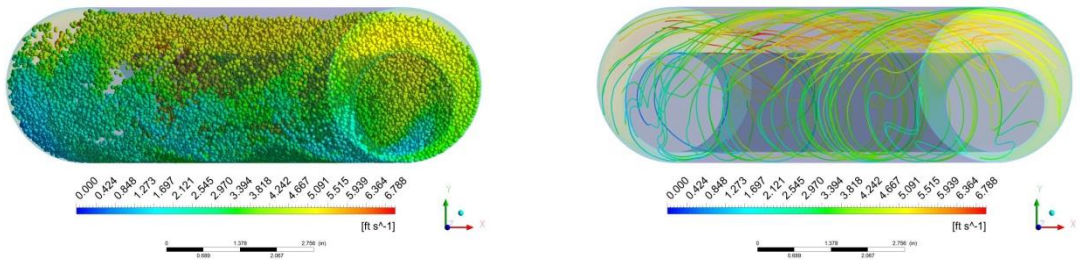

Figure 7-36: Trajectory of particles and 3D streamlines of fluid velocity for synchronous whirling [whirling speed: (+) 80 rpm, rotary speed: (+) 80 rpm] at 4 ft/s of fluid velocity

6 ft/s - Drill-pipe at 270°

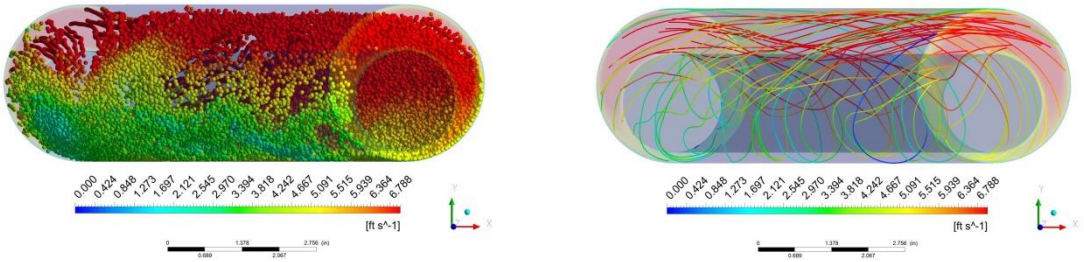

6 ft/s - Drill-pipe at 0°

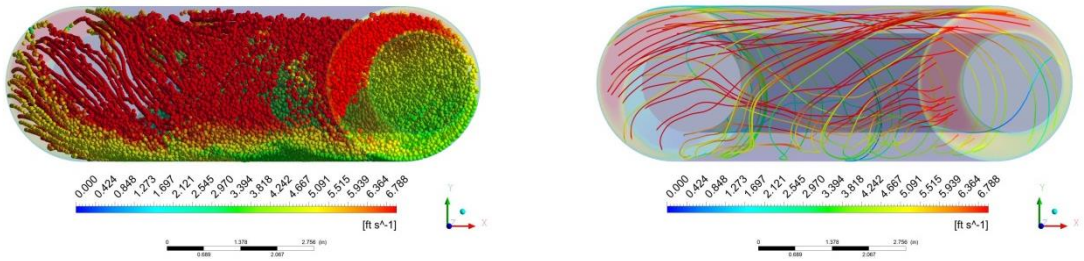

6 ft/s - Drill-pipe at 90°

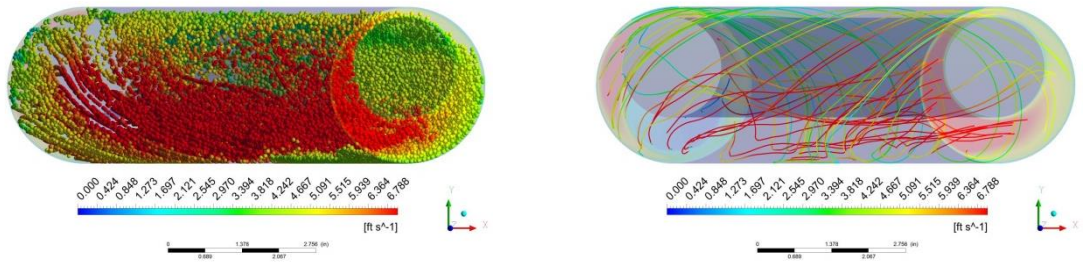

6 ft/s - Drill-pipe at 180°

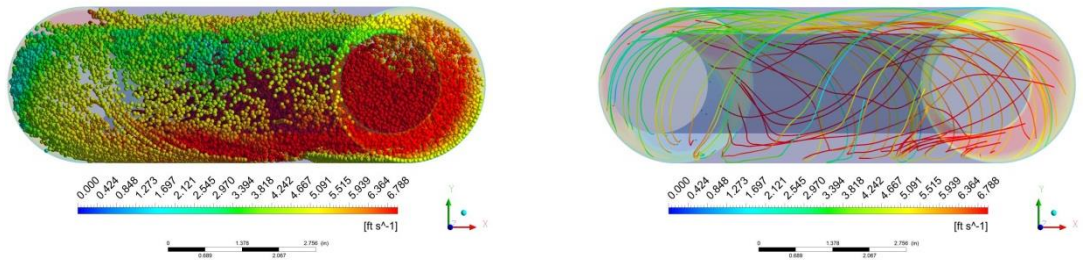

6 ft/s - Drill-pipe at 270° (1 whole cycle completed)

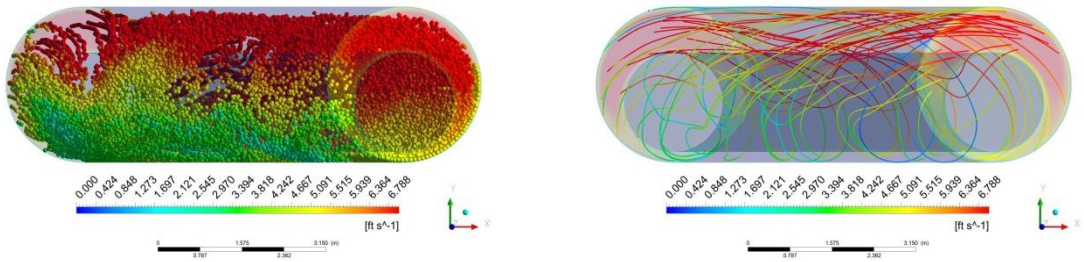

Figure 7-37: Trajectory of particles and 3D streamlines of fluid velocity for synchronous whirling [whirling speed: (+) 80 rpm, rotary speed: (+) 80 rpm] at 6 ft/s of fluid velocity

Moreover, it is deduced that an effective hole cleaning is provided at the transient and fully turbulent flow regimes at synchronous whirl. Significant increase in cuttings concentration at any drill-pipe rotation during the revolution was not observed; therefore, drilled cuttings are not tend to accumulate in the virtual region caused by plastering effect as shown in Figure 7-38.

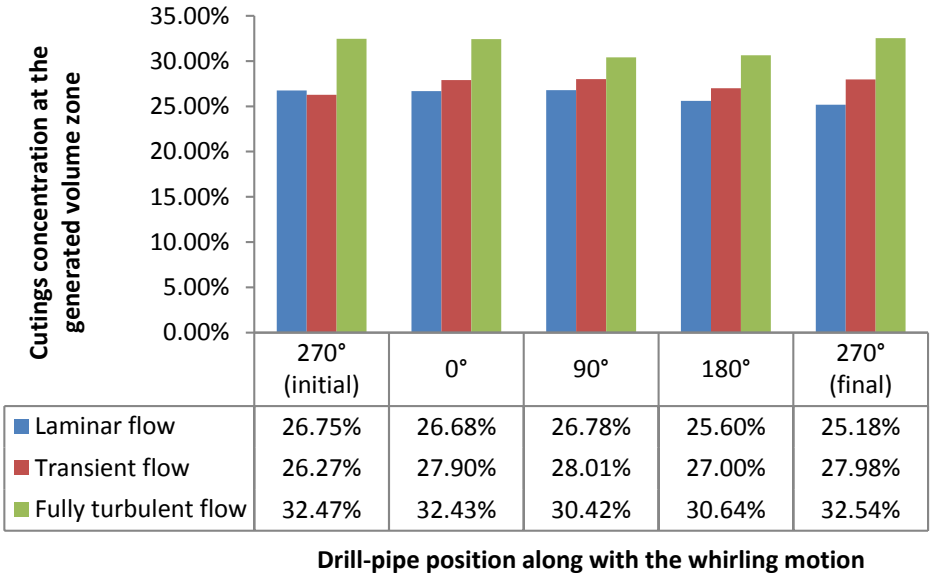

Figure 7-38: Cuttings distribution along the whirling rotary at the virtual region at forward whirl at 80 rpm

After the visual observations of various whirling motion on cuttings behavior, statistical evaluation of the whirling rotary on the cuttings transport performance with respect to annular pressure losses, cuttings concentration and average cuttings transport velocities is discussed after completing the 4 whole revolution of the drill-pipe. It is observed from Figure 7-39 that cuttings are mainly distributed in the sectors 4, 5 and 6 in backward whirl at 40 rpm in the laminar flow regime. On the contrary, cuttings concentration is observed more in the sectors 1, 7 and 8 in the forward whirl at 40 rpm for the same regime. This situation is explained by the direction of the whirling rotary. However, it is noted that more numbers of cuttings are present in the annuli when the whirling rotary is backward at 40 rpm than the whirling rotary is forward at 40 rpm. Backward whirl does not contribute the cuttings at the narrow part to carry into the main flow region. When the whirling rotary is taken account, cuttings which are dragged into the high

velocity region by the whirling direction begin to drop out of the suspension region because drill-pipe rotates at the clockwise direction, and causes the cuttings move through the bottom again.

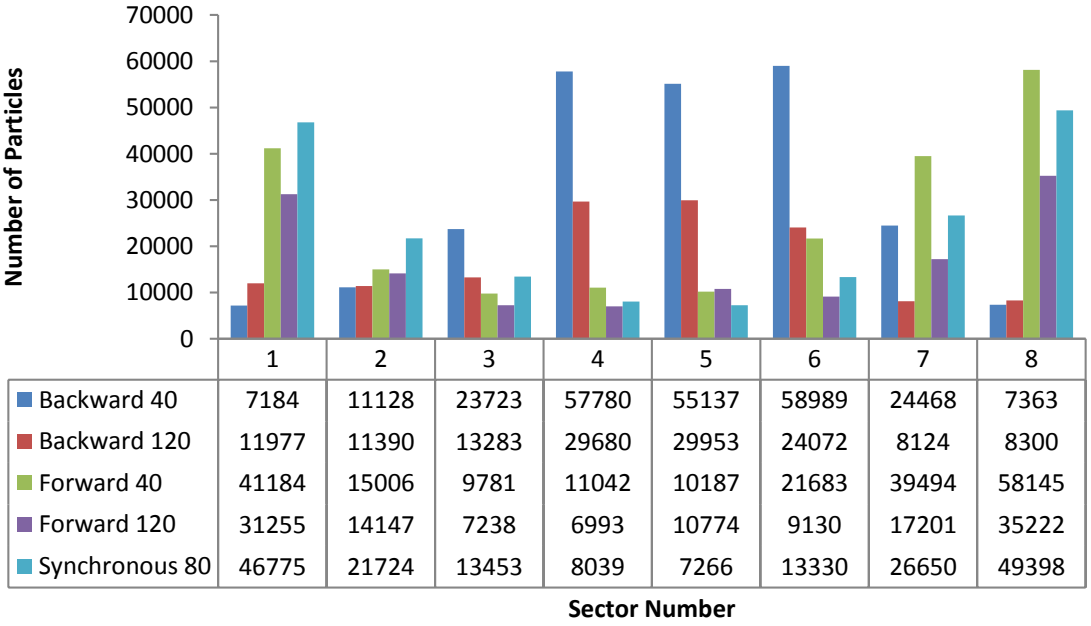

	1	2	3	4	5	6	7	8
Backward 40	7184	11128	23723	57780	55137	58989	24468	7363
Backward 120	11977	11390	13283	29680	29953	24072	8124	8300
Forward 40	41184	15006	9781	11042	10187	21683	39494	58145
Forward 120	31255	14147	7238	6993	10774	9130	17201	35222
Synchronous 80	46775	21724	13453	8039	7266	13330	26650	49398

Figure 7-39: Particle distribution along sectors for various whirling rotary at fluid velocity of 3 ft/s

Annular pressure losses are compared with respect to whirling motion and speed in the laminar flow regime, as seen in Figure 7-40. It is observed that pressure losses decrease with increasing whirling speed. However, this phenomenon is more obvious when the whirling motion is forward. In other words, the highest annular frictional pressure losses are obtained in the forward whirl at 40 rpm. Decreasing the annular pressure losses is provided by a reduction in the cuttings concentration and an increase in the shear rate due to the shear-thinning behavior of the drilling fluid. Therefore, annular frictional pressure reduces with increasing inner pipe rotation because shear thinning is more predominant than inertial effects in the low fluid velocities. Annular pressure losses are also the function of the whirling motion. In addition, average axial cuttings transport velocity increases with increasing whirling rotary speed when the flow is laminar as shown in Figure 7-41. Furthermore, the number of particles significantly decreases with increasing whirling rotary speed. Cuttings concentration decreases with increasing whirling rotary speed as shown in Figure 7-42. Similar results were obtained in the literature in terms of drill-pipe rotation [16, 18, 33, 40].

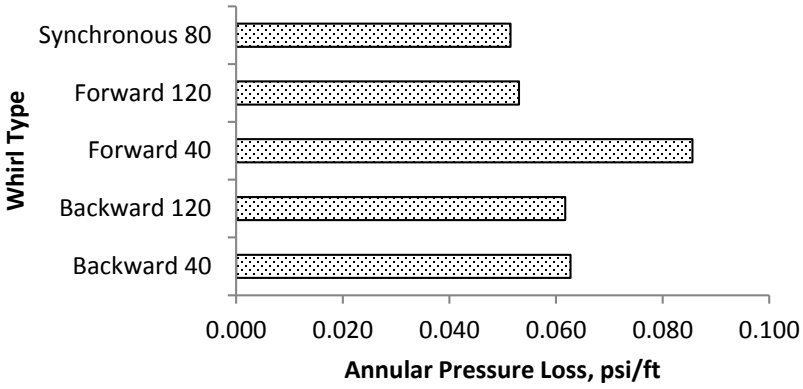

Figure 7-40: Annular pressure losses as a function of whirling rotary at fluid velocity of 3 ft/s

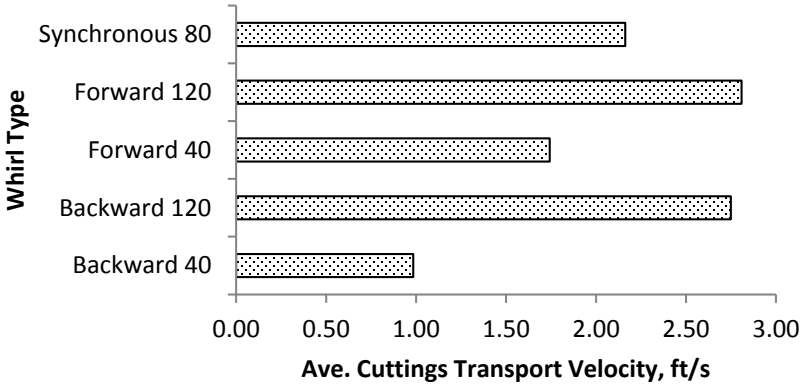

Figure 7-41: Average cuttings transport velocity as a function of whirling rotary at fluid velocity of 3 ft/s

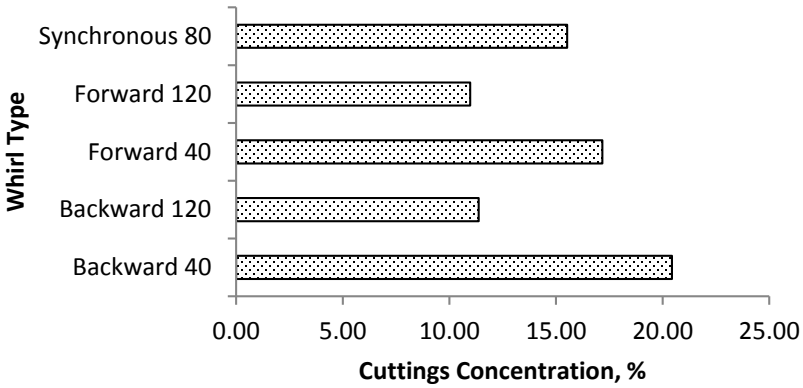

Figure 7-42: Cuttings concentration as a function of whirling rotary at fluid velocity of 3 ft/s

In the transient flow regime, cuttings distribution along the annuli is similar to what it is seen in the laminar flow. In the sectors 4, 5 and 6 in backward whirl at 40 rpm, the number of cuttings is more while cuttings concentration is more pronounced in the sectors 1, 7 and 8 in the forward whirl at 40 rpm as seen in Figure 7-43.

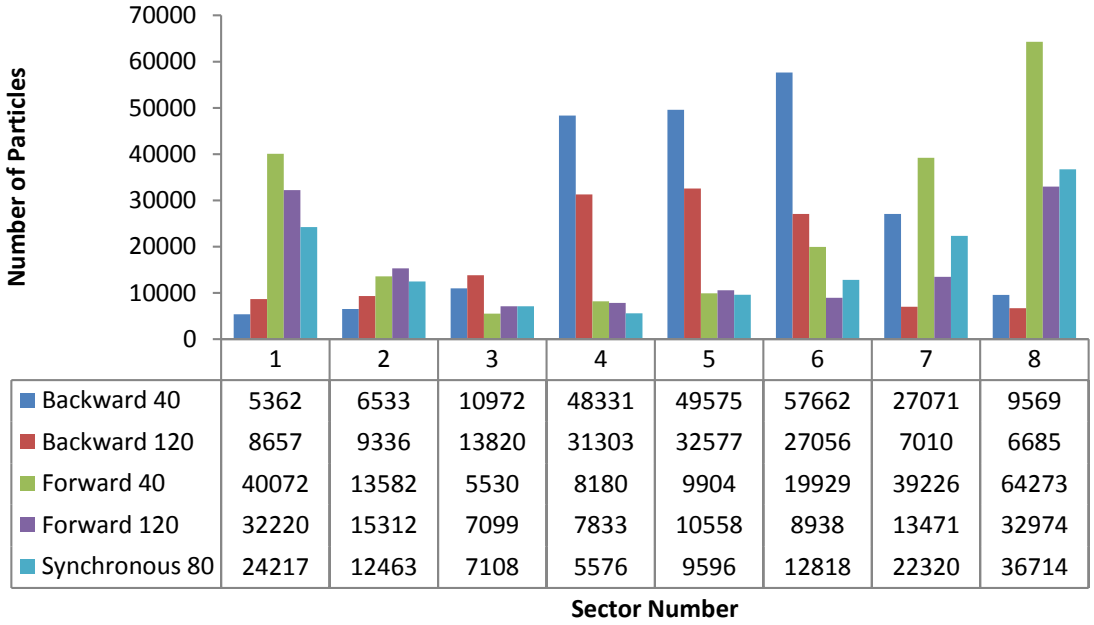

	1	2	3	4	5	6	7	8
Backward 40	5362	6533	10972	48331	49575	57662	27071	9569
Backward 120	8657	9336	13820	31303	32577	27056	7010	6685
Forward 40	40072	13582	5530	8180	9904	19929	39226	64273
Forward 120	32220	15312	7099	7833	10558	8938	13471	32974
Synchronous 80	24217	12463	7108	5576	9596	12818	22320	36714

Figure 7-43: Particle distribution along sectors for various whirling rotary at fluid velocity of 4 ft/s

Annular pressure losses also decrease with increasing whirling speed in the transient flow regime as seen in Figure 7-44. The highest annular frictional pressure losses are obtained in the forward whirl at 40 rpm. This behavior is already explained with the shear thinning behavior of the drilling fluid, particularly in the low flow rates. In addition, average axial cuttings transport velocity increases with increasing whirling rotary speed form 40 rpm to 80 rpm; however, it decreases at whirling rotary at 120 rpm as shown in Figure 7-45. The number of particles significantly decreases with increasing whirling rotary speed at the transient flow. Furthermore, cuttings concentration decreases with increasing whirling rotary speed as shown in Figure 7-46. However, there is no noticeable difference between whirling speed of 120 rpm and 80 rpm with respect to cuttings concentration.

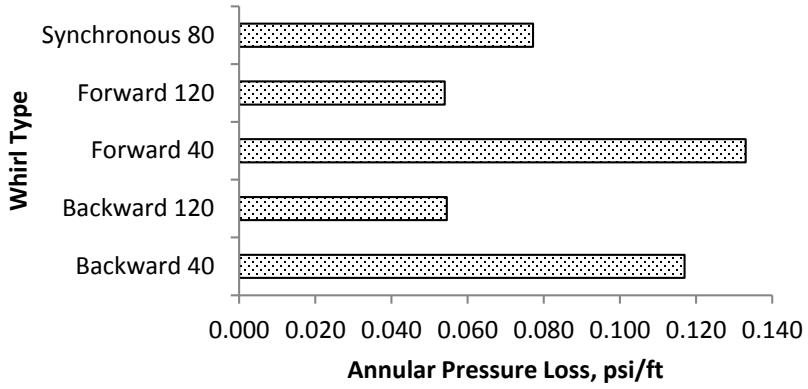

Figure 7-44: Annular pressure losses as a function of whirling rotary at fluid velocity of 4 ft/s

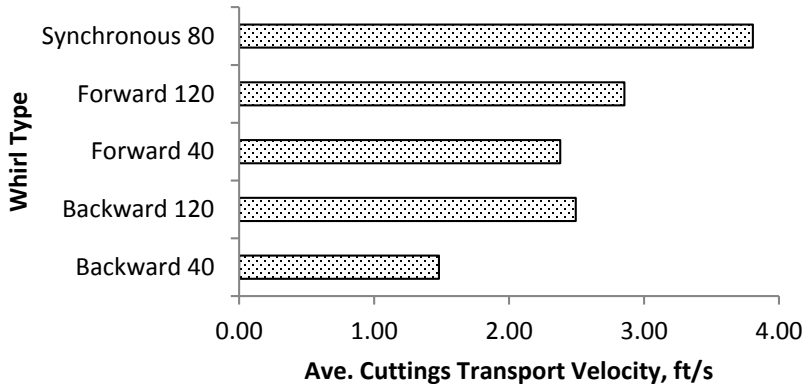

Figure 7-45: Average cuttings transport velocity as a function of whirling rotary at fluid velocity of 4 ft/s

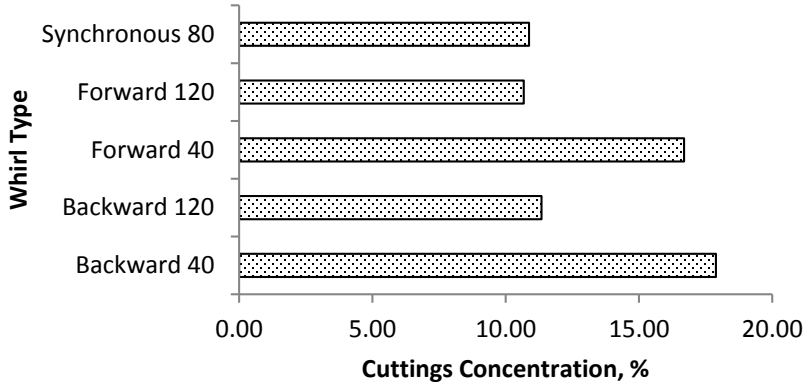

Figure 7-46: Cuttings concentration as a function of whirling rotary at fluid velocity of 4 ft/s

In the fully turbulent flow regime, cuttings distribution along the annuli is slightly different from what it is obtained in the laminar and transient flows. In the sectors 4 and 5 in backward whirl with 120 rpm, the number of cuttings is more pronounced while cuttings concentration is more in the sector 6 in the backward whirl at 40 rpm. In sector 7, forward whirl with 40 rpm causes the most cuttings concentration. More cuttings are distributed in the sector 8 with synchronous whirl at 80 rpm. Cuttings distribution along with the all sectors at fully turbulent flow regime can be seen in Figure 7-47.

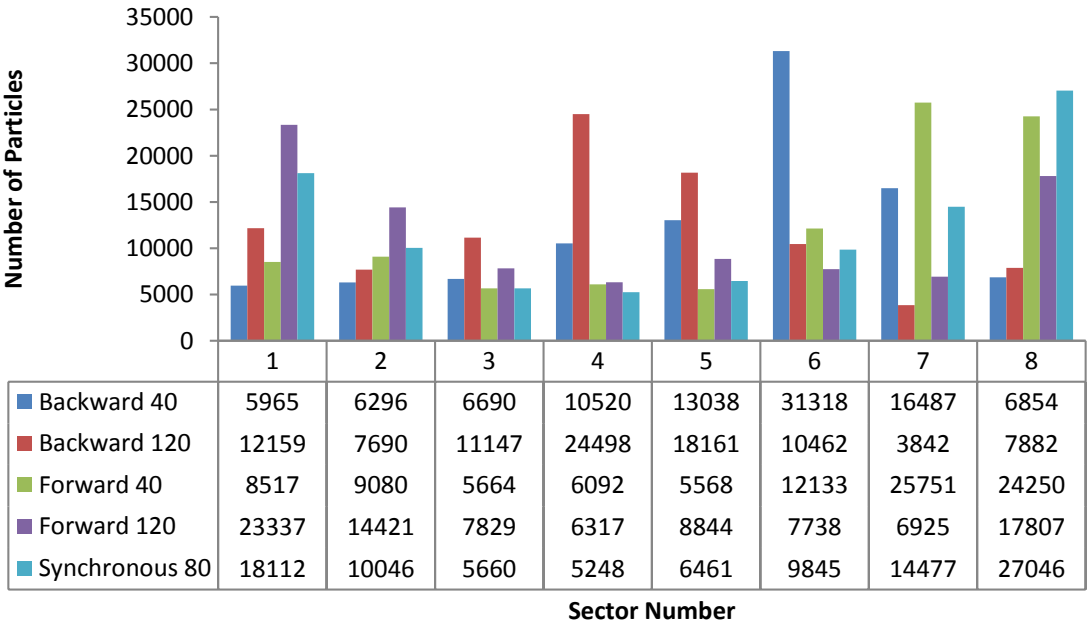

	1	2	3	4	5	6	7	8
Backward 40	5965	6296	6690	10520	13038	31318	16487	6854
Backward 120	12159	7690	11147	24498	18161	10462	3842	7882
Forward 40	8517	9080	5664	6092	5568	12133	25751	24250
Forward 120	23337	14421	7829	6317	8844	7738	6925	17807
Synchronous 80	18112	10046	5660	5248	6461	9845	14477	27046

Figure 7-47: Particle distribution along sectors for various whirling rotary at fluid velocity of 6 ft/s

Annular pressure losses decrease with decreasing whirling rotary speed in the turbulent flow regime as shown in Figure 7-48. This behavior is completely different in turbulent flows than what is observed in the laminar and transient flows. Flow is destabilized with the pipe rotation and some additional energy is contributed to the flow as discussed earlier. This causes an increase in pressure drop while whirling rotation of the drill-pipe because inertial effects become more dominant than shear thinning. Hence, an increase in the pressure drop occurs when the whirling rotary speed increases.

In addition to the annular pressure losses with respect to the whirling motion and speed, average axial cuttings transport velocity is also investigated for the fully turbulent flows as seen in Figure 7-49. It is deduced that average axial cuttings transport velocity increases with increasing whirling rotary speed from 40 rpm to 80 rpm; however, average axial cuttings transport velocity does not change when whirling rotary is increased from 80 rpm to 120 rpm. This behavior is also observed at the case#1 (no whirl, pure rotation) where drill-pipe rotates only around its axis. Moreover, it can also be seen from the Figure 7-49 that effect of increasing whirling rotary speed from 40 rpm to 80 rpm on cuttings transport efficiency is more pronounced at forward whirling. Therefore, increasing whirling speed at forward whirling makes a significant contribution to the cuttings transport efficiency at the higher flow rates.

Figure 7-50 illustrates that cutting concentration does not change with increasing whirling speed from 40 rpm to 80 rpm. However, cuttings concentration decreases with increasing whirling rotary speed from 80 rpm to 120 rpm. It is noted that whirling rotary is a function of the cuttings concentration at high rotary speeds. Particularly, there is a significant reduction in the cuttings concentration with increasing whirling speed at forward whirling.

To sum up, the highest and lowest values for the annular pressure losses, average cuttings transport velocity and cuttings concentration at different whirling rotary and flow regimes are summarized in Table 7-3. At lower flow rates, forward whirling with whirling speed of 120 rpm can provide the optimum hole cleaning. At higher flow rates, the minimum annular pressure losses are obtained at forward whirling with 40 rpm although the lowest cuttings concentration is observed at forward whirling with 120 rpm.

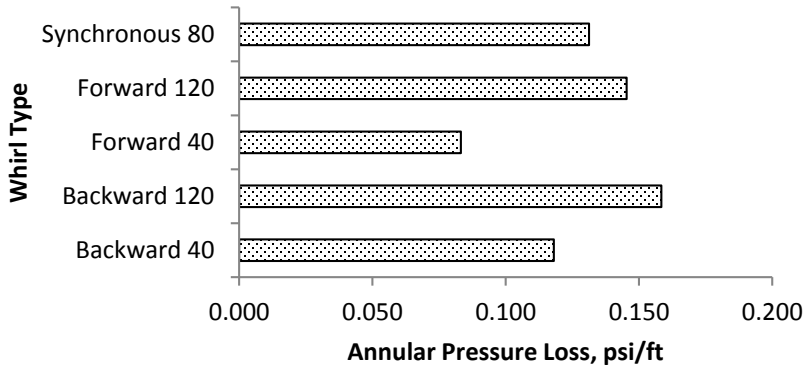

Figure 7-48: Annular pressure losses as a function of whirling rotary at fluid velocity of 6 ft/s

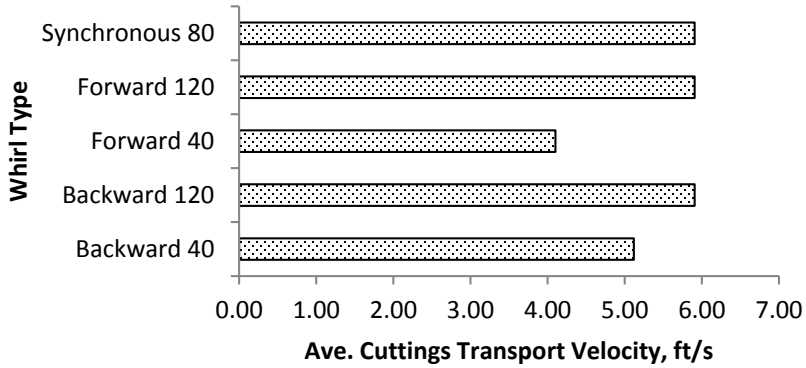

Figure 7-49: Average cuttings transport velocity as a function of whirling rotary at fluid velocity of 6 ft/s

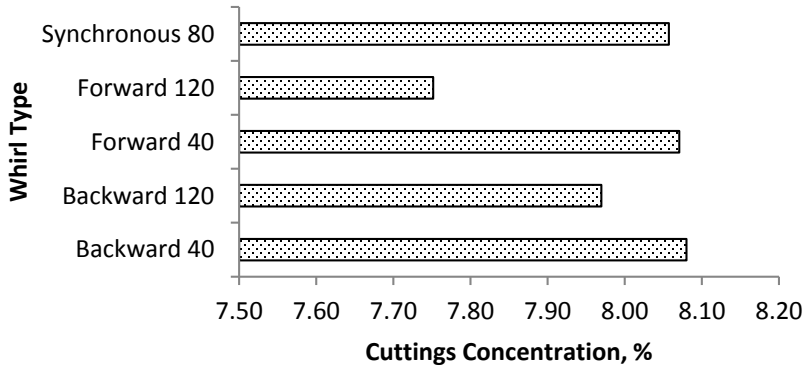

Figure 7-50: Cuttings concentration as a function of whirling rotary at fluid velocity of 6 ft/s

Table 7-3: Summary of the highest and lowest values for different cases

	Synchronous 80	Forward 120	Forward 40	Backward 120	Backward 40
			Laminar Flow Regime		
ΔP/L	Min		Max		
$\bar{V}_T$		Max			Min
C_c		Min			Max
			Transient Flow Regime		
ΔP/L		Min	Max		
$\bar{V}_T$	Max				Min
C_c		Min			Max
			Fully Turbulent Flow Regime		
ΔP/L			Min	Max	
$\bar{V}_T$	Max	Max	Min	Max	
C_c		Min			Max

CHAPTER 8: CONCLUSIONS AND RECOMMENDATIONS

The present study employs a coupled CFD-DEM method in order to investigate the effects of drill-pipe rotation as well as whirling rotary on prediction of pressure losses, cuttings concentrations and average cuttings transport velocities in an eccentric, horizontal, annular, geometry. First, cuttings transport performance was investigated by allowing only the rotation of the drill-pipe on its own axis. Second, various types of whirling rotary including backward, forward and synchronous whirling motions were analyzed in detail. It should be noted that numerical study for investigating the effect of rotation on hole cleaning efficiency was performed by using constant eccentricity, ROP, mud rheology, cutting size and diameter ratio during the simulations. The effect of drill-pipe and whirling rotation on cuttings transport performance was the preliminary scope of the research. On the basis of findings and observations made during the work, the following conclusions can be drawn:

1. Fluid velocity is an important factor on hole cleaning efficiency. Cuttings concentration decreases with increasing flow rate. When the flow regime is laminar and/or transient, the effect of fluid velocity on cuttings concentration is more predominant. However, increasing flow rate slightly decreases the cuttings concentration at high fluid velocities.
2. Increasing flow rate leads to significant increment in the annular pressure drop, but frictional losses also increase at higher rotary speeds when the flow is transient and turbulent. Generation of cuttings during drilling results in higher annular frictional losses because the presence of the particles increases the drag force and skin friction in the fluid-solid multiphase flows.
3. Cuttings concentration does not change significantly with the inner pipe rotary at any flow regime. When the drill-pipe rotary speed changes from 0 rpm to 80 rpm, reduction in cuttings volume is more pronounced. After 80 rpm rotary speed, there is no remarkable impact of drill-pipe rotation on the cuttings concentration.
4. Drill-pipe rotation plays a significant role on cuttings distribution in the annular section because cuttings are swayed and distributed asymmetrically along the circumference direction by the presence of the inner-pipe rotation.

5. Tangential velocity of the drilling fluid increases with increasing drill-pipe rotation; therefore, rotation of the drill-pipe leads to produce drag and lift forces along the tangential direction and contributes cuttings transport efficiency by removing the stationary cuttings bed.
6. Orbital motion of the drill pipe significantly contributes to hole cleaning performance.
7. In laminar and transient flow regimes, the highest annular frictional pressure loss is obtained at forward whirl with low whirling speed. Also, annular pressure drop is high at backward whirl with low whirling speed. In consequence, low whirling rotary results in higher annular pressure losses in low flow rates. Otherwise, annular pressure losses increase with increasing whirling speed in the turbulent flow regime.
8. Increasing whirling rotary speed mainly increases the average axial cuttings transport velocities in laminar, transient and turbulent flow regimes. However, average axial cuttings transport velocity is more at synchronous whirl in the transient flow.
9. Cuttings concentration increases with decreasing whirling speed at laminar, transient, and turbulent flows.
10. The presence of the plastering effect may be experienced in the backward whirling, particularly, at the low flow rates with backward whirl motion of the drill-pipe.

This research indicates that the further work needs to be done:

1. Eccentricity plays a significant role on cuttings transport and whirling orbit. The effect of eccentricity on the whirling motion of the drill-pipe should be investigated for a better understanding of orbital motion on the hole cleaning efficiency.
2. The plastering effect is a significant factor in drilling application, especially while casing drilling operation. In order to analyze this mechanism better, effect of the cutting size should be considered in the whirling rotary simulations. However, various diameter ratios between the wellbore and the drill-pipe should be included in the whirling rotary simulation with respect to the occurrence of the plastering effect.

3. In this study, motion mode is assumed to be whirling. However, effect of torque and dynamic buckling due to the nature of the drilling should be taken into account in the numerical model; therefore, drill-pipe may loss its stability as regarding the boundary conditions which are defined by the dynamic vibrations so that snaking or whirling mode is determined. As a result, coupling between the fatigue failure of the material due to the influence of the bending dynamics and transport phenomena should be considered simultaneously.
4. Parametric study can be conducted for the whirling motion of the drill-pipe in a horizontal well. Effect of mud rheology, ROP, hole inclination and rotary speed can be investigated.

REFERENCES

1. Caenn, R., H.C.H. Darley, and G.R. Gray, *Chapter 5 - The Rheology of Drilling Fluids,* in *Composition and Properties of Drilling and Completion Fluids (Sixth Edition)*, R. Caenn, H.C.H. Darley, and G.R. Gray, Editors. 2011, Gulf Professional Publishing: Boston. p. 179-269.

2. Lake, L.W., *Drilling Problems and Solutions,* in *Petroleum Engineering Handbook Volume II*, R.F. Mitchell, Editor. 2007, Society of Petroleum Engineers: USA. p. 433-454.

3. Tomren, P.H., A.W. Iyoho, and J.J. Azar, *Experimental Study of Cuttings Transport in Directional Wells.* SPE Drilling Engineering, 1986. **1**: p. 43-56.

4. Costa, S.S., *et al.*, *Simulation of Transient Cuttings Transportation and ECD in Wellbore Drilling*, in *2008 SPE Europec/EAGE Annual Conference and Exhibition*. 2008, Society of Petroleum Engineers: Rome, Italy. doi:10.2118/113893-MS.

5. Nazari, T., G. Hareland, and J.J. Azar, *Review of Cuttings Transport in Directional Well Drilling: Systematic Approach*, in *SPE Western Regional Meeting*. 2010, Society of Petroleum Engineers: Anaheim, California, USA. doi:10.2118/132372-MS.

6. Wang, K., *et al.*, *Review and Analysis of Cuttings Transport in Complex Structural Wells.* Open Energy & Fuels Journal, 2013. **6**: p. 9-17.

7. Xiaofeng, S., *et al.*, *Review of Hole Cleaning in Complex Structural Wells.* The Open Petroleum Engineering Journal, 2013. **6**: p. 25-32.

8. Brown, N.P., P.A. Bern, and A. Weaver, *Cleaning Deviated Holes: New Experimental and Theoretical Studies*, in *1989 SPE/IADC Drilling Conference*. 1989, Society of Petroleum Engineers: New Orleans, Louisiana. p. 171-180. doi:10.2118/18636-MS.

9. Duan, M., *et al.*, *Critical Conditions for Effective Sand-Sized Solids Transport in Horizontal and High-Angle Wells.* SPE Drillling & Completion, 2009: p. 229-238. doi:10.2118/106707-PA.

10. Cayeux, E., *et al.*, *Real-Time Evaluation of Hole Cleaning Conditions Using a Transient Cuttings Transport Model*, in *SPE/IADC Drilling Conference and Exhibition*. 2013, Society of Petroleum Engineers: Amsterdam, The Netherlands. doi:10.2118/163492-MS.

11. Zhu, H.P., *et al.*, *Discrete particle simulation of particulate systems: Theoretical developments.* Chemical Engineering Science, 2007. **62**(13): p. 3378-3396.

12. Williams, C.E., Jr. and G.H. Bruce, *Carrying Capacity of Drilling Muds.* 1951.

13. Haolin, Z., *et al.*, *A simplified mechanistic model for predicting the critical incipient velocity of cuttings in inclined pipes.* Journal of Chemical & Pharmaceutical Research, 2014. **6**(3): p. 735.

14. ANSYS, *ANSYS FLUENT Theory Guide*. 2013.

15. Peden, J.M., J.T. Ford, and M.B. Oyeneyin, *Comprehensive Experimental Investigation of Drilled Cuttings Transport in Inclined Wells Including the Effects of Rotation and Eccentricity*, in *Europec 90*. 1990, Society of Petroleum Engineers: Hague, The Netherlands. p. 393-404. doi:10.2118/20925-MS.

16. Sanchez, R.A., *et al.*, *Effect of Drillpipe Rotation on Hole Cleaning During Directional-Well Drilling.* SPE Journal, 1999. **4**(02): p. 101-108. doi:10.2118/56406-PA.

17. Duan, M., *et al.*, *Transport of Small Cuttings in Extended Reach Drilling*, in *International Oil & Gas Conference and Exhibition*. 2006, Society of Petroleum Engineers: Beijing, China. doi:10.2118/104192-MS.

18. Ozbayoglu, M.E., *et al.*, *Effect of Pipe Rotation on Hole Cleaning for Water-Based Drilling Fluids in Horizontal and Deviated Wells*, in *IADC/SPE Asia Pacific Drilling Technology Conference and Exhibition*. 2008, Society of Petroleum Engineers: Jakarta, indonesia. doi:10.2118/114965-MS.

19. Osgouei, R.E., *Determination of Cuttings Transport Properties Of Gasified Drilling Fluids*, in *Petroleum and Natural Gas Engineering*. 2010, Middle East Technical Univeristy: Ankara, Turkey.

20. Duan, M., *et al.*, *Experimental Study and Modeling of Cuttings Transport Using Foam With Drillpipe Rotation.* SPE Drilling & Completion, 2010. **25**(03): p. 352-362. doi:10.2118/116300-PA.

21. Han, S.-M., *et al.*, *Solid–liquid hydrodynamics in a slim hole drilling annulus.* Journal of Petroleum Science & Engineering, 2010. **70**(3/4): p. 308-319.

22. Ytrehus, J.D.M., *et al.*, *Experimental study of cuttings transport efficiency of water based drilling fluids - OMAE2014-23960*. 2014.

23. Gavignet, A.A. and I.J. Sobey, *Model Aids Cuttings Transport Prediction.* Journal of Petroleum Technology, 1989. **41**(09): p. 916-921.

24. Hyun, C., N.S. Subhash, and S.O. Osisanya, *A Three-Segment Hydraulic Model for Cuttings Transport in Horizontal and Deviated Wells*, in *SPE/CIM International Conference on Horizontal Well Technology*. 2000, Society of Petroleum Engineers: Calgary, Alberta, Canada. doi:10.2118/65488-MS.

25. Ramadan, A., P. Skalle, and S.T. Johansen, *A mechanistic model to determine the critical flow velocity required to initiate the movement of spherical bed particles in inclined channels.* Chemical Engineering Science, 2003. **58**(10): p. 2153.

26. Ramadan, A., P. Skalle, and A. Saasen, *Application of a three-layer modeling approach for solids transport in horizontal and inclined channels.* Chemical Engineering Science, 2005. **60**(10): p. 2557-2570.

27. Malekzadeh, N. and M. Mohammadsalehi, *Hole Cleaning Optimization in Horizontal Wells: A New Method To Compensate Negative Hole Inclination Effects*, in *Brasil Offshore*. 2011, Society of Petroleum Engineers: Macaé, Brazil. doi:10.2118/143676-MS.

28. Wang, Z.M., *et al.*, *A Study on the Thickness of a Cutting Bed Monitor and Control in an Extended Reach Well.* Petroleum Science and Technology, 2011. **29**(13): p. 1397-1406.

29. Haolin, Z., *et al.*, *A simplified mechanistic model for predicting the critical incipient velocity of cuttings in inclined pipes.* Journal of Chemical & Pharmaceutical Research, 2014. **6**(3): p. 735-744.

30. Bilgesu, H.I., *et al.*, *Computational Fluid Dynamics (CFD) as a Tool to Study Cutting Transport in Wellbores*, in *SPE Eastern Regional Meeting*. 2002, Society of Petroleum Engineers: Lexington, Kentucky. doi:10.2118/78716-MS.

31. Bilgesu, H.I., N. Mishra, and S. Ameri, *Understanding the Effect of Drilling Parameters on Hole Cleaning in Horizontal and Deviated Wellbores Using Computational Fluid Dynamics*, in *Eastern Regional Meeting*. 2007, Society of Petroleum Engineers: Lexington, Kentucky USA. doi:10.2118/111208-MS.

32. Mishra, N., *Investigation Of Hole Cleaning Parameters Using Computational Fluid Dynamics in Horizontal and Deviated Wells*, in *Petroleum and Natural Gas Engineering*. 2007, West Virginia University: Morgantown, West Virginia USA.

33. Wang, Z.-m., *et al.*, *Effect of drillpipe rotation on borehole cleaning for extended reach well.* Journal of Hydrodynamics, Ser. B, 2009. **21**(3): p. 366-372.

34. Wang, H.-g., X.-s. Liu, and G. Ding, *The model of cuttings bed thickness in horizontal well section.* Journal of China University of Petroleum, 1993. **17**(3): p. 25-32.

35. Sorgun, M., *Modeling Of Newtonian Fluids And Cuttings Transport Analysis In High Inclination Wellbores With Pipe Rotation*, in *Petroleum and Natural Gas Engineering*. 2010, Middle East Technical Univeristy: Ankara, Turkey.

36. Yilmaz, D., *Discrete Phase Simulations of Drilled Cuttings Transport Process in Highly Deviated Wells*, in *Petroleum Engineering*. 2012, Louisiana State University: Baton Rouge, Louisiana USA.

37. Tyagi, M., M. Zulqarnain, and D. Yilmaz, *Computational Fluid Dynamics Simulations of Horizontal Wellbore Cleaning and Cement Placement Processes in Drilling and Completions Engineering Applications.* Journal of Petroleum Engineering and Technology, 2012. **2**(2): p. 15-28.

38. Garcia-Hernandez, A.J., *et al.*, *Determination of Cuttings Lag in Horizontal and Deviated Wells*. 2007, Society of Petroleum Engineers. doi:10.2118/109630-MS.

39. Ofei, T.N., S. Irawan, and W. Pao, *CFD Method for Predicting Annular Pressure Losses and Cuttings Concentration in Eccentric Horizontal Wells.* Journal of Petroleum Engineering, 2014. **2014**: p. 16.

40. Sun, X., *et al.*, *Effect of drillpipe rotation on cuttings transport using computational fluid dynamics (CFD) in complex structure wells.* Journal of Petroleum Exploration & Production Technology, 2014. **4**(3): p. 255.

41. Magagnato, F., *The Modeling of Unsteady Turbulent Flows in Turbomachines.* Task Quarterly 5, 2001. **4**: p. 477-494.

42. Chung, S.Y., G.H. Rhee, and H.J. Sung, *Direct numerical simulation of turbulent concentric annular pipe flow: Part 1: Flow field.* International Journal of Heat & Fluid Flow, 2002. **23**(4): p. 426.

43. Feiz, A.A., M. Ould-Rouis, and G. Lauriat, *Large eddy simulation of turbulent flow in a rotating pipe.* International Journal of Heat & Fluid Flow, 2003. **24**(3): p. 412.

44. Liu, N.-S. and X.-Y. Lu, *Large eddy simulation of turbulent flows in a rotating concentric annular channel.* International Journal of Heat & Fluid Flow, 2005. **26**(3): p. 378-392.

45. Chung, S.Y. and H.J. Sung, *Large-eddy simulation of turbulent flow in a concentric annulus with rotation of an inner cylinder.* International Journal of Heat & Fluid Flow, 2005. **26**(2): p. 191-203.

46. Ninokata, H., *et al.*, *Direct Numerical Simulation of Turbulent Flows in an Eccentric Annulus Channel*, in *Annual Report of the Earth Simulator Center*. 2006, Tokyo Institute of Technology. p. 293-297.

47. Zhao, Z., *et al.*, *Evaluation of Various Turbulence Models in Predicting Airflow and Turbulence in Enclosed Environments by CFD: Part 2--Comparison with Experimental Data from Literature.* HVAC&R Research, 2007. **13**(6): p. 871-886.

48. Cleary, P.W. and M.L. Sawley, *DEM modelling of industrial granular flows: 3D case studies and the effect of particle shape on hopper discharge.* Applied Mathematical Modelling, 2002. **26**(2): p. 89.

49. Bertrand, F., L.A. Leclaire, and G. Levecque, *DEM-based models for the mixing of granular materials.* Chemical Engineering Science, 2005. **60**(8/9): p. 2517-2531.

50. Tsuji, T., K. Yabumoto, and T. Tanaka, *Spontaneous structures in three-dimensional bubbling gas-fluidized bed by parallel DEM–CFD coupling simulation.* Powder Technology, 2008. **184**(2): p. 132-140.

51. Martins, A.L., *et al.*, *CFD_DEM Modeling of the Gravel Packing Process During Petroleum Horizontal Well Completions*, in *Asociacion Argentina de Mechnica Computacional*. 2010: Buenos Aires, Argentina. p. 8651-8659.

52. Mezhericher, M.T.A., *Modeling of Particle Pneumatic Conveying Using DEM and DPM Methods.* Particulate Science & Technology, 2011. **29**(2): p. 197-208.

53. Chu, K.W., *et al.*, *Computational study of the multiphase flow in a dense medium cyclone: Effect of particle density.* Chemical Engineering Science, 2012. **73**: p. 123-139.

54. ANSYS, *ANSYS FLUENT User's Guide.* 2011.

55. Bagchi, P. and S. Balachandar, *Effect of turbulence on the drag and lift of a particle.* PHYSICS OF FLUIDS, 2003. **15**(11): p. 3496-3513.

56. Cayeux, E., *et al.*, *Real-Time Evaluation of Hole Cleaning Conditions Using a Transient Cuttings Transport Model*, in *SPE/IADC Drilling Conference*. 2013, Society of Petroleum Engineers: Amsterdam, The Netherlands. doi:10.2118/163492-MS.

57. Tu, J., G.H. Yeoh, and C. Liu, *Computational fluid dynamics : a practical approach*. 2008: Amsterdam ; Boston : Butterworth-Heinemann, 2008. 1st ed.

58. Davoudabadi, P., *The Most Accurate and Advanced Turbulence Capabilities*. 2012, ANSYS, Inc: Chicago, IL.

59. Speziale, C.G., *Analytical methods for the development of Reynolds stress closures in turbulence*. 1990: Hampton, Va. : National Aeronautics and Space Administration, Langley Research Center.

60. Nouri, J.M. and J.H. Whitelaw, *Flow of Newtonian and Non-Newtonian Fluids in a Concentric Annulus With Rotation of the Inner Cylinder.* Journal of Fluids Engineering, 1994. **116**(4): p. 821-827.

61. Nouri, J.M. and J.H. Whitelaw, *Flow of Newtonian and non-Newtonian fluids in an eccentric annulus with rotation of the inner cylinder.* International Journal of Heat and Fluid Flow, 1997. **18**(2): p. 236-246.

62. Hussain, Q.E. and M.A.R. Sharif, *Numerical modeling of helical flow of viscoplastic fluids in eccentric annuli.* AIChE Journal, 2000. **46**(10): p. 1937-1946.

63. Wan, S., D. Morrison, and I.G. Bryden, *The Flow of Newtonian and Inelastic Non-Newtonian Fluids in Eccentric Annuli with Inner-Cylinder Rotation.* Theoretical & Computational Fluid Dynamics, 2000. **13**(5): p. 349.

64. Neto, J.L.V., *et al., CFD applied to turbulent flows in concentric and eccentric annuli with inner shaft rotation.* Canadian Journal of Chemical Engineering, 2011. **89**(4): p. 636.

65. Nouri, J.M., H. Umur, and J.H. Whitelaw, *Flow of Newtonian and non-Newtonian fluids in concentric and eccentric annuli.* Journal of Fluid Mechanics, 1993. **253**: p. 617-641.

66. Greenwood, D.T., *Principles of dynamics*. 1965: Prentice-Hall.

67. Cundall, P.A. and O.D.L. Strack, *A discrete numerical model for granular assemblies.* Géotechnique, 1979. **29**(1): p. 47.

68. Zhu, H.P., *et al., Discrete particle simulation of particulate systems: A review of major applications and findings.* Chemical Engineering Science, 2008. **63**(23): p. 5728-5770.

69. Ahmadian, H., S. Nazari, and H. Jalali, *Drill string Vibration Modeling Including Coupling Effects.* International Journal of Industiral Engineering & Producion Research, 2007. **18**(4): p. 59-66.

70. Gao, G. and S. Miska, *Dynamic Buckling and Snaking Motion of Rotating Drilling Pipe in a Horizontal Well.* SPE Journal, 2010. **15**(03): p. 867 - 877. doi:10.2118/113883-PA.

71. Heisig, G. and M. Neubert, *Lateral Drillstring Vibrations in Extended-Reach Wells*. 2000, Society of Petroleum Engineers. doi:10.2118/59235-MS.

72. Van Puymbroeck, L. and H. Williams, *Increasing Drilling Performance in ERD Wells with New Generation Drill Pipe*. 2013, Society of Petroleum Engineers. doi:10.1190/URTEC2013-108.

73. Shyu, R.-J., *Bending Vibration of Rotating Drill String*, in *Ocean Engineering*. 1989, Massachusetts Institute of Technology: The U.S.A.

74. Saasen, A., *Annular Frictional Pressure Losses During Drilling—Predicting the Effect of Drillstring Rotation.* Journal of Energy Resources Technology, 2014. **136**(3): p. 034501-034501.

75. Skjold, T.L., *Drillpipe Rotation Effects on Pressure Losses*, in *Department of Petroleum Engineering and Applied Geophysics*. 2010, Norwegian University of Science and Technology.

76. Karimi, M., T.E. Moellendick, and C. Holt, *Plastering Effect of Casing Drilling; a Qualitative Analysis of Pipe Size Contribution*. 2011, Society of Petroleum Engineers: Denver, Colorado, USA. doi:10.2118/147102-MS.

APPENDIX A: CONTOURS OF SIMULATED RESULTS IN CONCENTRIC ANNULI

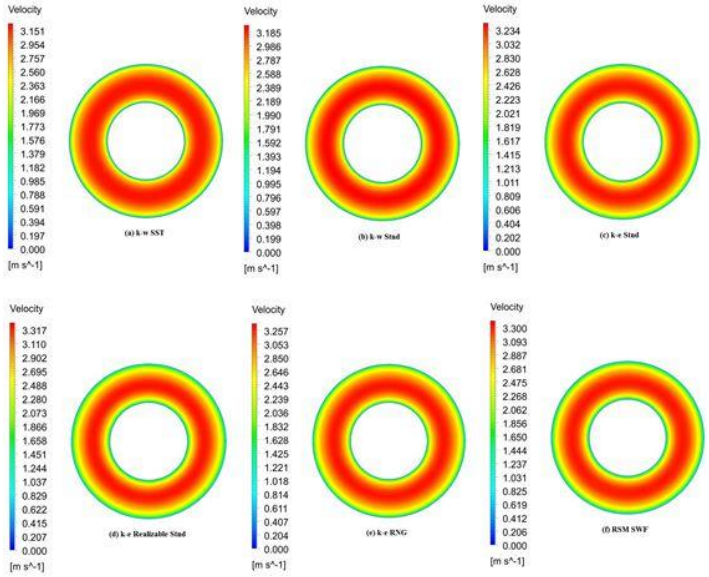

Figure A-1: Axial velocity contours in a concentric annulus without inner pipe rotation for each turbulence model: (a) k-w SST, (b) k-w Stnd, (c) k-e Stnd, (d) k-e Realizable Stnd, (e) k-e RNG, (f) RSM SWF

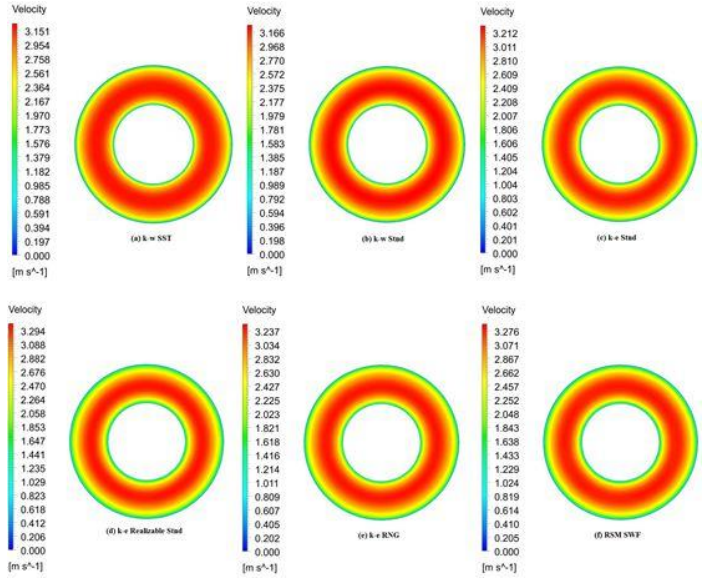

Figure A-2: Axial velocity contours in a concentric annulus with inner pipe rotation (300 rpm) for each turbulence model: (a) k-w SST, (b) k-w Stnd, (c) k-e Stnd, (d) k-e Realizable Stnd, (e) k-e RNG, (f) RSM SWF

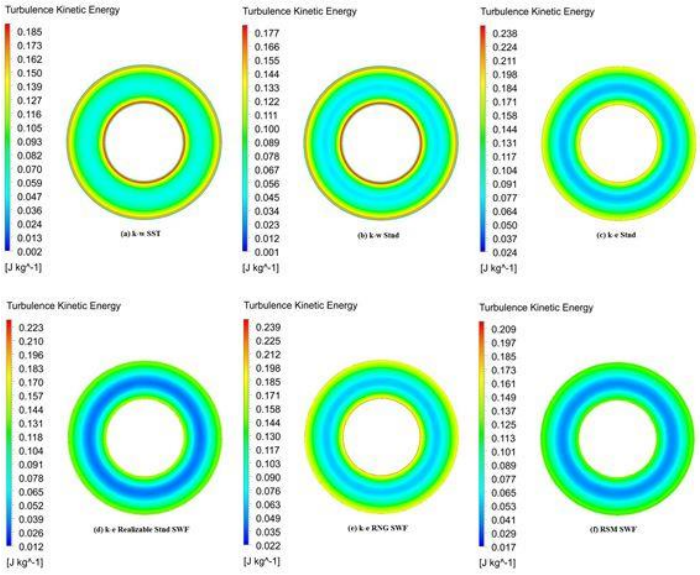

Figure A-3: Turbulence kinetic energy contours in a concentric annulus without inner pipe rotation for each turbulence model: (a) k-w SST, (b) k-w Stnd, (c) k-e Stnd, (d) k-e Realizable Stnd, (e) k-e RNG, (f) RSM SWF

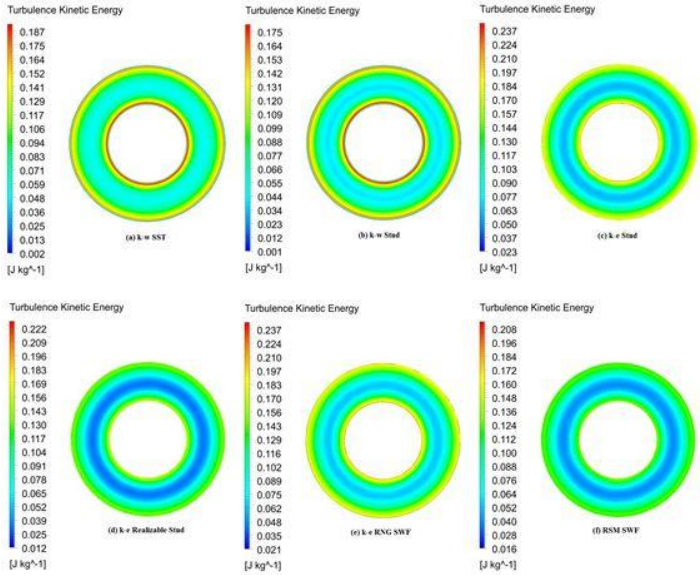

Figure A-4: Turbulence kinetic energy contours in a concentric annulus with inner pipe rotation (300 rpm) for each turbulence model: (a) k-w SST, (b) k-w Stnd, (c) k-e Stnd, (d) k-e Realizable Stnd, (e) k-e RNG, (f) RSM SWF

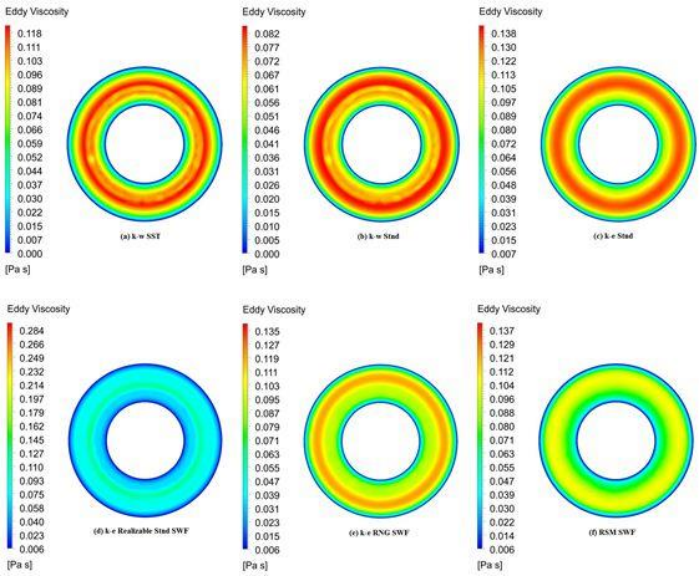

Figure A-5: Eddy viscosity contours in a concentric annulus without inner pipe rotation for each turbulence model: (a) k-w SST, (b) k-w Stnd, (c) k-e Stnd, (d) k-e Realizable Stnd, (e) k-e RNG, (f) RSM SWF

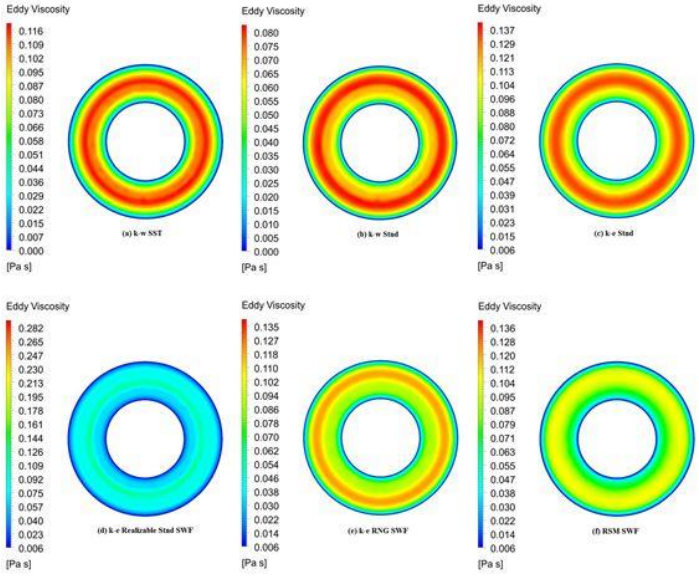

Figure A-6: Eddy viscosity contours in a concentric annulus with inner pipe rotation (300 rpm) for each turbulence model: (a) k-w SST, (b) k-w Stnd, (c) k-e Stnd, (d) k-e Realizable Stnd, (e) k-e RNG, (f) RSM SWF

APPENDIX B: CONTOURS OF SIMULATED RESULTS IN ECCENTRIC ANNULI

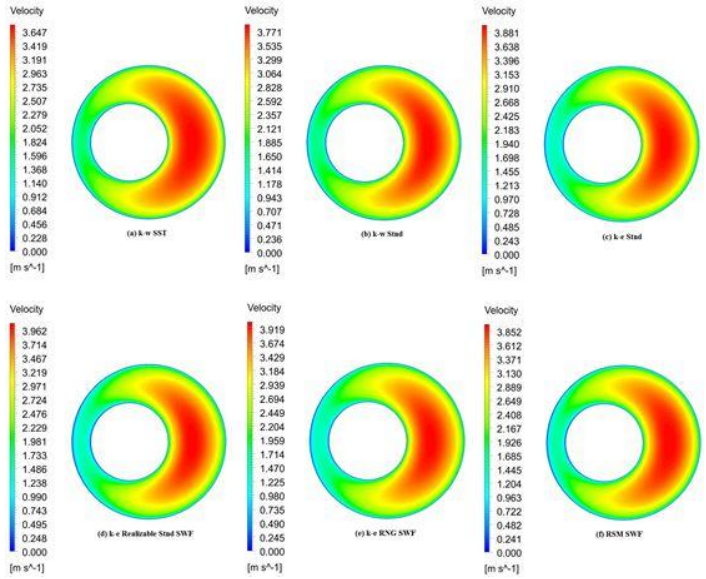

Figure B-1: Axial velocity contours in an eccentric (0.5) annulus without inner pipe rotation for each turbulence model: (a) k-w SST, (b) k-w Stnd, (c) k-e Stnd, (d) k-e Realizable Stnd, (e) k-e RNG, (f) RSM SWF

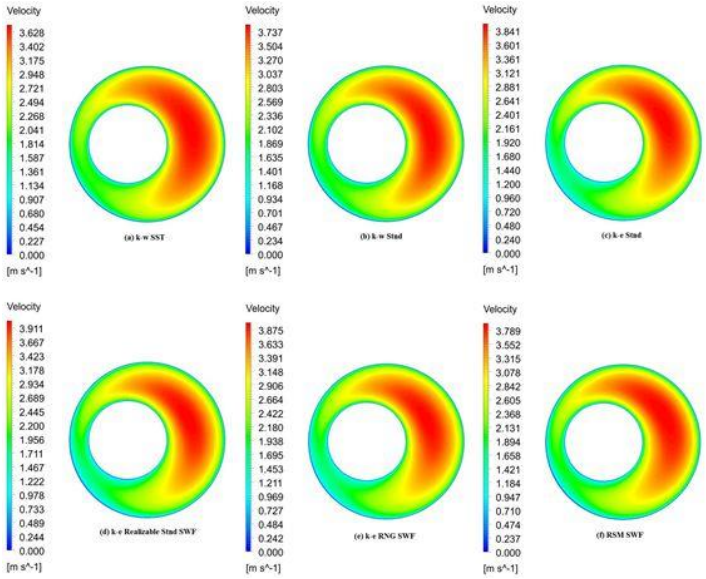

Figure B-2: Axial velocity contours in an eccentric (0.5) annulus with inner pipe rotation (300 rpm) for each turbulence model: (a) k-w SST, (b) k-w Stnd, (c) k-e Stnd, (d) k-e Realizable Stnd, (e) k-e RNG, (f) RSM SWF

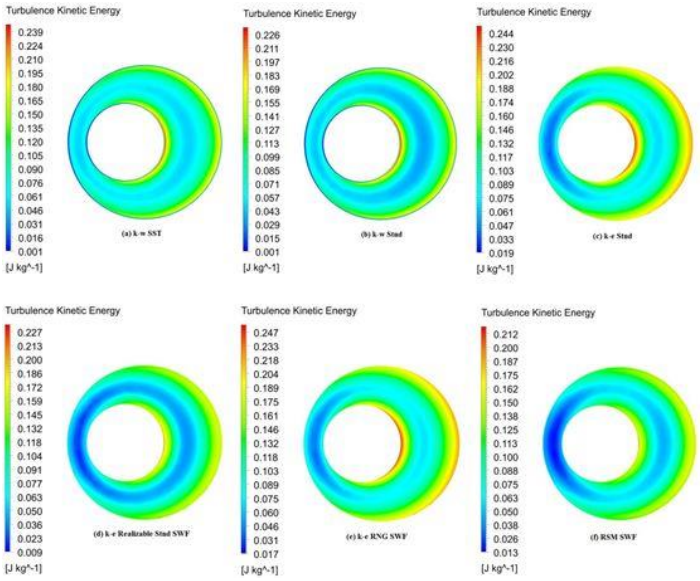

Figure B-3: Turbulence kinetic energy contours in an eccentric (0.5) annulus without inner pipe rotation for each turbulence model: (a) k-w SST, (b) k-w Stnd, (c) k-e Stnd, (d) k-e Realizable Stnd, (e) k-e RNG, (f) RSM SWF

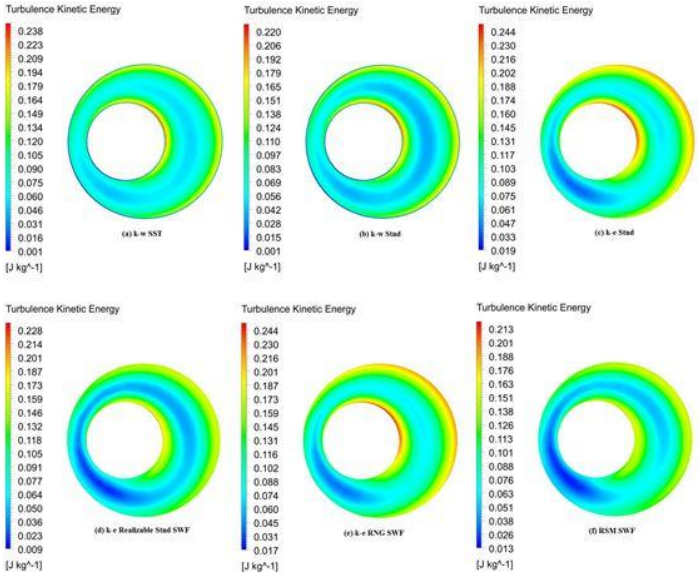

Figure B-4: Turbulence kinetic energy contours in an eccentric (0.5) annulus with inner pipe rotation (300 rpm) for each turbulence model: (a) k-w SST, (b) k-w Stnd, (c) k-e Stnd, (d) k-e Realizable Stnd, (e) k-e RNG, (f) RSM SWF

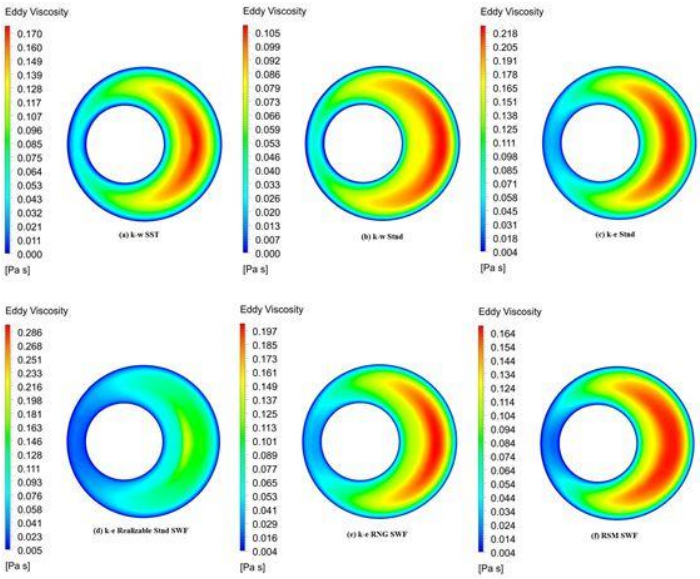

Figure B-5: Eddy viscosity contours in an eccentric (0.5) annulus without inner pipe rotation for each turbulence model: (a) k-w SST, (b) k-w Stnd, (c) k-e Stnd, (d) k-e Realizable Stnd, (e) k-e RNG, (f) RSM SWF

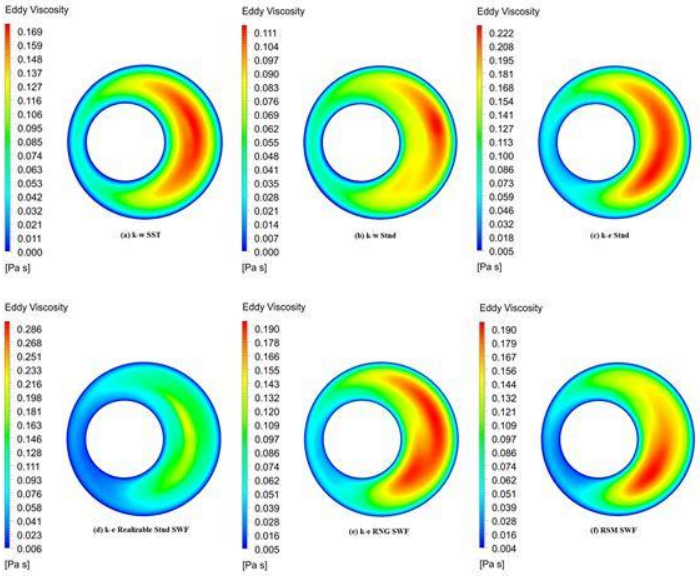

Figure B-6: Eddy viscosity contours in an eccentric (0.5) annulus with inner pipe rotation (300 rpm) for each turbulence model: (a) k-w SST, (b) k-w Stnd, (c) k-e Stnd, (d) k-e Realizable Stnd, (e) k-e RNG, (f) RSM SWF

VITA

Yasin Demiralp was born in Samsun/Turkey in 1987. He successfully received his bachelor's degree in Petroleum and Natural Gas Engineering at Istanbul Technical University (ITU) in 2010. Once obtained his B.Sc. degree, he began working in Turkish Petroleum International Company (TPIC). After 7 months work experience as a drilling engineer in geothermal fields in Turkey, he enrolled in the Craft & Hawkins Department of Petroleum Engineering at Louisiana State University (LSU) in Summer 2012 in order to pursue his Master of Science Degree. He is currently a candidate for the MSc in Petroleum Engineering, to be awarded in December 2014.